INVESTIGATION OF THE PRODUCTION OF SILICON NITRIDE FROM TURKISH RICE HUSKS

A THESIS SUBMITTED TO
THE GRADUATE SCHOOL OF NATURAL AND APPLIED SCIENCES
OF
MIDDLE EAST TECHNICAL UNIVERSITY

BY

BARIŞ YİĞİT ALPAY

IN PARTIAL FULFILLMENT OF THE REQUIREMENTS
FOR
THE DEGREE OF MASTER OF SCIENCE
IN
METALLURGICAL AND MATERIALS ENGINEERING

FEBRUARY 2014

Approval of the thesis:

INVESTIGATION OF THE PRODUCTION OF SILICON NITRIDE FROM TURKISH RICE HUSKS

submitted by **BARIŞ YİĞİT ALPAY** in partial fulfillment of the requirements for the degree of **Master of Science in Metallurgical and Materials Engineering Department, Middle East Technical University** by,

Prof. Dr. Canan Özgen
Dean, Graduate School of **Natural and Applied Sciences** _____

Prof. Dr. C. Hakan Gür
Head of Department, **Metallurgical and Materials Engineering** _____

Prof. Dr. Yavuz A. Topkaya
Supervisor, **Metallurgical and Materials Eng. Dept., METU** _____

Prof. Dr. Ahmet Geveci
Co-Supervisor, **Metallurgical and Materials Eng. Dept., METU** _____

Examining Committee Members:

Prof. Dr. Abdullah Öztürk
Metallurgical and Materials Engineering Department, METU _____

Prof. Dr. Yavuz A. Topkaya
Metallurgical and Materials Engineering Department, METU _____

Prof. Dr. Ahmet Geveci
Metallurgical and Materials Engineering Department, METU _____

Prof. Dr. İshak Karakaya
Metallurgical and Materials Engineering Department, METU _____

Prof. Dr. Ali İhsan Arol
Mining Engineering Department, METU _____

Date: **07.02.2014**

I hereby declare that all information in this document has been obtained and presented in accordance with academic rules and ethical conduct. I also declare that, as required by these rules and conduct, I have fully cited and referenced all material and results that are not original to this work.

Name, Last Name: Barış Yiğit Alpay

Signature :

ABSTRACT

INVESTIGATION OF THE PRODUCTION OF SILICON NITRIDE FROM TURKISH RICE HUSKS

Alpay, Barış Yiğit
M.S., Department of Metallurgical and Materials Engineering
Supervisor : Prof. Dr. Yavuz A. Topkaya
Co-Supervisor : Prof. Dr. Ahmet Geveci

February 2014, 101 pages

Production of Si_3N_4 by the carbothermal reduction and nitridation of SiO_2 in rice husk was investigated. For this purpose, rice husks from the Black Sea region (Bafra) of Turkey was obtained. The husks were subjected to a pretreatment step involving water washing, acid leaching and pyrolysis at 600°C. Pyrolyzed rice husks were found to have a C:SiO_2 molar ratio of about 5.2. Pyrolyzed rice husks were used as the starting material for the carbothermal reduction and nitridation experiments. Temperatures between 1300-1500°C were studied for 1 h to determine the optimum temperature for the process. Then, the reaction duration, N_2 flow rate and starting pyrolyzed rice husk amount was studied in order to examine their effect on the products of the process. Three different Si_3N_4 containing products were distinguished. Upon XRD analyses, it was seen that SiC was formed along with Si_3N_4 in all conditions. Si_3N_4 weight percentage was found to be increasing with the increasing reaction duration, increasing N_2 flow rate and decreasing pyrolyzed rice husk amount. SEM analyses showed that Si_3N_4 was mainly formed as nano/micro-fibers.

Keywords: Silicon Nitride, Silicon Carbide, Carbothermal Reduction and Nitridation, Pyrolysis, Rice Husk

ÖZ

TÜRK PİRİNÇ KABUKLARINDAN SİLİSYUM NİTRÜR ÜRETİMİNİN ARAŞTIRILMASI

Alpay, Barış Yiğit
Yüksek Lisans, Metalurji ve Malzeme Mühendisliği Bölümü
Tez Yöneticisi : Prof. Dr. Yavuz A. Topkaya
Ortak Tez Yöneticisi : Prof. Dr. Ahmet Geveci

Şubat 2014 , 101 sayfa

Pirinç kabuğundaki SiO_2'den karbotermal indirgeme ve nitrürleme reaksiyonu ile Si_3N_4 oluşumu incelenmiştir. Bu amaçla Karadeniz Bölgesinden (Bafra) pirinç kabukları temin edilmiştir. Pirinç kabukları suyla yıkama, asit liçi ve 600°C'de piroliz işlemlerini içeren bir sürece tabii tutulmuştur. Pirolize pirinç kabuklarındaki C:SiO_2 mol oranı yaklaşık 5.2 olarak bulunmuştur. Elde edilen pirolize pirinç kabukları karbotermal indirgeme ve nitrürleme deneyleri için hammadde olarak kullanılmıştır. 1300-1500°C arasındaki sıcaklıklar 1 saat süreyle çalışılarak optimum reaksiyon sıcaklığı belirlenmiştir. Ardından reaksiyon süresi, N_2 akış hızı ve kullanılan pirolize pirinç kabuğu miktarının reaksiyon sonucu elde edilen ürünlere olan etkileri incelenmiştir. Deneyler sonucunda üç farklı Si_3N_4 içeren ürünün oluştuğu fark edilmiştir. X-ışını kırınımı analizleri sonucunda, Si_3N_4 ile birlikte SiC'in de tüm şartlarda oluştuğu gözlemlenmiştir. Si_3N_4 ağırlık yüzdesinin reaksiyon süresi ve azot akış hızı arttıkça arttığı, kullanılan pirolize pirinç kabuğu miktarı arttıkça ise azaldığı görülmüştür. Taramalı elektron mikroskopunda yapılan incelemeler sonucunda Si_3N_4'ün genel olarak nano/mikro-fiber morfolojisine sahip olduğu gözlemlenmiştir.

Anahtar Kelimeler: Silisyum Nitrür, Silisyum Karbür, Karbotermal İndirgeme ve Nitrürleme, Piroliz, Pirinç Kabuğu

To my father

ACKNOWLEDGMENTS

I must express my deepest gratitude to my excellent supervisors Prof. Dr. Yavuz A. Topkaya and Prof. Dr. Ahmet Geveci for their kind support, patient supervision and constant encouragement throughout the research.

I would like to thank Saeid Pournaderi for sharing his experience and friendship with me. I benefited greatly from many discussions with him. I would also like to thank him for XRD and SEM analyses.

Technical assistance of Serkan Yılmaz for SEM, Nilüfer Özel and Levent Sıtkı for XRD analyses are gratefully acknowledged. I am thankful to Şerif Kaya for his helps in the hydrometallurgy laboratory. I would also like to express my gratitude to the staff of METU Central Laboratories for many analyses they have conducted.

I am thankful to my colleagues Can Altıparmak, Utku Burgaz, Mustafa Dedeoğlu and Gökhan Erian, who have contributed to this study in various ways, for their friendship and support.

I would like to express my deepest gratitude to my parents Dilek and Faruk Alpay for their love and support.

Finally, I would like to thank my brother and climbing partner Murat Can Alpay for sharing great adventures with me, which I hope to go on many more.

This study was financially supported by the Scientific Research Projects Fund of Graduate School of Engineering, Grant No: BAP-03-08-2013-010.

TABLE OF CONTENTS

LIST OF TABLES

TABLES

LIST OF FIGURES

FIGURES

LIST OF ABBREVIATIONS

BP	Black Powder
DSC	Differential Scanning Calorimetry
EDS	Energy Dispersive Spectrometry
ICP	Inductively Coupled Plasma
PRH	Pyrolyzed Rice Husk
RH	Rice Husk
RHA	Rice Husk Ash
SEM	Scanning Electron Microscopy
TGA	Thermogravimetric Analysis
WCM	White Cotton-like Material
WSL	White Surface Layer
XRD	X-Ray Diffraction

CHAPTER 1

INTRODUCTION

The 20th century has produced the greatest advancement in materials technology in human history, especially in the field of metallurgy. Metallurgical improvements in this time-line have now produced almost every reasonable combination of metal alloys and the capabilities of those alloys are fairly well known and exploited. As the need for new materials which are capable of operating under higher temperatures, higher speeds, longer life factors and lower maintenance costs are required to maintain the pace with technological advancements, limits of metal based systems are being exceeded. Recent developments in ceramics technology favor them as possible solutions in keeping up with the higher requirements of today [1].

Ceramics used for modern engineering applications are considered as non-traditional and defined as advanced or technical ceramics. These advanced ceramics, when used as engineering materials, posses several properties which can be viewed as superior to metal-based systems, like high resistance to abrasion, excellent hot strength, chemical inertness and dimensional stability [1]. Among technical ceramics, non-oxide silicon based materials exhibit a better high-temperature performance up to 1500°C [2].

Silicon nitride (Si_3N_4) is a non-oxide, advanced structural ceramic material, which is known to mankind for approximately a hundred and fifty years and it has been studied intensively for the last fifty years. Its high mechanical strength, high thermal shock resistance, high wear and corrosion resistance, higher fracture toughness compared to most other ceramics, low density and low coefficient of thermal expansion with high thermal conductivity makes it a desirable material for investigation. Among several methods of producing silicon nitride, the carbothermal reduction and nitridation of

silica (SiO_2) is the main method for manufacturing silicon nitride powder [3].

Rice husk is one of the by-products of rice production where rice is one of the most widely consumed food products by the human population as reported by the Food and Agriculture Organization [4]. Husks are composed of organic and inorganic parts, of which the inorganic part is mainly composed of SiO_2 and organic part is mainly composed of complex compounds of C-H-O, like cellulose, lignin and other organic materials. Upon controlled burning of rice husk, it is possible to decompose the organic part while keeping the carbon non-oxidized, thus obtaining a C and SiO_2 containing coke of rice husk. For approximately forty years, first reported in a U.S. patent, it is known that by using this rice husk coke, it is possible to produce Si_3N_4 by the carbothermal reduction method in the presence of nitrogen gas [5].

In this study, the optimum production conditions of silicon nitride by carbothermal reduction and nitridation of Turkish rice husks from Black Sea region (Bafra) was investigated. Although similar studies have been conducted in the past using rice husks originating from various locations in the world, the findings of these studies were reported to have large disagreements with each other. In this regard, this study was conducted with the motivation of the investigation and resolution of the disambiguation present in the literature by making its own contribution. For these purposes, temperatures between 1300-1500°C were studied for 1 h. After determining the optimum temperature, three more sets of experiments were conducted to examine the effect of duration, N_2 flow rate and amount of starting material on the product. Experimental studies were backed-up with thermodynamic calculations and studies conducted on the reaction mechanism.

CHAPTER 2

LITERATURE SURVEY

2.1 Silicon Nitride

2.1.1 Background

It is speculated that, in the prehistoric earth, when the atmosphere was hot and chemically reducing, silicon reacted with nitrogen to give silicon nitride, which eventually lead to the reaction of hot silicon nitride with water, which formed ammonia (NH_3). Therefore, the introduction of nitrogen into organic compounds was achieved, perhaps even the creation of life [6]. The earliest report about a synthetic Si_3N_4 was written in 1859 [7]. A patent written in 1896 explains the carbothermal reduction and nitridation of SiO_2 to produce Si_3N_4 [8].

In 1955, Si_3N_4 was being used as a refractory material. Potential of Si_3N_4 as a high-temperature structural engine material gained popularity in the beginning of 1960s, leading to intensive studies on the material. The need for good high-temperature properties as well as high thermal shock resistance for an internal combustion engine part lead to the development, testing and also commercial marketing of Si_3N_4. In 1970s, Si_3N_4 was extensively studied in the United States in partnership with Ford Motor Company, in order to find a suitable ceramic material for the stationary and mobile gas-turbine engine parts [6]. From late 1980s to 1990s, the development of larger size gas turbine engines for co-generation applications have been started in the United States and Japan, focusing on Si_3N_4 [9].

The ceramic engine programs in the United States and Japan were very expensive

and they have been estimated to have cost several thousand million dollars during almost forty years of effort, at the end of which no ceramic engine was successfully produced. The reasons for that were, in part, the lack of reliability and high material costs as well as the serious difficulties in making major changes in the engine design or component material. Thus, the early programs have been unsuccessful in achieving its goals. Nonetheless, thanks to these studies, great amount of knowledge on Si_3N_4 and its performance characteristics under severe conditions have been obtained and the introduction of several engine parts made of Si_3N_4 in commercially available engines was achieved [6].

2.1.2 Phases and Crystal Structure

Si_3N_4 exists in two hexagonal crystallographic modifications which are defined as α-Si_3N_4 and β-Si_3N_4 [6, 10]. Their crystallographic data is given in Table 2.1. These phases are built up from a three dimensional network of SiN_4 tetrahedrons as schematically shown in Figure 2.1. Each silicon atom is at the center of a tetrahedron and each nitrogen atom is in trigonal and approximately planar coordination by three silicon atoms, so as to link three SiN_4 tetrahedra. This rigid structure and strong covalent bonds are the cause of the extraordinary hardness, durability, and mechanical strength of this material [6, 11].

Table 2.1: Crystallographic Data of Si_3N_4 [10]

Phase	**Structure**	**Lattice Parameters (nm)**
α-Si_3N_4	Hexagonal	a=0.7748, c=0.5618
β-Si_3N_4	Hexagonal	a=0.7608, c=0.2911

Figure 2.2 shows the crystal structure of β-Si_3N_4 which is built up from Si_6N_8 unit cells and assigned to $P6_3/m$ space group. There exists channels of 300 pm diameter along the crystallographic c-axis between the layers, which play an important role in the diffusion of atoms, even large ones [6, 11].

The crystal structure of α-Si_3N_4, as shown in Figure 2.3, was determined to be closely related to that of β-Si_3N_4, consisting of alternate basal layers of β-Si_3N_4 and a mirror image of β-Si_3N_4, which results in the doubled c-axis dimension compared to

β-Si_3N_4. It has a unit cell composition of $Si_{12}N_{16}$ under the space group $P3_1c$. Although the β structure is almost strain free, the α structure contains considerable strain, which is expressed by the lattice distortion and the displacement of atoms from the idealized positions [6].

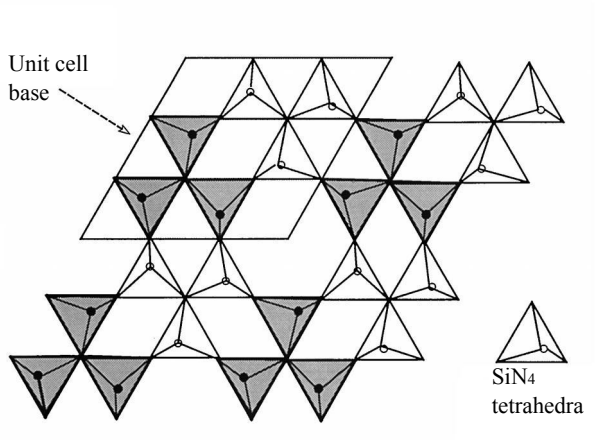

Figure 2.1: Si_3N_4 crystal structure outline [6].

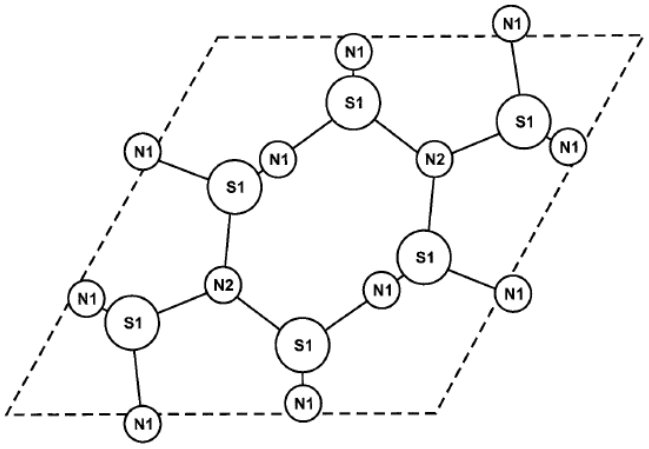

Figure 2.2: β-Si_3N_4 unit-cell [6].

Furthermore, in the α-Si_3N_4 structure, although having the double length c-axis compared to β structure, because of the operation of a c glide plane, the continuous voids are interrupted to form a series of large interstices, linked by 140 pm diameter tunnels, causing the diffusion process to become much more difficult through the layers. The bond lengths in the α-Si_3N_4 structure are indefinite and they vary much more so than in the β-Si_3N_4. There exist small variations in the unit-cell dimensions of materials obtained from different sources and with different particle morphologies [6, 11].

The crystal structure of α-Si_3N_4 is very complex. Upon studies, it is concluded that α phase has a range of homogeneity. This can be explained by a defect structure as shown in Figure 2.3, with approximately 25% nitrogen vacancies in the N(4) sites and partial replacement of nitrogen by oxygen in N(1) sites with electrical neutrality being obtained by an appropriate number of silicon vacancies or Si^{3+} species. Thus, the empirical formula suggested for the α phase is $Si_{11.4-11.5}N_{15}O_{0.3-0.5}$ which is actually an oxynitride phase [6, 11].

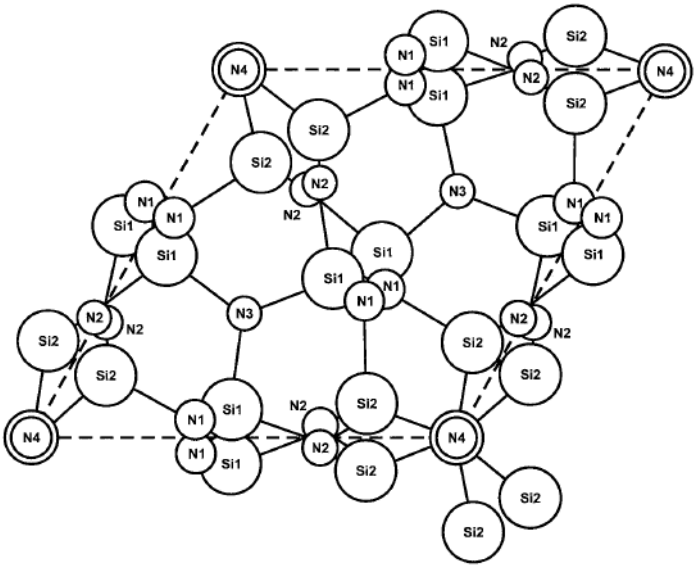

Figure 2.3: α-Si_3N_4 unit-cell [6].

Today, α and β phases are considered as polymorphic modifications of Si_3N_4. α-Si_3N_4 is considered to be the stable low temperature modification because of the increase in α-Si_3N_4 content of the powder with the decrease in synthesis temperature. Moreover, α to β transformation only occurs at temperatures greater than 1650°C. Presumably for kinetic reasons, β to α transformation has not been observed yet, but it would be expected to be too slow to be detected at temperatures lower than 1400°C [6, 11].

2.1.3 General Properties

2.1.3.1 Physical Properties

In the production of advanced ceramics, application of different methods and even small variations in the control of parameters affecting these processes result in different properties in the final product. This scatter in the property data is mainly due to the starting powder characteristics (size, shape, purity, etc.), amount and kind of sintering additives and binders, powder shaping and sintering techniques, temperature, pressure and soaking time during sintering, which affects the ultimate microstructure in the product [11]. Perfect control of these process parameters, as well as good powder characteristics is a must to obtain a high quality material with the desired microstructure. Furthermore, it is difficult to obtain a reliable and reproducible Si_3N_4 ceramic body. This can be attributed to the complex microstructure and the difficulties in tailoring it [12]. Table 2.2 shows the scattered data of important properties of the densified Si_3N_4 ceramics.

Table 2.2: Physical Properties of Dense Si_3N_4 Material. Reproduced from H. Lange et al. [11].

Property	**Value**
Decomposition temperature	2173 K
Theoretical density (th. D.)	α phase: 3.168 - 3.118 g/cm^3
	β phase: 3.19 - 3.202 g/cm^3
Material density	95-100% th. D.
Thermal expansion coefficient (293 - 1473 K)	2.9 - 3.6 x 10^{-6} K^{-1}
Specific heat	700 J·Kg^{-1}K^{-1}
Electrical resistance [a]	$10^{13}\Omega$cm
Micro-hardness (Vickers)	1400 - 1700 MNm^{-2}
Bending strength [a] [b]	600 - 1000 MPa
Fracture toughness [a]	5-8 MPa·m$^{1/2}$
Elastic modulus [a]	280 - 320 GPa
Thermal conductivity	15 - 30 Wm^{-1}K^{-1}
Critical temperature difference in thermal shock	600 - 800 K

[a] = Room temperature, [b] = Four-point bending

The mechanical properties of Si_3N_4 are determined by the interfacial strength be-

tween Si_3N_4 grains. Weak interfacial strength between the grains results in Si_3N_4 with high room temperature strength and high fracture toughness. On the other hand, strong interfaces result in creep resistant, but brittle materials [12].

Fracture strength is the main characteristic property which is mostly determined as a key criterion of quality. In the evaluation of the strength of Si_3N_4 components, the scatter of property data must be taken into account statistically. For this reason, the influence of sintering parameters on material is reflected in the Weibull distribution[1], which is used to characterize the scattering of fracture strength and thus the reliability of the material. Following values are typical for Weibull modulus of commercially available Si_3N_4 ceramics: pressureless sintered Si_3N_4 >10, gas pressure sintered Si_3N_4 >15, isostatitacally hot pressed Si_3N_4 >20 (the higher the Weibull modulus is, the more reliable the material). However, a general comparison of fracture strength is still difficult, since materials for specialized applications have been developed. Here, the main criteria of quality include not only fracture strength, but also the strength level at high temperatures [11]. Figure 2.4 shows a schematic diagram of the bending strength of Si_3N_4 as a function of temperature for two types of Si_3N_4, produced for different applications [12].

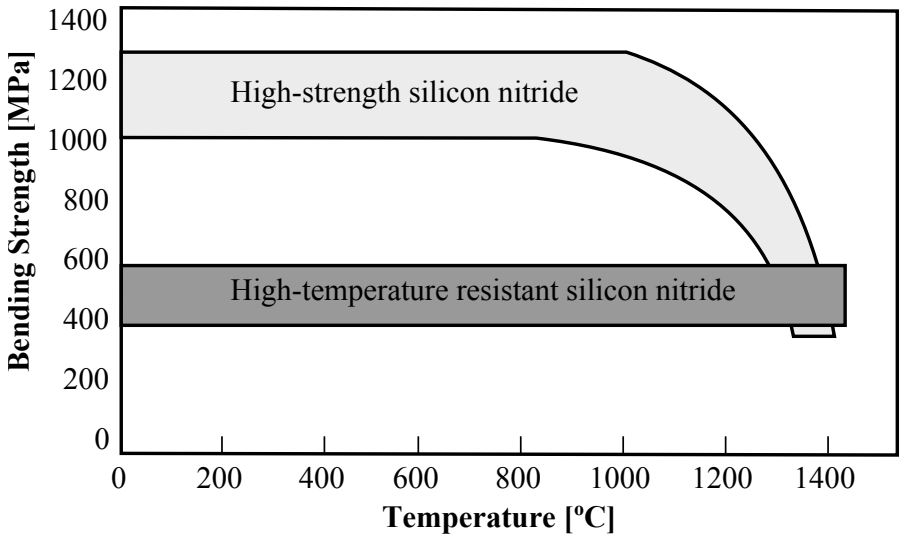

Figure 2.4: Schematic representation of the bending strength as a function of temperature for two types of Si_3N_4 ceramics. Reproduced from M. J. Hoffmann [12].

[1] The strength of brittle materials such as glasses and ceramics, is not Gaussian; it is given by the Weibull distribution. The Weibull distribution is an indicator of the variability of strength of materials resulting from a distribution of flaw sizes. This behavior results from critical sized flaws in materials with a distribution of flaw sizes (i.e. failure due to the weakest link of chain) [13].

By controlled structure development (in situ whisker reinforcement) it is possible to increase fracture toughness of Si_3N_4 materials from a level of about 7 MPa·$m^{1/2}$ to almost 10 MPa·$m^{1/2}$ [9, 10]. It is also known that the ratio of α to β phase as well as the production method, has an effect on the fracture toughness of the material [6].

2.1.3.2 Chemical Properties

Si_3N_4 is an inert material to a wide range of molten metals like Al, Zn, Sn, Pb, Cu, Ag and Cd, however when in contact with molten transition metals like Fe, Co, Ni, V and Cr, it reacts with the metal to form metal silicides and N_2. When it is in contact with molten salts, oxidic slags, and glasses, the occurring corrosion is slow. Si_3N_4 ceramics are resistant to mineral acids with the exception of hydrofluoric acid (HF). Porous Si_3N_4 components are known to be attacked by hot strong caustic solutions and melts with the formation of NH_3 [11].

Most actual and anticipated applications for Si_3N_4 ceramics require exposure to high temperatures under oxidizing conditions, like gas turbine engine parts. Si_3N_4 is thermodynamically unstable to oxidation under normal oxygen pressures, however it is protected against catastrophic oxidation by a blocking layer of SiO_2 and Si_2N_2O film formed naturally at elevated temperatures in air, which is able to prevent oxygen diffusion into the nitride surface. Ability of Si_3N_4 ceramics to withstand high temperatures under oxidizing conditions without excessive oxidation, therefore rests on the integrity and stability of the surface oxide layer [6, 9]. It is known that Si_3N_4 has a good oxidation resistance up to 1400°C, mainly due to these protective layers [11].

2.1.4 Applications

The improvements in the efficiency of heat engines generally require the structural materials to operate under severer conditions. The turbine inlet temperature of most advanced gas turbines has already far exceeded the melting point of the super alloys [9]. The general requirements of high temperature structural materials for heat engines, like gas turbines and diesel engines are listed as;

Table 2.3: Silicon Nitride as High-Temperature High-Strength Ceramic. Reproduced from Miyahara et al. [9].

Characteristics as substance	**Characteristics as material**	**Characteristics as heat engine components**
Compound formed between Si and N	Abundance as element materials	Abundance as resources
	Oxidation to form SiO_2 layer with low O permeability	High oxidation resistance
	Low specific gravity	Light weight
Covalent Bonding	High temperature deformation resistance	High fracture strength High creep resistance High fatigue resistance
	High Young's modulus	High rigidity
	Low thermal expansion	Low thermal deformation Thermal shock resistance
	High hardness	Wear resistance

- high fracture strength at ambient and high temperatures, especially high specific strength;
- high fatigue strength at ambient and high temperatures;
- high thermal shock and thermal fatigue resistance;
- high creep resistance at high temperatures;
- high oxidation and corrosion resistance;
- high wear resistance;
- high impact resistance [9].

Considering the listed requirements, as well as the incapabilities of metals to withstand the ever rising severity of operation conditions for the sake of better efficiency, Si_3N_4 is the most promising replacement of alloys in regard to structural engine parts [9]. Table 2.3 summarizes the characteristics of Si_3N_4 as a high-temperature high-strength ceramic material.

Silicon nitride turbocharger rotors for diesel engines and gasoline engines were commercialized in the 1980s (Figure 2.5). Furthermore, several components of automotive diesel engines have been commercialized successively, including igniter plugs, swirl chambers, cams, and valves [9]. The major hot-section components in diesel

engines such as piston-head, piston-cylinder are still in the process of development, but the full incorporation of Si_3N_4 as engine hot-zone moving components remains many years away. Serious obstacles in this regard are the lack of detailed knowledge about the long-term reliability of the components and their high cost [6].

In the 300kW-class, ceramic gas turbine engine CGT301, which is developed by Ishikawajima-Harima Heavy Industry in Japan for co-generation use, Si_3N_4 was used in the making of the blades, nozzles, heat exchanger, fuel nozzle, combustion liners, nose cone, inlet liner, inner ring, shroud rings, retaining rings and seal rings. Successful assembly of Si_3N_4 based advanced ceramics into CGT301 engine have enabled a high engine efficiency of 35% or more, which usually shows efficiency around 20% with metallic components [9]. It is estimated that more than 300000 sintered Si_3N_4 turbocharger rotors are manufactured annually [6].

Another application area of Si_3N_4, other than engine parts, is cutting tools. With its high hot hardness, high cutting speed (up to 15 m/s), high wear resistance and chemical inertness, it has the required properties for making cutting tools. Unlike other cutting tool materials like boron nitride and diamond, the decrease in its microhardness value is very low above 1273 K, which makes it a suitable material for cutting tool, especially for high speed milling of cast iron [9]. Sintered Si_3N_4 cuts cast iron, hard steel and nickel-based alloys with surface speeds up to 25 times those obtainable with conventional materials, such as tungsten carbide [6].

As a result of technological progress, the conditions under which the bearings operate become severer and bearings made of advanced ceramics like zirconia, silicon carbide, alumina and silicon nitride are replacing steel bearings. Considering the load carrying capacity, rolling contact fatigue life, heat, corrosion and wear resistances, Si_3N_4 shows the most superior performance. Unlike other advanced ceramics, Si_3N_4 is able to withstand high-speed rotation and it is suitable for high vacuum applications [9]. Applications in which Si_3N_4 is used include abrasive environments in oil drilling, vacuum pumps, and sterilizable and un-lubricated dental drills [6]

Si_3N_4 is also being used in the making of ceramic composites. SiC (particle or whisker)-Si_3N_4 composites/nano-composites show higher flexural strength at high temperatures up to 970 MPa at 1400°C [9].

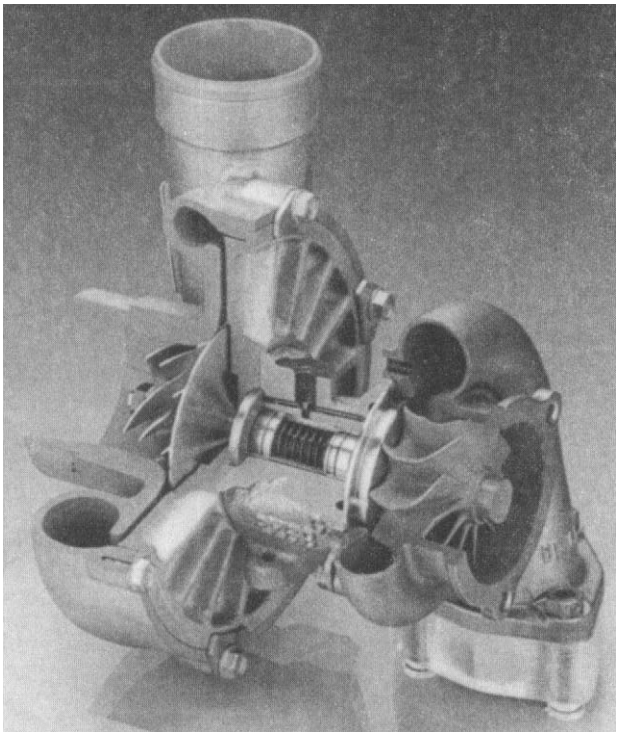

Figure 2.5: Automotive turbocharger with a silicon nitride rotor [9].

Internally threaded shroud nozzles for inert-gas welding and cutting torches, thermocouple sheaths, thin films in microelectronics area, dental porcelain firing trays and supports are other application areas where Si_3N_4 is used steadily [6].

2.1.5 Production Methods

Si_3N_4 can be fabricated by a variety of methods depending on whether the final product is desired to be a component, thin film or powder. Some methods can be used interchangeably to produce different kinds of products, however most of the methods focus on the synthesis of Si_3N_4 powders which are to be further treated in powder based production techniques of advanced ceramics. Properties of the final product will be affected by the chosen method of fabrication. Properties of commercially available Si_3N_4 powders produced by different methods are given in Table 2.4. The three most important methods for Si_3N_4 synthesis are listed as direct nitridation of silicon powders, reaction of silicon compounds with ammonia and carbothermal reduction of silica in the presence of nitrogen [11, 14–19].

Table 2.4: Properties of Commercially Available Silicon Nitride Powders. Reproduced from M. N. Rahaman [19].

	Method of Preparation			
	Liquid-Phase Reaction of $SiCl_4/NH_3$	**Nitridation of Si in N_2**	**Carbothermic Reduction of SiO_2 in N_2**	**Vapor-Phase Reaction of $SiCl_4/NH_3$**
Manufacturer	UBE	H. C. Starck	Toshiba	Toya Soda
Grade	SN-E 10	H1	—	TSK TS-7
Metallic Impurities (wt%)	0.02	0.1	0.1	0.01
Nonmetallic Impurities (wt%)	2.2	1.7	4.1	1.2
α-Si_3N_4 (wt%)	95	92	88	90
β-Si_3N_4 (wt%)	5	4	5	10
SiO_2 (wt%)	2.5	2.4	5.6	—
Surface area (m^2/g)	11	9	5	12
Average particle size (μm)	0.2	0.8	1.0	0.5
Tap density (g/cm^3)	1.0	0.6	0.4	0.8

2.1.5.1 Direct Nitridation of Silicon

Direct nitridation of elemental silicon is the most widely used method for the industrial synthesis of Si_3N_4 powders [11]. The flowchart for this method is given in Figure 2.6. Using this method, it is also possible to produce Si_3N_4 components, which is known as reaction bonded silicon nitride. Depending on the silicon source, the purity level of the product changes, thus high purity silicon powders are desired for nitridation. For the synthesis of Si_3N_4 powders, piles of silicon powders are allowed to react with nitrogen in chamber or conveyor-type pusher furnaces for 10 to 30 hours at 1200 to 1400°C [11, 20]. Although the mechanism is complex, the overall reaction can be written as [20]:

$$3Si_{(s)} + 2N_{2(g)} \rightarrow Si_3N_{4(s)} \tag{2.1}$$

On the other hand, by consolidating the silicon powders by one of the ceramic forming methods to form a shaped article and preheating it in an argon environment at 1200°C to develop some strength to withstand the machining operations, followed by heating in nitrogen gas at atmospheric pressure at around 1250 to 1400°C, where reaction bonding and nitriding occurs simultaneously, Si_3N_4 components can be produced [19]. This way, it is possible to produce complex shaped articles without the time consuming and expensive finishing operations [6].

Temperature must be kept at higher than 1100°C to keep the reaction rate at a reasonable level. Additionally, reaction rate is strongly affected by the particle size and purity of silicon powder. Iron is known to act as a catalyst in this method, increasing the reaction rate. After the synthesis process, the sintered product is crushed and milled to a desired particle size for powder production. Possible metallic impurities introduced during milling are removed by subsequent acid leaching [11].

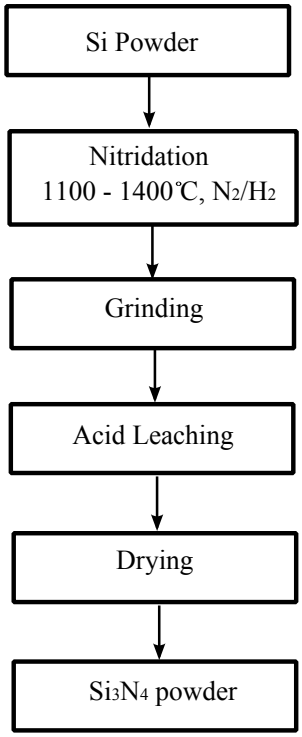

Figure 2.6: Process for Si_3N_4 powder synthesis by direct nitridation. Reproduced from H. Lange et al. [11].

This method produces 100% crystalline product. Lower temperatures and mixture of hydrogen in the nitriding gas tend to form α-Si_3N_4, whereas higher temperatures tend to form β-Si_3N_4 [11].

2.1.5.2 Reaction of Silicon Compounds with Ammonia

This method can be divided in two parts as liquid-phase reactions and gas-phase reactions. For the liquid phase reaction method to produce Si_3N_4 powders, which is also known as the imide precipitation method, the reaction between liquid $SiCl_4$ and liquid NH_3 is used [19]. The flowchart for this method is given in Figure 2.7. Although the

reactions are more complex, they can be written as [19]:

$$SiCl_{4(l)} + 6NH_{3(l)} \rightarrow Si(NH)_2 + 4NH_4Cl \tag{2.2}$$

$$3Si(NH)_2 \rightarrow Si_3N_4 + N_2 + 3H_2 \tag{2.3}$$

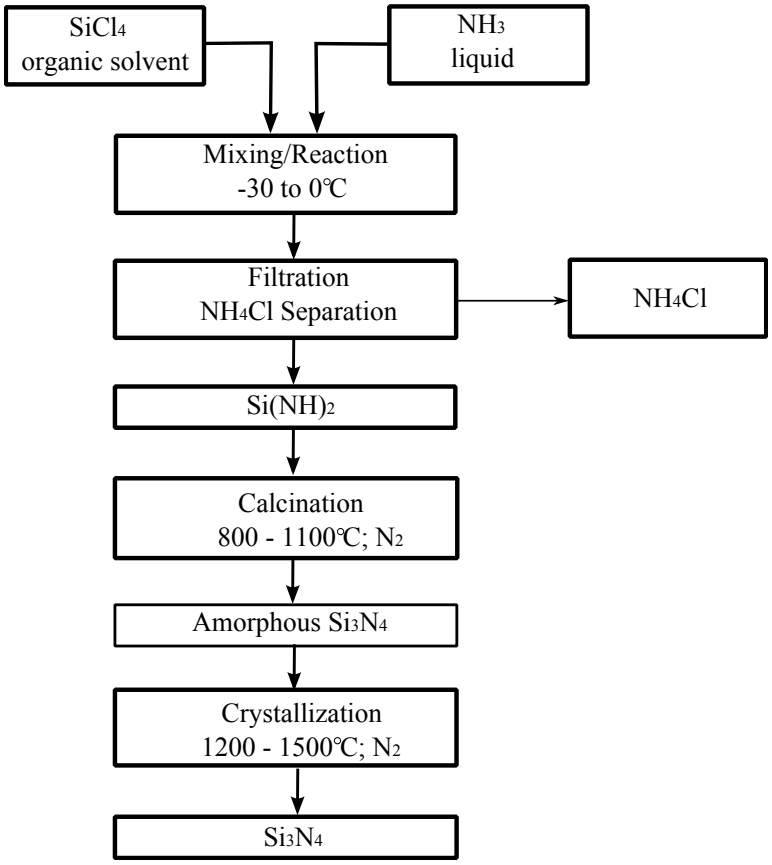

Figure 2.7: Process for Si_3N_4 synthesis by $SiCI_4/NH_3$ liquid-phase reaction. Reproduced from H. Lange et al. [11].

Pyrolysis of $Si(NH)_2$ below 1200 K forms amorphous Si_3N_4 powder. Heating at temperatures between 1200-1400°C favors the crystallization of α phase accompanied by particle coarsening. At temperatures above 1500°C, mainly β phase forms [11]. UBE Industries (Japan) produces Si_3N_4 powders commercially using this method [19].

Equations 2.2 and 2.3 still apply for the gas phase production of Si_3N_4 powders except that the staring materials are gases instead of liquids. SiH_4 can also be used as the starting gas instead of $SiCl_4$. The corrosive NH_4Cl by-product must be separated

from the system through either hot-gas filtration, extraction, or sublimation. Instead of using expensive pressure vessels, gas-phase reactions run at atmospheric pressure in heated tube reactors. Like liquid phase reactions, this method produces amorphous Si_3N_4 precursors which are to be crystallized in a step that follows. It is possible to produce extremely fine, spheroidal and amorphous particles using this method at temperatures between 300-1700°C [11].

2.1.5.3 Carbothermal Reduction and Nitridation of SiO_2

This method uses a mixture of SiO_2 and C powders to react at temperatures about 1500°C in a N_2 atmosphere. The flowchart regarding to this method is given in Figure 2.8. Because of the widespread availability of pure, fine and low cost SiO_2 and C powders, this method is an attractive alternative to direct nitridation of silicon in the production of Si_3N_4. This process is used to produce Si_3N_4 powders industrially by Toshiba (Japan) [11]. The overall reaction can be written as

$$3SiO_{2(s)} + 6C_{(s)} + 2N_{2(g)} \rightarrow Si_3N_{4(s)} + 6CO_{(g)} \tag{2.4}$$

however the formation mechanism is believed to be more complex, as follows [11]:

$$3SiO_{2(s)} + 3C_{(s)} \rightarrow 3SiO_{(g)} + 3CO_{(g)} \tag{2.4a}$$

$$3SiO_{(g)} + 3C_{(s)} + 2N_{2(g)} \rightarrow Si_3N_{4(s)} + 3CO_{(g)} \tag{2.4b}$$

Although the stoichiometric requirement of SiO_2:C ratio by weight is 1:0.4 for equation 2.4 to take place, a considerable amount of excess carbon is needed in practice. Usually SiO_2:C ratio of 1:2 to 1:10 by weight is used [11]. The excess carbon is used as oxygen sink to form CO gas and reduce the oxygen content on powder surface. After nitridation, any unreacted carbon has to be burnt out in an oxidizing atmosphere, which may cause some re-oxidation of Si_3N_4 surfaces [19].

CO formed during the course of reactions have to be removed from the system in order to prevent the reverse reaction. For this reason, CO partial pressure has to be kept low

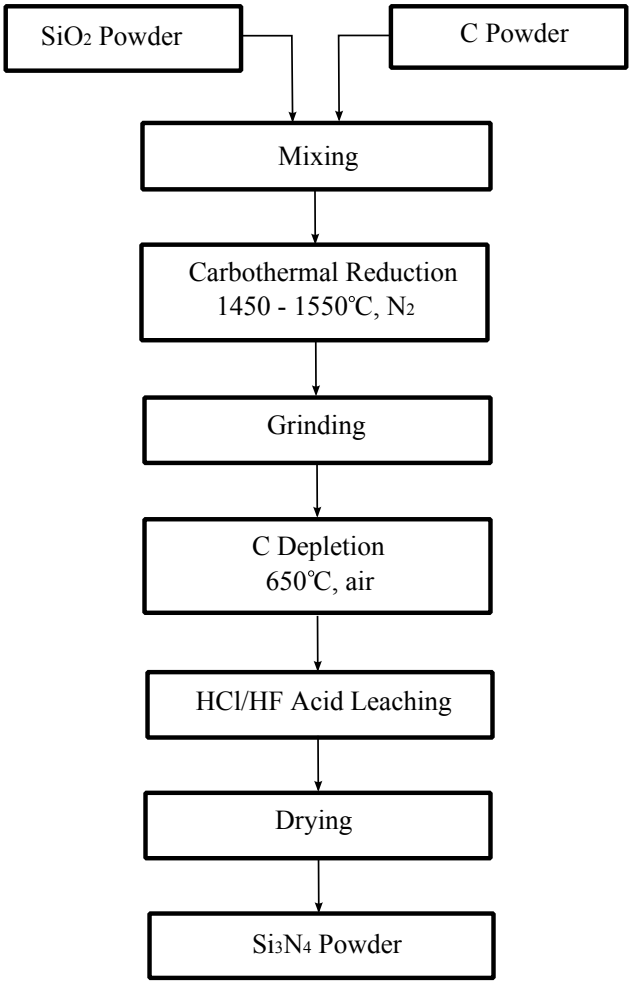

Figure 2.8: Process for Si_3N_4 synthesis by carbothermal reduction. Reproduced from H. Lange et al. [11].

by a flow of N_2. Si_3N_4 formation is enhanced at higher temperatures, however at temperatures above 1450°C, SiC also starts to form, which is practically inseparable from Si_3N_4. Particle size and morphology can be altered by adding spherical or whisker type Si_3N_4 to the starting mixture. Particle size of carbon also affects Si_3N_4 powder characteristics since it acts as a nucleation center in the Si_3N_4 formation. Fine and high specific surface area carbon powder enhances the formation of spherical Si_3N_4 particles, however coarse and low specific surface area carbon powders favor whisker Si_3N_4 [11].

This method produces strongly agglomerated mass of Si_3N_4 which requires milling, washing and classification. However, the impurities introduced at this communition stage may adversely affect the mechanical properties of the final product at elevated

temperatures [19]. Unreacted carbon and unreacted SiO_2 can be removed from the product by heating under air atmosphere around 600-800°C and HF leaching, respectively [11].

In this thesis study, this method has been utilized to produce silicon nitride. However, instead of using pure carbon and silica as the raw materials as described above, rice husks were used as the starting material, which are known to contain both C and SiO_2. In order to be able to point out the differences in the production of silicon nitride using commercial powders and rice husks as raw materials, a literature review on the production of Si_3N_4 by carbothermal reduction and nitridation of SiO_2 is given next. The details regarding the production of Si_3N_4 by carbothermal reduction and nitridation of rice husks are explained in a separate section, later in the thesis.

D. Mallette et al. studied the parameters affecting the carbothermal production of silicon nitride. They used commercial amorphous silica, activated carbon and alumina powders as raw materials. After mixing the powders for 3 h and pressing uniaxially to form a pellet, carbothermal reduction of silica was carried out in a resistance furnace under 0.6 L/min of N_2 flow. They have determined the optimum temperature for silicon nitride production between 1425 and 1450°C, stating the increasing formation of SiC above 1450°C. The optimum C:SiO_2 molar ratio for the production of α-Si_3N_4 was found to be 10, above which β-Si_3N_4 started to form in increasing amounts. They also detected the catalytic effect of silicon nitride powder seeding in the pellets in the conversion of silica to silicon nitride [21].

A. O. Kurt et al. used synthetic silica and carbon black to produce silicon nitride by carbothermal reduction of silica under nitrogen atmosphere in an alumina tube furnace. After mixing the raw materials and forming a pellet, it was placed into a graphite cylinder and introduced into the tubular furnace. Unlike other studies in the field, with the help of a servo-motor attached, they have managed to rotate the alumina tube at a certain speed to a certain direction throughout the nitridation process at 1450°C. They have concluded that the reaction rate was significantly increased by this method. Reaction was stated to be completed after 1.5 h at 1450°C with a product rich in α-Si_3N_4 phase and small amounts of β-Si_3N_4 present [22].

M. Ekelund et al. examined the effect of starting materials on the carbothermal reduction and nitridation of silica by mixing different types of C and SiO_2 powders and subjecting them to temperatures between 1410-1550°C at different nitrogen pressures. Highest conversion percentage of C and SiO_2 to Si_3N_4 was achieved by a mixture of very fine-grained carbon black with 115 m^2/g specific surface area and larger grain sized amorphous silica powder with 50 m^2/g specific surface area at 1470°C and 2.8 MPa nitrogen pressure. They have stated that the conversion to Si_3N_4 was highly sensitive to CO pressures, even low pressures could reversely affect the reaction [23].

A. Ortega et al. studied the kinetics of the carbothermal reduction of silica in nitrogen atmosphere to obtain silicon nitride. They kept the CO pressure in the tubular furnace at a constant value with the help of an integrated CO sensor. Since the reaction rate was proportional to CO pressure generated in the furnace, reaction rate was kept at a constant value for the entire process by controlling the CO pressure. They have concluded that the α-Si_3N_4 fraction of the product was not affected by the reaction rate, provided that the rate was kept at a constant value. Thus, it was stated that the reaction temperature did not affect the final composition of the product. Also a mechanism was proposed for the carbothermal production of silicon nitride. According to this mechanism, first the C and SiO_2 which is in intimate contact would react to form SiO gas at high temperature. Then, SiO would react with carbon and nitrogen at the surface of the C-SiO_2 aggregate to form a layer of Si_3N_4 on top of the aggregate. After the formation of the Si_3N_4 layer, N_2 gas would have to diffuse through this layer to get into contact with C and SiO gas to form a new Si_3N_4 layer. The diffusion process would get more difficult with time, reducing the reaction rate. Thus, the rate limiting step of the reaction was proposed as the diffusion of the reactant gas through the Si_3N_4 layer [24].

S. J. P. Durham et al. studied the effect of C:SiO_2 ratio, reaction temperature and precursor mixing on carbothermal synthesis of silicon nitride. Carbon black and fumed silica was used as raw materials and they were mixed by dry mixing and sol-gel route. Full conversion to silicon nitride was found to occur between 1500 to 1550°C. It was stated that to obtain full conversion, the C:SiO_2 ratio must be greater than the stoichiometric requirement of the overall reaction responsible for Si_3N_4 production. They concluded that the increase in the specific surface area of carbon resulted in an

increase in silicon nitride conversion, on the other hand higher specific surface area of SiO_2 did not affect the conversion. High flow rate of nitrogen was found to be an essential to prevent the formation of SiC and Si_2N_2O phases [25].

T. H. Liou et al. studied the parameters affecting the kinetics of carbothermal reduction and nitridation of silicon dioxide and carbon mixture. High purity commercial SiO_2 and C powders were mixed and then pelletized before nitridation experiments. Alumina reaction tube furnace was used for the reduction and nitridation process. By the investigation of outlet gas composition, only carbon monoxide and nitrogen was detected. It was detected that the products obtained were a mixture of unreacted carbon, unreacted silica and silicon nitride. No significant amount of SiC were detected. The authors found that the increase in nitrogen gas flow rate resulted in an increase in silica to silicon nitride conversion. However, the increase was negligible above gas flow of 400 ml/min. The increase in reaction rate due to gas flow rate was explained by both sweeping away of CO gas which is known to prevent Si_3N_4 formation and a better diffusion of N_2 into C-SiO_2 mixture. It was detected that the diameter of the C-SiO_2 pellet was not affecting the reaction when smaller than 5 mm. However, larger diameters were found to be decreasing the reaction rate, since the diffusion of nitrogen into pellet was hindered and most of the silicon nitride was formed on the surface. It was also found that the increase in pellet forming pressure had a slightly increasing effect on the reaction rate. However, pellet forming pressures above 10^5 kPa had no significant effect. The increase in reaction rate due to increasing pressure was explained by the increase of intimate contact of C and SiO_2 grains, which is essential for SiO gas formation which later reacts with C and N_2 to form Si_3N_4. Higher carbon content in the starting mixture was found to have a beneficial effect on the reaction rate. C:SiO_2 molar ratio above 4 was found to be affecting the reaction rate less. It was detected that smaller grain sizes of silicon dioxide increased the reaction rate. Carbon was also found to have a similar effect. Increasing the reaction temperature had a positive effect on the reaction rate. This was explained by the increasing SiO formation at higher temperatures. However, the authors have stated that at temperatures above 1500°C other byproducts would form [26].

S. C. Zhang et al. studied the carbothermal production of silicon nitride by silica at a N_2 flow rate of 275 ml/min at 1400°C in an alumina tube furnace. They have found

that with increasing reaction duration and C:SiO_2 molar ratio, the reaction rate was increased. They have stated that silicon nitride formation was greatly influenced by the specific surface area of carbon used. Increasing specific surface area of SiO_2 was also found to have a beneficial effect on the reaction rate. However, when the carbon specific surface area was 680 m^2/g, neither the effect of reaction duration nor specific surface area of SiO_2 was found to be as strong. The authors have also detected that there was no significant silicon nitride formation when pure SiO_2 was placed into a graphite boat without any carbon in the mixture and introduced into reaction tube. This result showed that the intimate mixing of C and SiO_2 was of great importance in the formation of Si_3N_4 [27].

Y. W. Cho et al. studied the effect of various parameters on the reaction rate of carbothermal production of silicon nitride by silica. They used mixtures of fine amorphous silica and fine carbon powders as raw material. A vertical tube furnace was used for experiments. An experiment at 1400°C for 10 h at 200 ml/min N_2 flow rate produced only α-Si_3N_4 with small amounts of crystalline SiO_2 (cristobalite). Some unreacted amorphous SiO_2 was also detected by the X-ray diffractogram. At 1450°C, α-Si_3N_4 formation was significantly increased and small amounts of β-Si_3N_4 was formed after 5 h. At 1500°C, SiC formation was detected even after 2 h. It was concluded that the increase in reaction temperature had a positive affect on reaction rate probably by increasing the formation rate of SiO gas. Both at 1450 and 1500°C, the amount of SiC formed decreased with increasing flow rate of N_2. No SiC was present at 1450°C when the flow rate was above 200 ml/min. Higher carbon content in the starting mixture was found to increase the reaction rate. At 1450°C, formation of SiC was detected when C:SiO_2 molar ratio was above 4 [28].

2.2 Rice Husk

2.2.1 Background

Rice is a major food source in most of the developing countries. Rice husks (RH), also called as rice hulls, as shown in Figure 2.9, serve as protective coverings of individual rice grains, which are removed during the production of consumable rice.

For every ton of consumable rice produced, around 200 kg of rice husk is obtained as a by-product. Considering the 700 million tonnes of annual worldwide production of 'rice paddy' (rice which has not been separated from its husk) in 2011 as announced by Food and Agricultural Organization, around 100 million tonnes of rice husk is produced in a year [29]. Other than some low value applications such as cattle feeding, land filling, building material, insulation material in farms and burning as fuel, the efforts in making use of rice husks are limited. This limitation is due to its tough, bulky and abrasive nature, low nutritional properties, resistance to degradation and high ash content. For these reasons, rice husks are basically left as agricultural waste products or burnt, which causes serious storage and disposal problems as well as environmental pollution [30].

Figure 2.9: Rice husks.

In the past few decades, rice husks gained popularity for researchers because of its high SiO_2 content, which have significantly widened the usage of rice husks. At present, rice husks can be used as raw materials for the production of silicon, silica, silicon carbide, silicon nitride, silicon tetrachloride, zeolite and more. Rice production of Turkey is steadily increasing for the last decade and reported in 2011 as 540000 tonnes by the Rice Millers Association which corresponds to annual rice husk production of around 110000 tonnes [31]. Using them as raw materials for the production of

these silicon based materials would cause economical benefits to producers and thus to national economy of Turkey.

2.2.2 Structure and Components

Rice husks are composed of organic and inorganic parts. The organic part, which is around 72% of the husk by weight is mainly composed of lignin, cellulose, pentosans and other organic matters. Table 2.5 represents the detailed information on the organic constituents of the rice husk, as analyzed by Sharma et al. [32]. The inorganic part, which forms the ash upon burning, is mainly composed of SiO_2 (87 to 97 wt%) and some impurity metal-oxides such as CaO, Fe_2O_3, MgO, Al_2O_3 [33, 34].

The exact chemical composition of rice husks vary from region to region and sample to sample. The reasons for the compositional variation could be climatic and geographical conditions, crop year, soil chemistry, chemical fertilizers used and type of paddy. In an extensive literature review done by Govindarao [35], all reported data on the chemical analysis of rice husks from different regions of the world were considered and it was calculated that 20 wt% ash, 22 wt% lignin, 38 wt% cellulose, 18 wt% pentosans and 2 wt% other organic matter were present in rice husks on a dry basis as an average [33].

Table 2.5: Organic Constituents of Rice Husk. Reproduced from Sharma et al. [32].

Constituent	**Amount present in rice husk (wt%)**
α-cellulose	43.30
Lignin	22.00
D-xylose	17.52
l-arabinose	6.53
Methylglucuronic acid	3.27
D-galactose	2.37
Total	94.99

It is obvious that the potential of rice husks, for them to be used as raw materials for the production of a wide variety of silicon based materials is originated from its high SiO_2 content. Silicon, in a soluble form, enters the rice plant through the root

as a silicate or molosilicic acid and moves to the outer layers of the plant. There, it becomes concentrated by evaporation and polymerization to form a cellulose silica membrane. Silicon is present in inner and outer epidermal regions of rice husks, as hydrated amorphous form of SiO_2 [3].

Figure 2.10: Close-up view showing different surfaces of rice husks.

Figure 2.10 shows a close-up view of rice husks. As it is seen, they have a boat-like shape with a fibrous structure. It is observed from the figure that the inner concave surfaces of boat-like structures are smooth, on the other hand outer convex surfaces tend to have a longitudinal pattern with hundreds of small globules and small hair-like structures. Cellulose and lignin are concentrated on the concave surfaces and silica is concentrated on the convex surfaces [36]. Upon optical microscopy observations, the globules on the outer layers were found to be small protuberances, formed in a regular pattern. Although silica in the rice husk is present all over the surface, it is mainly concentrated on these small protuberances [33].

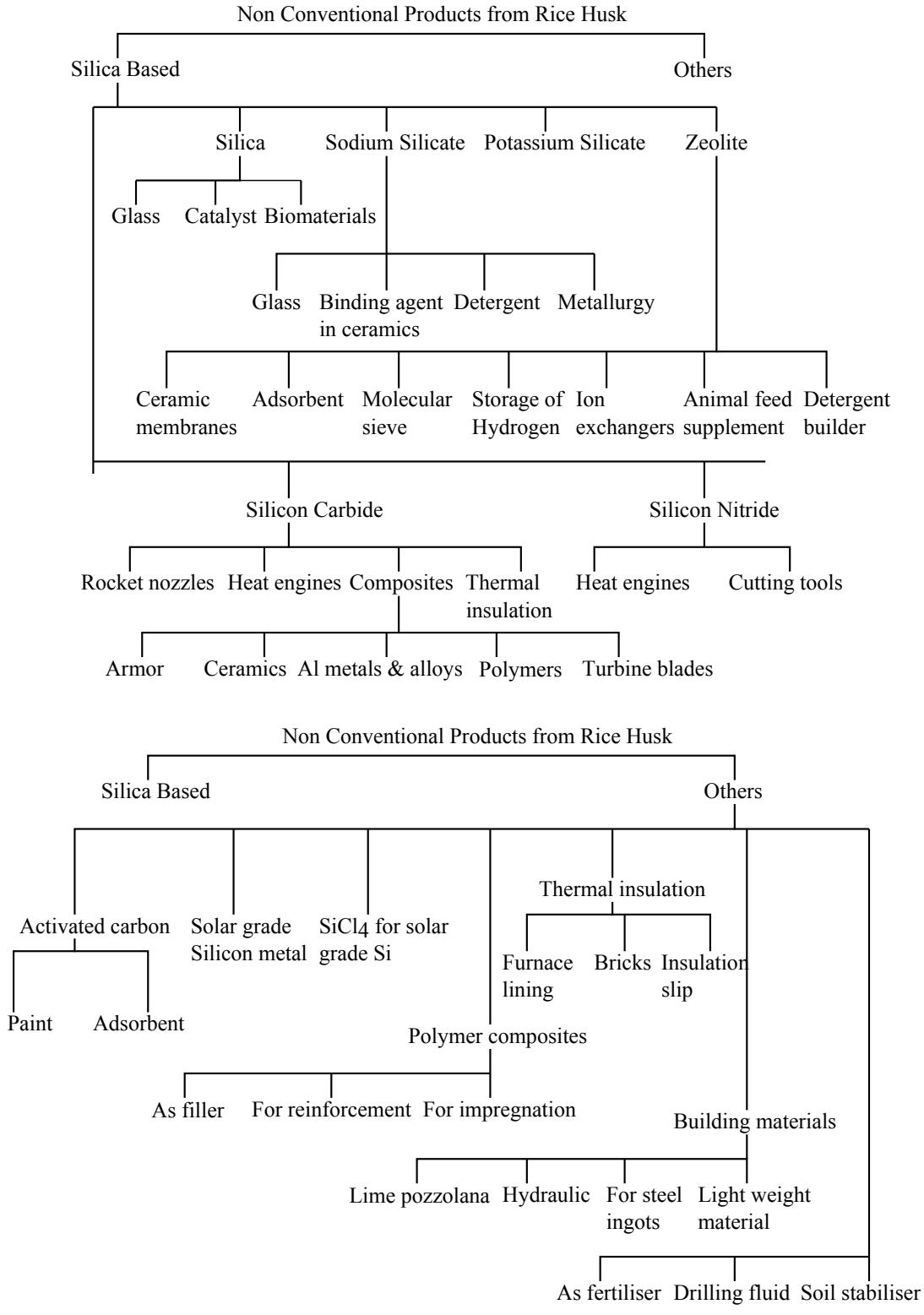

Figure 2.11: Scheme of non-conventional products from rice husks and applications based on silica and others than silica [38].

2.2.3 Applications

Rice husks can be consumed directly without any treatments for low value applications. These include fuels, cattle feeding, land filling and insulation materials. However, rice husks are known to have a low calorific value of around 3585 kcal/kg and high ash content to cause environmental problems which makes it less desirable as a fuel [37]. Also rice husks being fibrous materials, can prove to be fatal for the cattle feeding. Application of rice husk or its ash in land filling is also an environmentally hazardous route of disposing the waste [30].

Rice husks are now mainly considered as raw materials for the production of non-conventional materials. Rice husks are used as raw materials for the production of a variety of inorganic materials. The non-conventional products produced by rice husks are summarized in Figure 2.11.

2.3 Carbothermal Reduction and Nitridation of Rice Husks

Although the production of silicon nitride by carbothermal reduction and nitridation of silica was explained in detail in its own section, there are some major differences when the starting material is changed as rice husks instead of silica. It was stated earlier that rice husk contain both silica and carbon, thus it is a possible candidate for the carbothermal production of silicon nitride. One major advantage of using rice husks is that, silica and carbon present in the husk is already in intimate contact and homogeneously mixed with high specific surface area [3]. This would affect the reaction kinetics in a positive manner and cause the reaction to occur more easily than the conventional mechanical mixing of commercial silica and carbon powders. On the other hand, rice husks usually contain high amounts of impurities, which ends up with affecting the product properties and/or produced phases.

In order to use the rice husks as the raw materials for carbothermal production of silicon nitride, first the organic matter of rice husks should be eliminated while keeping the carbon non-oxidized. Thus, generally an extra pyrolysis step (heating of rice husks to 600-900°C in an inert atmosphere) is introduced to the process when rice

husks are used.

The final composition of the reaction products is affected by various parameters. Among them C:SiO_2 ratio, gas flow rate, reacting gas composition, reaction temperature, reaction duration, heating rate, addition of catalysts and particle size of starting mixture are studied extensively in the literature. A literature review regarding the use of rice husks in carbothermal production of silicon nitride is given next.

The patent for the production of silicon nitride from rice husks was first claimed by I. B. Cutler, in 1974. In his work, he claimed that it was possible to produce silicon nitride from rice husks by subjecting the husks to coking (pyrolysis), which is followed by placing the coked product within an enclosure with oxygen free atmosphere at temperatures between 1100-1350°C, under nitrogen flow. It was stated that the rate of the carbothermal reduction and nitridation reaction was controlled by the partial pressure of CO formed by the reaction. He claimed that increasing the nitrogen gas flow rate would increase the reaction rate since the CO gas, produced by the reaction, would be swept away from the system, therefore decreasing its partial pressure, which was shown to be increasing the rate of reaction. He also found that the addition of iron and/or iron-oxide (Fe_2O_3) into coked product before nitridation had a catalytic effect on the reaction, increasing its rate. He concluded that at temperatures above 1400°C, SiC was produced instead of Si_3N_4. He recommended that the temperature should be kept at maximum at 1350°C [5].

T. H. Liou et al. studied the leaching parameters and pyrolysis kinetics of rice husk. They found that it was possible to remove the impurities in rice husk effectively with various acid leaching methods. Best purification was obtained by leaching rice husks with 3 N HCl solution for 1 h at 100°C. It was reported that the pyrolysis of rice husks took place in two distinct stages and a pyrolysis temperature above 700°C was needed for full conversion of organic matter into carbon. They proposed a pyrolysis mechanism of de-polymerization of organic matter into gaseous volatiles and intermediates in the first stage up to 600 K and then further decomposition of these intermediates into other gases and char in the second stage up to 800 K [39].

N. Kuşkonmaz et al. studied the effect of reaction temperature and duration on the product composition. They pyrolyzed the rice husks at 700°C for 1 h without leach-

ing. Pyrolyzed rice husks were ground and formed into pellets. They found the optimum temperature for Si_3N_4 production as 1400°C. SiC was detected at 1450°C among Si_3N_4. At 1500°C no Si_3N_4 was detected, only phase present was SiC. Si_3N_4 content was found to be increasing up to 1400°C with increasing reaction duration. At 1450°C, SiC content was found to be increasing with increasing reaction duration. They also stated that the nitride product was in the form of α-Si_3N_4 with whisker morphology [14].

V. Pavarajarn et al. studied the carbothermal production of silicon nitride by rice husks at temperatures between 1400-1470°C for 3-10 h. They observed three different Si_3N_4 products with different morphologies. These were listed as; silicon nitride powder mixed with residual pyrolyzed rice husk, a layer of whiskers on top of pyrolyzed rice husks and long fibers formed at the edges of the crucible. Powder and whiskers were found to be α-Si_3N_4, on the other hand small amount of β-Si_3N_4 was also detected within the fibrous material. It was observed that both of the fiber and whisker Si_3N_4 was formed by vapor-solid mechanism, which required SiO vapor as a key intermediate. Silicon nitride powder formed within the pyrolyzed rice husk was proposed to be produced by solid-state reaction. It was also reported that the whisker and fiber content was increased with increasing reaction duration and temperature [16].

C. Real et al. studied the synthesis of silicon nitride by carbothermal reduction and nitridation of rice husks using constant rate thermal analysis. They first pyrolyzed the rice husks at 600°C for 3 h. A reactive gas mixture containing 95% N_2 and 5% H_2 were used during the nitridation experiments. They used a sensor to control the CO concentration at a constant level which was predefined by the user. Temperature of the sample was automatically adjusted to reach the desired CO level. It was reported that as CO concentration was increased Si_3N_4 content in the product was also increased. Higher CO concentration favored the production of α phase on the other hand lower CO concentration favored β phase. Products having 83-98% of α-Si_3N_4 was produced at various CO partial pressures. They concluded that it was possible to produce a product with pre-determined phase composition, morphology and particle size by adjusting the CO composition in the vicinity of the sample [17].

I. A. Rahman studied the effect of introduction of V_2O_5 as a catalyst in the carbothermal production of silicon nitride from rice husks. Rice husks were pyrolyzed at 800°C for 1 h under argon. Pyrolyzed rice husks were ball-milled to provide the starting material for nitridation. Nitridation took place at 1430°C, under flowing nitrogen gas for 2-6 h. It was found that the presence of V_2O_5 favored the production of β-Si_3N_4 when C:SiO_2 ratio was above the stoichiometric requirement of equation 2.4. He also concluded that Si_2ON_2 was the predominant phase when C and SiO_2 content in the rice husk was decreased to the stoichiometric ratio [40].

T. H. Liou et al. studied the parameters affecting the nitridation of pyrolyzed rice husks. They prepared the starting material for nitridation experiments by acid leaching and pyrolysis of rice husks. Rice husks were pyrolyzed at 900°C for 1 h and then formed into pellets. Nitridation temperatures between 1200-1450°C were investigated. They found that silica to silicon nitride conversion was increased with increasing nitrogen flow rate up to 200 mL/min. A further increase in flow rate did not affect the conversion. They stated that when pellets with diameters larger than 7 mm were used, nitrogen could not easily diffuse into the pellets, thus the reaction only occured on the surface layer of the sample which caused a decrease in the conversion. It was also found that the pellet-forming pressure did not affect the nitridation reaction. They also stated that initial grain sizes of pyrolyzed rice husk samples did not have an effect on nitridation. This was explained by the naturally high specific surface area and intimate contact between C and SiO_2 in the rice husk. It was concluded that the silica to silicon nitride conversion increases with increasing temperature. They also found that the nitridation rate of rice husk was significantly faster than that of pure C/SiO_2 commercial mixtures [18].

I. A. Rahman, in another study, investigated the effect of digestion of rice husks by various concentrations of HNO_3, on the carbothermal production of Si_3N_4. Rice husks were digested at 60°C for up to 7 h at varying nitric acid concentrations between 10-14 M. Pyrolysis temperature of the digested husk was chosen as 800°C to a constant weight under argon flow. Weight loss after digestion was detected as 50-60%. C/SiO_2 molar ratio was calculated to be less than the stoichiometric requirement for the carbothermal reduction and nitridation reaction (equation 2.4) for 14 M acid solution. The digestion in 12 M solution for 3-6 h, however, resulted in a ratio of

2, which was the exact requirement. Using this digested rice husk for pyrolysis and subsequent nitridation at 1430°C for 6 h, sub-micrometer sized α-Si_3N_4 powder with equiaxed morphology was successfully produced [41].

I. A. Rahman et al., in a further study, examined the parameters affecting the morphology of silicon nitride, produced by carbothermal reduction and nitridation of rice husks. After water washing process, rice husks were pyrolyzed at 700°C for about 0.5 h under argon flow. The pyrolysis product was then ground and leached in acid solution in order to obtain the starting powder for nitridation. Nitridation experiments took place at temperatures between 1260-1500°C for up to about 8 h. They used a gas mixture of 5 % hydrogen and 95 % nitrogen during the experiments. They concluded that silicon nitride with high purity and mostly α phase could be obtained. Hydrogen in the gas mixture was found to be speeding up the reaction. They stated that, sub-micrometer sized, equiaxed α-Si_3N_4 grains were favored by the addition of pre-formed Si_3N_4 powder into pyrolyzed rice husk powder before nitridation. It was found that the morphology of silicon nitride produced was also affected by the particle size of starting powder. Particle dimensions smaller than 53 μm favored hexagonal symmetry in the silicon nitride crystals, on the other hand greater particle sizes favored a whiskery formation. Addition of iron oxide and nickel oxide as catalysts were found to cause SiC production during the reaction, even at temperatures as low as 1300°C [42].

An important fact to point out about using the rice husks as raw materials for the carbothermal reduction and nitridation process is about the purity of the product. It is known that this method usually produces impure silicon nitride, which is accompanied by silicon carbide [3]. This can be a result of both the impurities (alkali metals other than SiO_2) in rice husks or the high carbon to silica ratio which causes excess carbon to result in silicon carbide during nitridation [3]. Thus, this method is also a possible candidate for the production of the popular Si_3N_4/SiC composite powder. Brief information regarding the performance and properties of Si_3N_4/SiC composites is given in the next section.

2.4 Silicon Nitride/Silicon Carbide Composite

Both silicon nitride and silicon carbide are important structural ceramics which are commonly known for their good combination of thermal and mechanical properties. Thus, most of the application areas of silicon carbide and silicon nitride are common such as bearings, cutting tools, refractories, wear and corrosion resistant applications. Silicon carbide materials have extremely high hardness (harder than silicon nitride) and thus good wear resistance. However, the low fracture toughness of silicon carbide ceramics which usually does not exceed about 3.5 $MPa{\cdot}m^{1/2}$ is a major disadvantage compared to silicon nitride ceramics [43]. On the other hand, silicon nitride has a lower resistance to oxidation at high temperatures. Silicon carbide is also listed as a semiconductor material which has a much lower electrical resistance compared to silicon nitride [38]. Some important properties of silicon carbide ceramics are given in Table 2.6 and a comparison of mechanical properties of commercially available silicon nitride and silicon carbide based ceramics is given in Table 2.7. It is seen from Table 2.7 that the main disadvantage of SiC based ceramics compared to Si_3N_4 based ceramics is their low fracture toughness values.

Table 2.6: Physical Properties of Silicon Carbide. Reproduced from Y. Yücel [38].

Property	**Value**
Decomposition temperature	3100 K
Melting temperature	2573 - 2773 K
Density	3.22 g/cm^3
Poisson's ratio	0.19
Thermal expansion coefficient (273 - 1273 K)	4.7 x $10^{-6\circ}C^{-1}$
Electrical resistance	$10^{-2}\Omega m$
Hardness (Knoop)	2500 kg/mm^2
Elastic modulus	414 GPa
Modulus of rupture (sintered)	450 - 520 MPa
Thermal conductivity	90 $Wm^{-1}K^{-1}$

To improve the properties, reliability and lifetime of monolithic ceramic materials, it is reported that the introduction of a second ceramic material to produce ceramic-based nano/micro-composites possess a great opportunity, even at high temperatures [44]. In the case of Si_3N_4 based ceramic materials, with the introduction of SiC

particles, Si_3N_4/SiC nano/micro-composites have been developed and studied in the last few decades, to improve its performance and properties [45].

Table 2.7: Comparison of Mechanical Properties of Commercially Available Si_3N_4/SiC-based Ceramics. Reproduced from P. Klimczyk [43].

	Si_3N_4 based ceramics			**SiC based ceramics**		
	StarCeram N 7000 H.C. Starck	**StarCeram N 8000 H.C. Starck**	**EKatherm Ceradyne**	**StarCeram S H.C. Starck**	**Hexaloy SA St. Gobain**	**Ceralloy 146-S5 Ceradyne**
E	290	310	310	395	410	430
HV	1500	1520	1450	2500	2800	2600
K_{1c}	6.7	6	7	3	4.6	4.3

E: Young's modulus (GPa), HV: Hardness Vickers, K_{1c}: Fracture toughness (MPa·$m^{1/2}$)

Various production methods are reported for the synthesis of Si_3N_4/SiC composites. Several of these methods are listed as; crystallization and hot pressing of amorphous Si-N-C sub-micrometer size powders or mechanical mixtures of sub-micrometer size crystalline SiC and Si_3N_4 powders, gas-pressure sintering of SiC powders with in-situ reaction pyrolysis of carbon-coated Si_3N_4 powders and reaction-bonding and gas-pressure sintering of a mixture of Si and SiC powders in a flow of N_2/H_2 gas mixture [46].

M. Balog et al. studied the effect of SiC nano-particle content in the Si_3N_4 matrix, on the hardness and fracture toughness of the composite. The composite was synthesized from crystalline Si_3N_4 powder doped with Si-N-C amorphous precursor and yttria as the sintering aid. They found that, as SiC content was increased, both nano and macro-hardness of the Si_3N_4/SiC composite was also increased. It was suggested that SiC nano-inclusions increased the hardness by the presence of harder SiC particles in the softer Si_3N_4 matrix. It was also reported that, with the addition of 8 wt% SiC, the fracture toughness of the composite reached its maximum of 5.8 MPa·$m^{1/2}$ [47].

M. Herrmann et al. studied the oxidation resistance of Si_3N_4/SiC composites at high temperatures, compared to monolithic Si_3N_4 ceramics. Materials were tested at 1500°C for up to 1000 h. The composites were prepared by mixing of Si_3N_4 and SiC powders and sintering additives in a ball mill and subsequent hot pressing. They reported that the residual strength after oxidation experiments was twice as high for the best nano/micro-composite materials than for monolithic Si_3N_4 materials. The

lifetime of the composites were also found to be longer than the pure materials. They concluded that this behavior was due to a change in oxidation and damage mechanism at high temperatures. A layer of Si_2N_2O (silicon oxynitride) was reported to form on the composite material at the beginning of the oxidation process, which prevents the pit formation greatly, therefore decreasing the internal stresses and increasing the lifetime of the material [48].

J. F. Yang et al. studied the mechanical properties of Si_3N_4/SiC composites with various SiC content. The composites were prepared by mixing of α-Si_3N_4/SiC powders and sintering additives in a ball mill and a subsequent cold isostatic pressing and sintering. They stated that, as the SiC content was increased, the fracture toughness of the composite was decreased. On the other hand, up to 20 vol.% addition of fine SiC particles, the flexural strength of the composite was found to be increased. Maximum flexural strength attained was more than 1 GPa. However, SiC additions beyond 20 vol.% resulted in a drastic decrease in the flexural strength of the material. It was reported that the increase in the flexural strength and the decrease in the fracture toughness was due to the refined microstructure. The drastic decrease of flexural strength at large amounts of SiC additions was explained by the flaws associated with SiC agglomerates [49].

P. Sajgalik et al. studied the mechanical properties of Si_3N_4/SiC composites produced by various SiC content. The composites were prepared from a mixture of α-Si_3N_4, amorphous Si-N-C, and sintering additives of Y_2O_3 and Al_2O_3. The micro/nano-composite produced by the addition of 10 wt% SiC was found to have a high room temperature bending strength of 1.2 GPa and a moderate fracture toughness of about 7 MPa·$m^{1/2}$. It was also found that the composite produced by the addition of 20 wt% SiC was able to keep 60% of its bending strength up to 1300°C. Creep resistance of this composite was found to be about 1 magnitude greater than the pure material between 1200 - 1400°C [45].

Piotr Klimczyk prepared micro, sub-micro and nano-structured Si_3N_4/SiC composites by High Pressure-High Temperature (HPHT) sintering and investigated their mechanical properties in his study. He stated that the composites obtained from sub-micron powders provided the best mechanical properties compared to nano and micro com-

posites. He reported a Young's modulus of 377 GPa, Vickers hardness of 3000 HV and a relatively moderate fracture toughness of 4.9 MPa·$m^{1/2}$ for Si_3N_4–70 vol.% SiC composite sintered at 1880°C. He also reported that a lower sintering temperature of 1690°C produced a composite with higher fracture toughness, but lower hardness and Young's modulus. It was concluded that the sub-micron Si_3N_4–70 vol.% SiC composites had better combination of mechanical properties than that of commercially available Si_3N_4 and SiC materials [43].

L. Hegedusova et al. studied the room temperature strength and high temperature creep behavior of carbon-derived Si_3N_4/SiC micro/nano-composites. Amount of SiC in the sintered composite was detected as 5 vol.% with some sintering additives and silicon oxynitride present. They found that the room temperature bending strength of the composite was between 675 to 832 MPa. They also reported that the composite material had higher creep resistance compared to monolithic silicon nitride. It was concluded that the higher creep resistance was a result of the improved viscosity of the intergranular phase, which caused silicon nitride grains to be locked by the SiC nano-particles [44].

Koichi Niihara studied the mechanical behaviors of a wide variety of ceramic nano-composite materials. He found that, for Si_3N_4/SiC nano-composites prepared by liquid-phase sintering, the fracture toughness was increased with the increasing content of SiC. A maximum fracture toughness of 6.7 MPa·$m^{1/2}$ was achieved with 25 vol.% SiC content, which was higher than that of monolithic Si_3N_4. He also stated that, fracture strength was improved by nano-sized SiC dispersions. Maximum fracture strength was detected at 25 vol.% SiC as 1.5 GPa. The increase in fracture toughness and fracture strength was attributed to the promotion of the growth of fine and uniformly elongated Si_3N_4 grains by nano-size SiC dispersions. It was also stated that the fracture strength of the composite with 32 vol.% SiC at 1400°C was over 1 GPa and about 900 MPa at 1500 °C. This has been found to be a quite important discovery since monolithic silicon nitride materials show a drastic decrease in their fracture strength at above 1200°C due to grain boundary sliding and/or softening of grain boundary impurity phases. The reason of the high strength at high temperatures was explained by the dispersion of nano-size SiC particles at the grain boundaries which prevents grain boundary sliding [50].

A. S. Saygıner studied the effect of gas flow rate, reaction duration and temperature on the production of Si_3N_4/SiC composite powders by carbothermal reduction and nitridation of rice husks. He found that SiC formation was favored with decreasing flow rate of nitrogen. It was stated that the optimum reaction duration was determined to be 3 h at 1450°C. SiC formation was found to be increasing with increasing reaction temperature and time [51].

CHAPTER 3

EXPERIMENTAL PROCEDURE AND SET-UP

The aim of this study was to investigate the optimum conditions for the carbothermal reduction and nitridation of carbon-silica mixtures obtained from Turkish rice husks to produce silicon nitride. For this purpose, rice husks originating from the Black Sea region (Bafra) of Turkey were acquired as the raw material. They were first sieved, water washed and acid leached to get rid of their impurities in a pretreatment step. Then, to obtain the starting powder for the carbothermal reduction and nitridation experiments, the purified rice husks were pyrolyzed and ground to a certain size. The flowchart of the process is given in Figure 3.1. The pretreatment and pyrolysis steps are explained in detail in the following sections.

3.1 Pretreatment of Rice Husks and Characterization

3.1.1 Purification of Rice Husks

Rice husks, obtained from the Black Sea region (Bafra) of Turkey, were containing high amounts of solid, visible impurities such as soil, dirt and stone pieces. Thus, they were first subjected to coarse sieving to a size of below 4.75 mm to separate the larger stone and soil pieces present with the husks. After the coarse sieving, 40 g of rice husks were washed with 2 L of tap water in a beaker for 5 minutes by magnetic stirring. The dirty water was decanted from the beaker after the washing was complete. This process was repeated for four times until the decanted water turned colorless. Water washed rice husks were dried in a drying oven at 105°C. Approximately 1 kg of water washed and dried rice husks were obtained as a stock

by repeating this procedure.

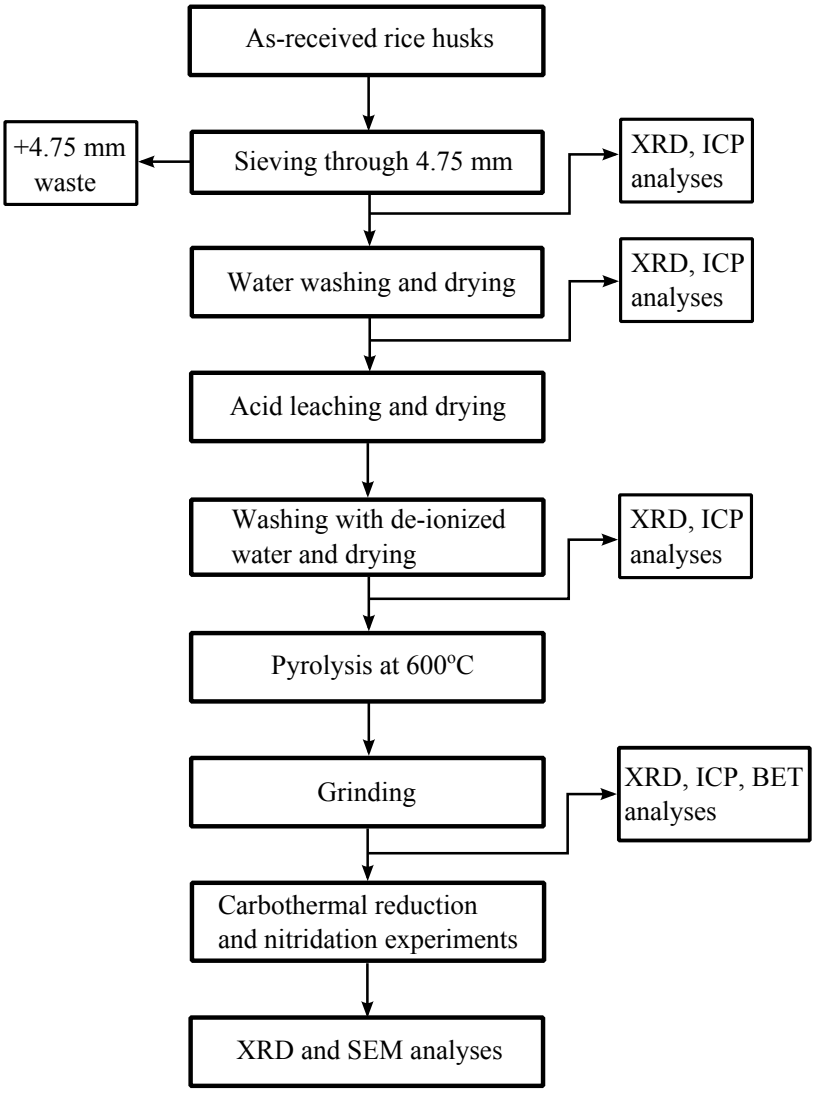

Figure 3.1: Flowchart followed for the production of silicon nitride through carbothermal reduction and nitridation of rice husks.

To remove the chemical impurities in rice husks, such as the metal-oxides MgO, Al_2O_3 and Fe_2O_3, an acid leaching method was used as a further purification process. 40 g of water washed rice husks were leached in a 2 N hydrochloric acid (HCl) solution at 55°C for 2 h in a beaker with magnetic stirring. To remove the acid residue on rice husks after leaching, tap water washing was done for 5 minutes. The contaminated water was decanted from the beaker after the washing. This process was repeated for three times, by checking the pH of the decanted solution after each step, until it became the same with the pH of the tap water. The process was continued

until all of the stock was subjected to leaching.

As a final step, the acid leached rice husks were washed with de-ionized water to get rid of the possible impurities introduced on the husks by tap water and dried at 105°C. A stock of approximately 750 g of clean rice husks were obtained by this method and used in the rest of the study.

3.1.2 Pyrolysis of Acid Leached Rice Husks

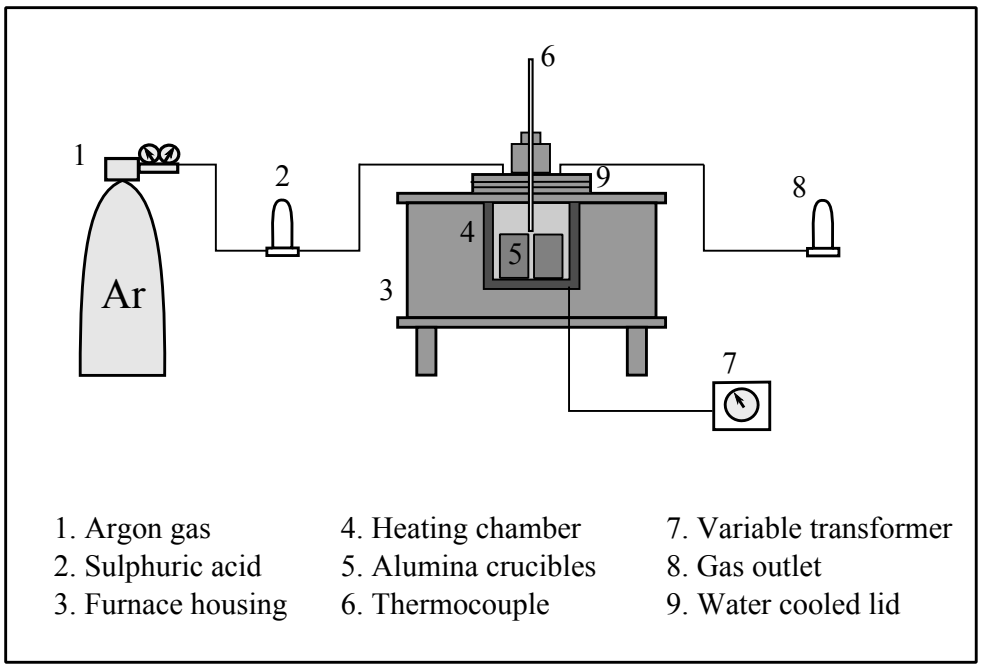

Figure 3.2: Schematic representation of the pyrolysis system.

In order to obtain the C-SiO_2 mixture which served as the starting material for the carbothermal reduction and nitridation experiments, the acid leached rice husks were pyrolyzed. In this process, by heating the rice husks to a high temperature in an inert atmosphere, the organic constituents of the rice husks were degraded while the carbon and inorganic matter were not oxidized, therefore the C-SiO_2 mixture was obtained.

An electrical furnace with a capacity of 50 g of rice husk was used for this purpose. The acid leached rice husks were put into cylindrical alumina crucibles and placed into the heating chamber of the furnace. The cylindrical heating chamber had a radius of 70 mm and a height of 140 mm. Schematic drawing of the pyrolysis system is given in Figure 3.2.

The pyrolysis process was conducted under argon atmosphere at 600°C. The furnace was switched off when it reached to the desired temperature and allowed to cool down to room temperature with a continuous flow of argon while the rice husks were still in the chamber. The process was repeated until all of the acid leached rice husk stock was consumed. About 300 g of pyrolyzed rice husk (PRH) was obtained by this method, as a stock.

3.2 Experimental Set-Up

For the carbothermal reduction and nitridation experiments conducted with the ground PRH powders, a horizontal tube furnace with a 1000 mm long alumina tube was used. Schematic drawing of the furnace is given in Figure 3.3. The inner and outer diameters of the alumina tube were 50 and 60 mm, respectively. Both ends of the tube were enclosed by silicon stopples at the edges. Six SiC elements were installed in the furnace for heating purposes. To protect the stopples from the heat generated by the hot-zone of the furnace, two radiation shields were placed into the tube 150 mm away from each of the stopples. At the ends of the tube, water cooling was employed by copper windings. The hot-zone of the furnace was determined to be 50 mm long at the middle zone of the tube by preliminary experiments.

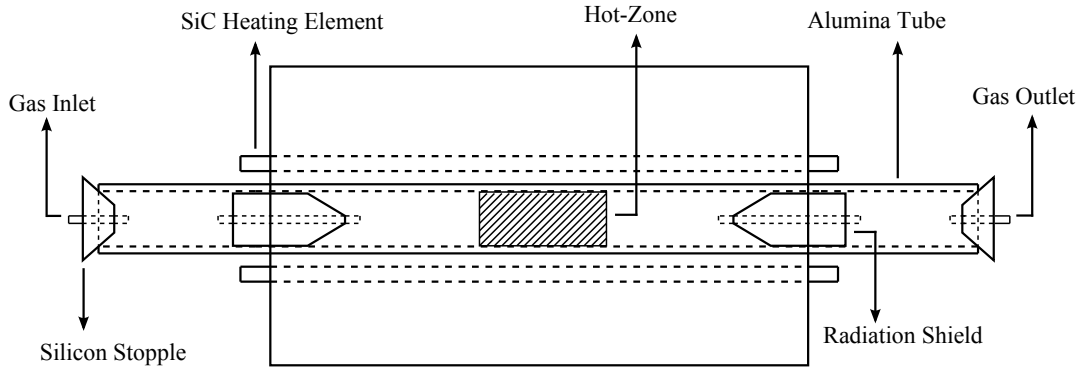

Figure 3.3: Schematic representation of the tubular furnace.

Schematic drawing of the experimental set-up for the carbothermal reduction and nitridation experiments is given in Figure 3.4. Nitrogen flow into the tube was adjusted by a flowmeter to a desired gas flow rate and overflow gas was allowed to exit the system through the overflow exit. The temperature and heating rate of the furnace

were controlled by a digital temperature control device (Elimko E-210). The PRH samples were introduced into the furnace by alumina crucibles with dimensions of 50 x 25 x 20 mm (length x width x depth).

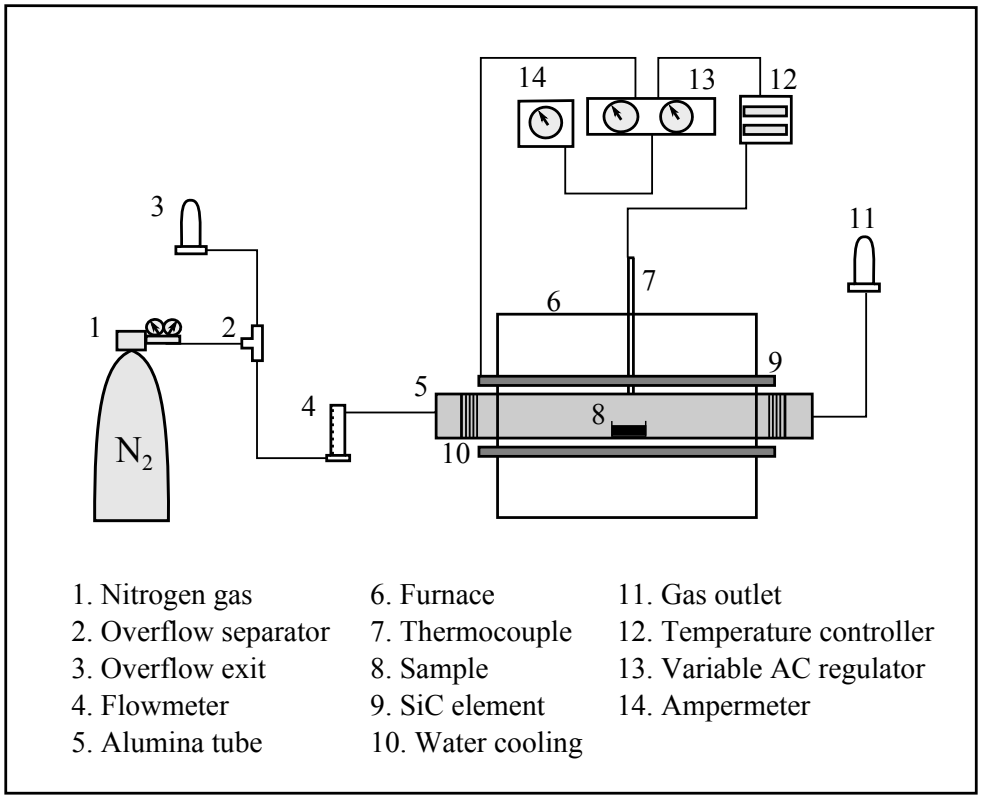

Figure 3.4: Schematic representation of the experimental set-up.

3.3 Experimental Procedure

The carbothermal reduction and nitridation experiments of acid leached and pyrolyzed rice husks were carried out in the following fashion. First, PRH samples were ground to less than 100 μm in size by hand grinding in a ceramic mortar. Then, 3 g of PRH samples were weighed and placed into the alumina crucibles. A flat surface of PRH was achieved by carefully shaking and tapping the crucibles to avoid dusting. After that, the alumina crucibles were introduced into the hot-zone of the tubular furnace at room temperature. Two small pieces of graphite were placed into the alumina tube in front of the radiation shield near the gas inlet, to act as an oxygen sink. High purity N_2 gas, containing 5 vpm O_2 and 3 vpm H_2O was used in the experiments. Gas flow rate was adjusted to 5 L/h between room temperature to 1200°C and increased to the

desired flow rate from 1200°C to the desired temperature. Heating rate was adjusted as 2.5°C/min between 0-200°C, 4.2°C/min between 200-700 °C, 4.5°C/min between 700°C to the reaction temperature. After the experiments, the sample was allowed to cool down to the room temperature in the furnace, with a continuous 5 L/h flow of nitrogen.

First set of experiments were conducted to determine the optimum temperature for Si_3N_4 production. Temperatures between 1300-1500°C were investigated for 1 h at a N_2 flow rate of 50 L/h on 3 g PRH samples.

In the second set of experiments, the effect of reaction duration between 1-24 h on the reaction products at the decided temperature and a N_2 flow rate of 50 L/h on 3 g PRH samples was studied.

A third set of experiments were conducted to investigate the effect of N_2 flow rate on the reaction products while keeping other parameters constant. Gas flow rates between 10-50 L/h were studied.

Finally, a fourth set of experiments were done to examine the effect of starting PRH amount on the products. PRH amounts changing between 0.25-3 g were introduced into the furnace while keeping other parameters unchanged.

The products obtained by the experiments were investigated by a Rigaku DMAX 2200 X-ray diffractometer with Cu-Kα radiation at a scanning rate of 2°/min to identify the phases and composition. The reaction products were also analyzed by Nova NanoSEM 430 and Jeol JSM 6400 scanning electron microscopes in order to examine the morphology of the products.

CHAPTER 4

RESULTS AND DISCUSSION

4.1 Characterization of Rice Husks

4.1.1 Physical Characterization

Rice husks were yellow in color with a boat-like shape as previously shown in Figures 2.9 and 2.10. The color turned from dull yellow to bright yellow as the purification process continues from water washing to acid leaching step. A simple sketch of a rice husk is given in Figure 4.1.

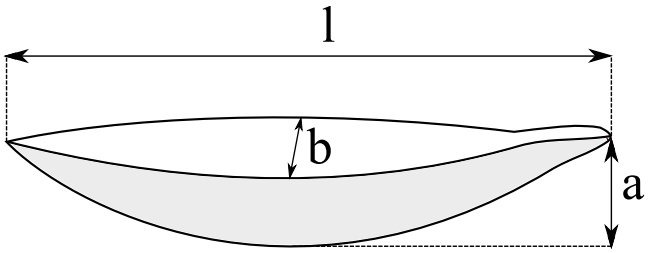

Figure 4.1: Sketch of a rice husk.

After the pyrolysis, the rice husks got thinner and transformed into a more needle-like shape as shown in Figure 4.2. PRHs were black in color due to their high carbon content. It was observed that most of the PRHs were preserving their initial RH shapes, however got thinner. The globules on the outer surface of the RHs were observed to be still present in the PRHs as seen in Figure 4.2. It was also detected that the PRHs were much more fragile than the RHs due to their brittle nature. Therefore, it was possible to grind them by hand in a ceramic mortar easily.

Figure 4.2: Pyrolyzed rice husks.

Table 4.1 shows the physical properties of the rice husks before and after pyrolysis. As-sieved (unwashed) rice husks were used in the determination of these parameters. Bulk densities were measured by weighing the sample in a 1 L cylinder several times and taking the average. Specific gravities were measured by a helium pycnometer in METU Central Laboratories on ground samples with particle size less than 154 μm. Moisture content was calculated by heating the samples to 105°C for 24 hours and noting the weight difference.

Table 4.1: Physical Properties of Rice Husks Before and After Pyrolysis

Property	**Rice Husk**	**Pyrolyzed Rice Husk**
Shape	Boat- like	Needle-like
Color	Yellow	Black
Length, l (mm)	7-10	6-9
Depth, a (mm)	1-3	1-2
Width, b (mm)	1-2	1-1.5
Bulk Density (g/cm^3)	0.11	0.10
Specific Gravity	1.62	1.74
Moisture Content (wt%)	6.3	2.4

4.1.2 Chemical Characterization

In order to understand the effect of pretreatment steps on the purification of rice husks, Inductively Coupled Plasma - Optical Emission Spectrometry (ICP-OES) analyses were conducted on as-sieved, water washed, acid leached and pyrolyzed samples of rice husks. Table 4.2 summarizes the results of chemical analysis done by ICP-OES in METU Central Laboratories.

As seen from Table 4.2, the main impurities present in the as-sieved rice husks were found as oxides of Al, Ca, Fe, Mg, K and Na in a descending order of magnitude. It was observed that most of the impurities in the form of metal-oxides were effectively removed by a simple water washing step. Furthermore, the subsequent acid leaching after water washing step has resulted in a substantial decrease in the impurity amount. It is interesting to note that the initial SiO_2 content of as-sieved rice husks was much higher than expected. However, approximately half of it was removed by the water washing step. This result showed that the adhering soil and clay pieces on the as-sieved rice husks were quite rich in SiO_2.

Decrease in the SiO_2 content of water washed rice husks after acid leaching was quite low and it may mean that either the residual SiO_2 containing impurities in the husks were not completely removed or some of the chemically present SiO_2 was being leached out during the leaching process. However, since SiO_2 is known to be insoluble in HCl, former is thought to be true. Considering the compounds given in Table 4.2 alone and treating the leached out SiO_2 as impurity, it was calculated that the impurity level of the as-sieved, water washed and acid leached rice husks were changed as 67 wt%, 23 wt% and 1 wt% of the husks, respectively. Thus, after the purification steps, a 99 wt% purity level in the rice husks was achieved.

Table 4.2 also showed that the SiO_2 percentage of rice husks increased to about 44.5% upon pyrolysis treatment. Due to the weight loss in pyrolysis, the percentage of the present compounds increased accordingly. However, it was observed that the impurity content remained low. After all subsequent treatments and pyrolysis, a purity level of about 98.8 wt% was achieved. Thus, it was observed that the purity level of the acid leached rice husks decreased slightly after pyrolysis.

Table 4.2: Chemical Analyses Results of As-sieved, Water Washed, Acid Leached and Pyrolyzed Rice Husk Samples

Compound (wt%)	**As-sieved***	**Water Washed***	**Acid Leached***	**Pyrolyzed****
SiO_2	47.57	24.64	20.46	44.57
CaO	3.75	0.55	0.13	0.27
Al_2O_3	4.67	0.40	0.02	0.06
Fe_2O_3	2.59	0.29	0.03	0.07
MgO	1.37	0.17	0.02	0.05
K_2O	1.07	0.24	0.01	0.02
Na_2O	0.90	0.11	0.01	0.02
TiO_2	0.35	0.03	0.002	0.005
MnO_2	0.11	0.04	0.001	0.005
ZnO	0.09	0.03	<0.003	0.02
NiO	<0.0019	<0.0019	<0.0019	<0.00004
CoO	<0.0017	<0.0017	<0.0017	<0.00001
V_2O_5	<0.0016	<0.0016	<0.0016	<0.00005
CuO	<0.0016	<0.0016	<0.0016	0.0013
P_2O_5	<0.032	<0.032	<0.032	0.00023

* Rest were organic compounds.

** Rest were carbon, etc.

Table 4.3 shows the results of the elemental analyses conducted on the acid leached rice husk sample in comparison with the PRH sample. Oxygen amount was not possible to determine by the elemental analyzer, thus it was calculated by subtracting the total of the other elements and the amount of SiO_2 as given by the ICP results, from 100. Ash content was calculated by treating the samples at 900°C for 5 hours under air atmosphere and weighing the residue.

It was seen from Table 4.3 that the acid leached rice husks were rich in carbon and oxygen, due to their high organic material content, such as cellulose, hemicellulose and lignin. C and SiO_2 concentration was calculated to be increased about 25 wt% and 120 wt%, respectively, after the pyrolysis treatment, due to the decomposition of organic matter and the resulting weight loss.

Comparing the SiO_2 percentages given by the ICP results in Table 4.2 and ash percentages given in Table 4.3, it was concluded that the ash was almost completely composed of SiO_2 since the values were very similar to each other. Table 4.3 also shows

Table 4.3: Elemental Composition of Acid Leached Rice Husk Samples Before and After Pyrolysis

Sample (wt%)	**C**	**H**	**N**	**S**	**O**	**Ash**	**C:SiO_2 (molar)**
Acid leached RH	36.8	5.2	none	none	37.5	19.7	9.0
PRH	46.0	2.0	none	none	7.5	44.6	5.2

an important result concerning the C:SiO_2 molar ratios. According to the reaction governing the carbothermal reduction and nitridation of SiO_2 as given in Equation 2.4, a C:SiO_2 molar ratio of at least 2 is needed for the reaction to take place. As seen from Table 4.3, C:SiO_2 molar ratios in the rice husks before and after the pyrolysis process were both significantly greater than 2, which was necessary for the reaction to take place. It was observed that the C:SiO_2 molar ratio was decreased with the pyrolysis treatment, since the weight loss was accompanied with the pyrolysis process.

Table 4.4 shows the proximate analysis results of the acid leached rice husks based on the pyrolysis and further heat treatment. The volatile matter content was calculated by noting the weight difference between the beginning and end of the pyrolysis treatments and taking the average of all pyrolysis treatments conducted. The ash content was calculated by burning a sample of pyrolyzed rice husk in air at 900°C for 5 hours to remove the carbon.

Table 4.4: Proximate Analysis of Acid Leached Rice Husk Sample

Volatile Matter (wt%)	**Fixed Carbon (wt%)**	**Ash (wt%)**
52.5	27.8	19.7

4.1.3 Phase Characterization

In order to determine the phases present in the rice husks and their crystallinity, X-ray diffraction (XRD) analyses were conducted on as-sieved, water washed, acid leached and pyrolyzed samples of rice husks by an X-ray diffractometer (Rigaku Ultima-IV) with Cu Kα radiation between 10-60° at a scanning rate of 2°/minute. The results of the XRD analyses are given in Figure 4.3.

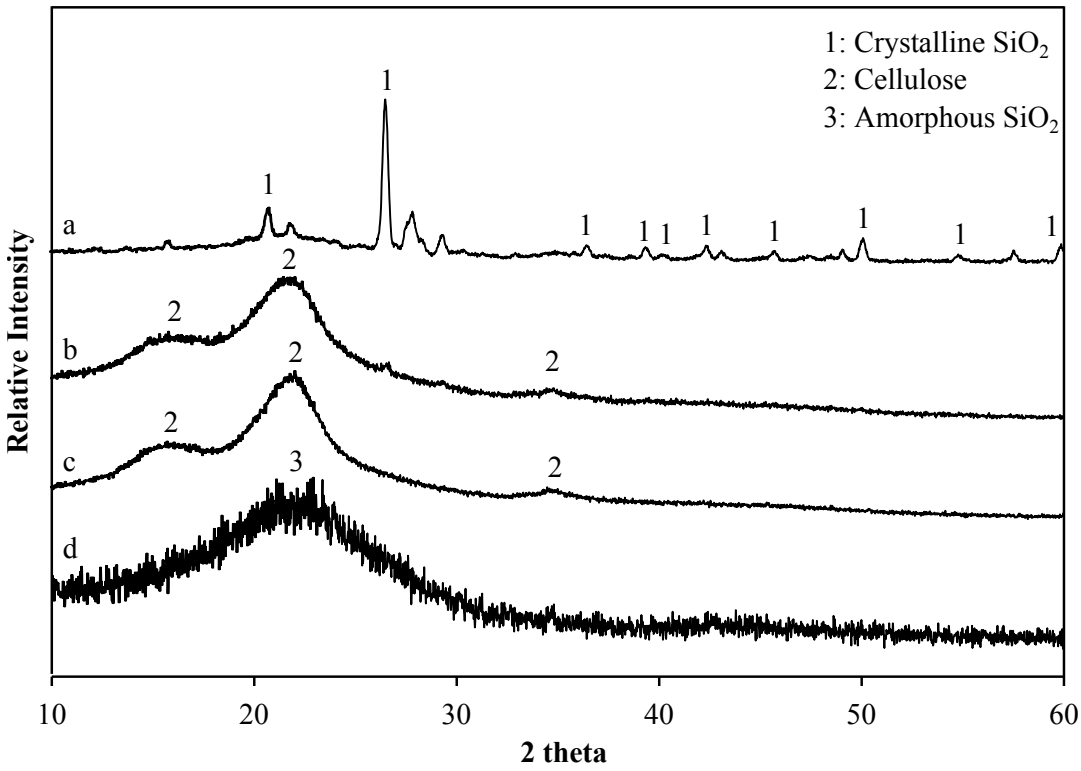

Figure 4.3: XRD patterns of (a) as-sieved, (b) water washed, (c) acid leached and (d) pyrolyzed rice husks.

As seen from Figure 4.3, as-sieved rice husks were observed to be containing high amounts of crystalline material peaks which were almost completely removed upon the water washing step. Thus, the crystalline phases that were present in the as-sieved rice husks were considered to be impurities, which were resulting from adhering clay and soil pieces. The impurity peaks were mainly identified as crystalline SiO_2, which is in agreement with the ICP results given in Table 4.2. Three main peaks, which were identified as cellulose, became easily visible after the water washing step [52]. It was observed that the acid leaching step had resulted in complete elimination of impurity peaks in the detection limit of the X-ray diffractometer and only visible peaks were identified as cellulose. It is also interesting to note that the crystallinity of cellulose phase was increased after the acid leaching step, as shown by the sharper peaks, which indicated the effect of acid leaching on the crystallinity of the material. The increase in crystallinity upon leaching was ascribed to the progressive removal of amorphous non-cellulosic materials [52].

After the pyrolysis treatment, the cellulose peaks were removed and only phase de-

tected was amorphous SiO_2 as seen in Figure 4.3. It is interesting to note that the main cellulose and SiO_2 peaks were almost at the same 2-theta degrees. N. Johar et al. [52] has identified these three peaks shown in Figure 4.3c as cellulose, on the other hand M. Sarangi et al. [53] has identified the peak at 22° as SiO_2 and did not comment on the other ones.

It is important to obtain an amorphous SiO_2 phase instead of a crystalline one after the pyrolysis process, since amorphous SiO_2 is considered to be more reactive and therefore beneficial in increasing the rate of carbothermal reduction and nitridation reaction, which is the following step after pyrolysis. Keeping the pyrolysis temperature as low as 600°C was the key in the production of amorphous SiO_2. Figure 4.4 shows the X-ray diffraction pattern of an acid leached rice husk ash sample, which was obtained by heating the rice husks to 900°C for 5 hours at air atmosphere. It was seen that some of the amorphous SiO_2 was transformed into crystalline SiO_2, making it less reactive and undesired if it were to be used in the nitridation experiments due to its ordered atomic structure with low energy.

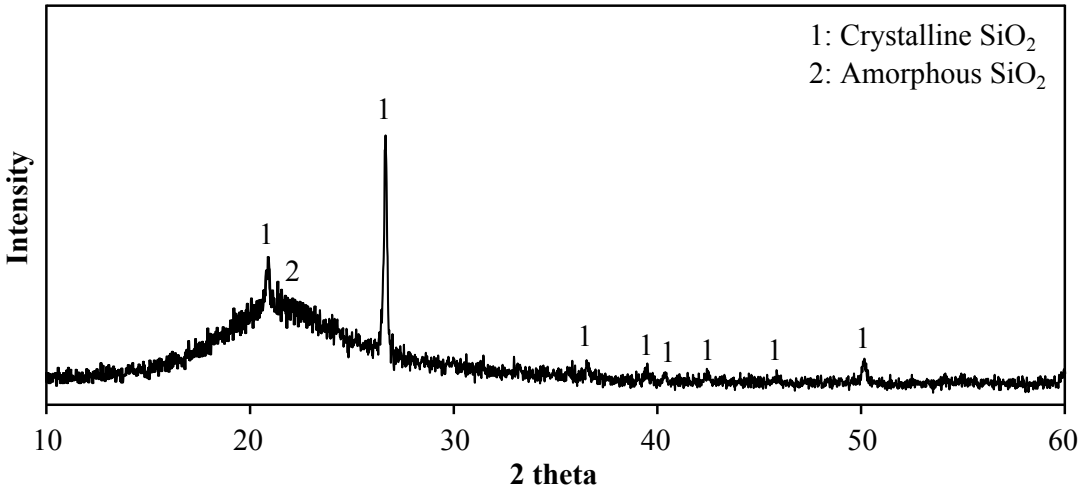

Figure 4.4: XRD pattern of acid leached rice husk ash.

4.1.4 Thermal Analysis

In order to investigate the thermal behavior of as-sieved and acid leached rice husks under inert atmosphere (pyrolysis), a thermogravimetric and differential scanning calorimetry analysis (TGA + DSC) was conducted between room temperature and

900°C with a heating rate of 4°C/min under N_2 atmosphere, in METU Central Laboratories. Figures 4.5 and 4.6 show the results of the TGA and DSC analysis respectively.

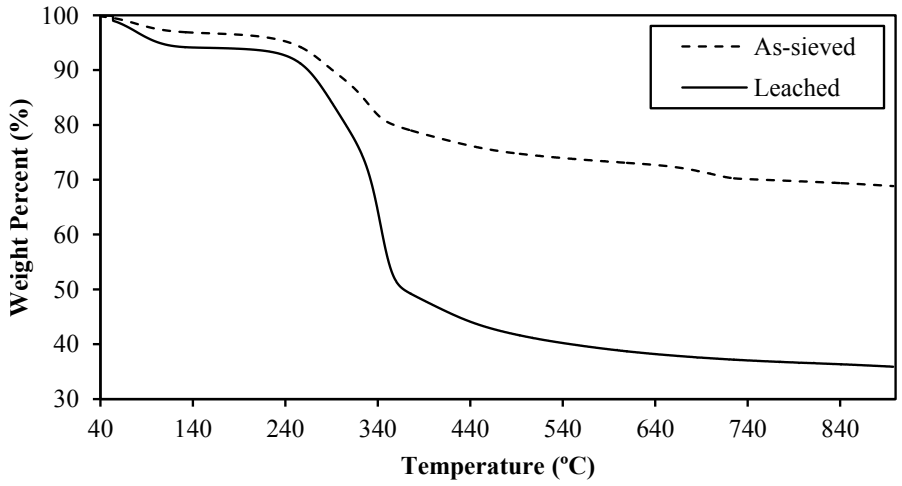

Figure 4.5: TGA curves of as-sieved and acid leached rice husk samples under N_2 atmosphere.

As seen from Figure 4.5, the thermal degradation of both as-sieved and acid leached rice husks took place in three distinct stages under N_2 atmosphere. First stage was from room temperature to approximately 150°C. This stage was corresponding to the evaporation of adsorbed water in the rice husks, accompanied with a small weight loss around 6% and 4% for acid leached and as-sieved samples, respectively [29, 31].

Second stage of the thermal degradation took place approximately between 150°C to 400°C with a fast and high amount of weight loss. This stage was mainly found to be responsible for the weight loss during pyrolysis process. About 50% and 20% of weight losses were observed for the leached and as-sieved samples, respectively at this stage. The large difference between these percentages of as-sieved and leached rice husks was due to the high impurity content of as-sieved rice husks which remained within the sample unchanged during the pyrolysis treatment, resulting in a small loss of weight. The information regarding the impurity content can be seen in Table 4.2. Among the organic constituents of rice husk, hemicellulose decomposes first at temperatures between 150-350°C and cellulose from 275-380°C [37]. Their degradation is responsible for the evolution of the volatile gases at this stage, as well as the weight loss. The breakdown of the organic matter releases the com-

bustible volatiles, water, carbon dioxide and char [37]. Lignin decomposes between 250-550°C and is mainly responsible for the char production [37].

Third stage took place approximately from 400°C to 900°C with a small weight loss, at a slow rate. After the second stage, almost all of the organic part of the husk has been decomposed, leaving mainly inorganic compounds like SiO_2, which is more stable at high temperatures and remains mainly unchanged [36]. Total weight losses were found to be about 65% and 30% for leached and as-sieved rice husks, respectively.

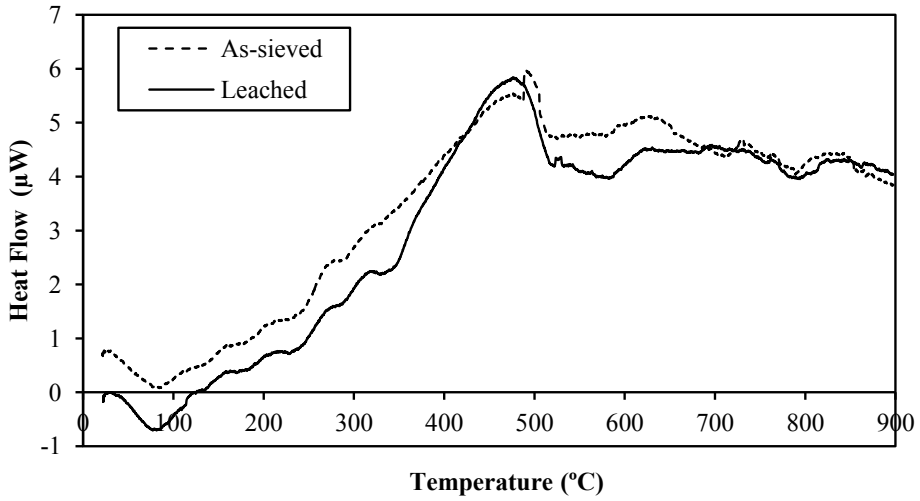

Figure 4.6: DSC curves of as-sieved and acid leached rice husk samples under N_2 atmosphere.

The DSC curves of as-sieved and acid leached rice husk samples were mainly in the same fashion with small differences as shown in Figure 4.6. Both samples exhibited a heat absorption at about 70°C due to the evaporation of adsorbed water as shown with a negative bump on the curve. Both samples exhibited two enthalpy changes due to degradation of organic matter at around 215°C and 280°C as shown by negative bumps on the curve. A large exothermic peak was observed for both samples at about 475°C which was suspected to be related with the decomposition of lignin. This exothermic peak explains the temporary temperature drop observed in the heating chamber of the furnace at around 475°C, during the pyrolysis treatment of acid leached rice husks.

4.1.5 Surface Analysis

Single point BET surface analyses were conducted in METU Central Laboratories on PRH samples in order to compare the effect of grinding on specific surface area. Since higher specific surface area is known to increase the reactivity of the sample, PRH stock is desired to have a high specific surface area to be used in the carbothermal reduction and nitridation process. Table 4.5 shows the BET analyses results of unground and ground samples of PRH.

Table 4.5: BET Surface Area of Pyrolyzed Rice Husk Samples

Sample	**BET Surface Area (m^2/g)**
Unground PRH	76.1
Powder ground to under 154 μm	117.8
Powder ground to under 100 μm	118.0

As seen from Table 4.5, grinding of the PRH resulted in a significant increase in the specific surface area. Although the ground samples had quite high specific surface areas, there was negligible difference between the specific surface area values of PRH samples which were ground to below 100 and 154 μm. This was considered to be due to the destroying of the pores present in the PRHs to its maximum by grinding to both under 100 and 154 μm. Thus, it was decided to grind the PRH stock to 100% below 100 μm to be used in the carbothermal reduction and nitridation experiments. The PRH stock was ground by hand using a ceramic mortar to avoid any contamination.

4.2 Carbothermal Reduction and Nitridation Experiments

4.2.1 General Inspection of the Products of Carbothermal Reduction and Nitridation of Rice Husks

Three distinct products were formed by the carbothermal reduction and nitridation experiments of rice husks, in agreement with the findings of V. Pavarajarn et al [16]. The products were easily distinguishable by the naked eye. Each of the products were formed in a different region of the alumina crucible containing the PRH sample,

making them effortless to detect. However, not all three of the products were always formed together. Certain conditions were found to favor the formation of certain products. Figure 4.7 indicates the positions of the products formed in the alumina crucible.

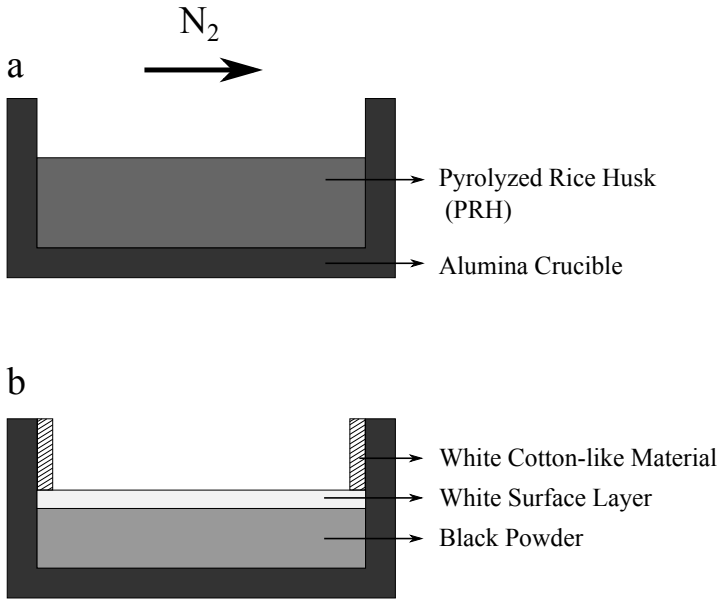

Figure 4.7: Cross-sectional view of the alumina crucibles showing the positions of reactant and products (a) before and (b) after the carbothermal reduction and nitridation reaction (not to scale).

Representation of PRH sample in alumina crucible is shown in Figure 4.7a. When N_2 is provided to flow on the sample at high temperatures, it was found to transform into Figure 4.7b. The Black Powder (BP) shown in Figure 4.7b was detected to contain high amounts of unreacted carbon, which gave it the black color. White Surface Layer (WSL) was a very thin layer formed on top of the BP. White Cotton-like Material (WCM) was detected to be formed on the crucible walls under certain conditions.

4.2.2 Effect of Reaction Temperature

Carbothermal reduction and nitridation of acid leached and pyrolyzed rice husks were conducted on 3 g PRH samples at 1300, 1350, 1400, 1450 and 1500°C for 1 h at a N_2 flow rate of 50 L/h. The aim for this experiment set was to determine the temperature at which the other experiment sets would be carried out. This experiment set was

conducted twice to examine all of the reaction products separately and as a whole, both morphologically and qualitatively.

Upon the visual inspection of the reaction products, it was noticed that at 1300 and 1350°C only BP was formed with occasional bright white dots on the surface. However at 1400, 1450 and 1500°C a continuous WSL was observed to be formed on top of the BP. Figure 4.8 shows the photographs of various products obtained after the experiments that were conducted at different temperatures.

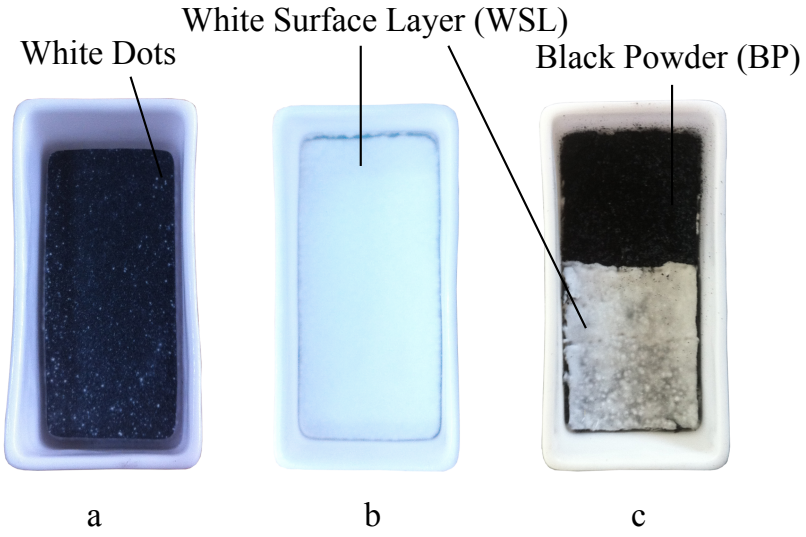

Figure 4.8: Photographs showing the top-view of the products formed at (a) 1300°C, (b) 1400°C and (c) 1400°C with half of the WSL removed for demonstration.

It was observed that it was not possible to separate pure WSL from BP. The separated layer was white on one side and black on the other side due to attached BP. No significant formation of White Cotton-like Material was detected in this experiment set. XRD analyses were conducted on the reaction products for characterization purposes. The results of the XRD analyses are given in Figure 4.9 for the BP products and in Figure 4.10 for the WSL products.

Figure 4.9 shows the XRD patterns of various products formed in BPs after 1 h reaction duration in comparison with the commercial Si_3N_4 powder obtained from Undersecretariat for Defence Industries of Turkey. It was seen that the dominant peaks in BPs formed after 1 h were SiC, regardless of the temperature. Significant amount of C was left unreacted in all of the BPs, detected by the distorted peak at around 26°. There were no Si_3N_4 peaks detected at 1300°C. Si_3N_4 formation was detected

first at 1350°C and its formation rate was increased with increasing temperature. This finding was in agreement with T. H. Liou et al. [18]. Increasing reaction rate with increasing temperature was explained by the higher rate of SiO vapor production at higher temperatures by Y. W. Cho et al. [28]. Amorphous SiO_2 was detected at 1300 and 1350°C by a broad hump at around 22°. Si_2N_2O peaks were also detected at 1350 and 1400°C along with some crystalline SiO_2, indicating that some of the amorphous SiO_2 in PRH was transformed into crystalline form at the reaction temperature.

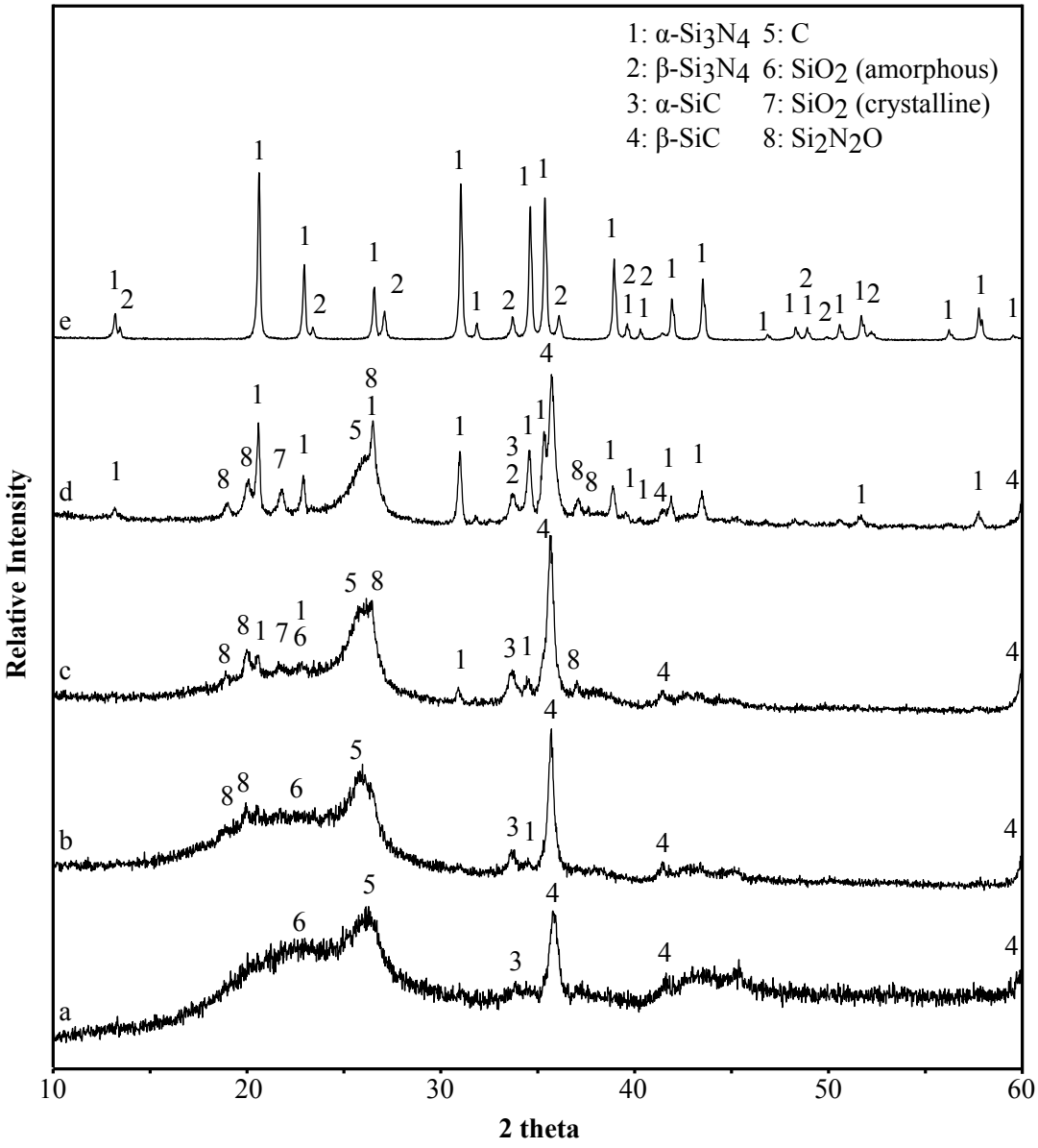

Figure 4.9: XRD patterns of BP products formed at (a) 1300°C, (b) 1350°C, (c) 1400°C, (d) 1450°C after 1 h at 50 L/h N_2 flow rate on 3 g PRH samples, before the removal of unreacted carbon and (e) commercial Si_3N_4 powder.

As indicated by Figure 4.10, the WSL products were mainly identified as α-Si_3N_4. In fact, at 1500°C a pure α-Si_3N_4 WSL was formed. SiC was detected in WSLs formed at 1400 and 1450°C. The presence of SiC was probably due to the contamination of WSLs with BPs during sampling. Also, BP attached to the opposite side of WSL product could cause SiC peaks on the diffractogram since data from the depths of the material was also retrieved during the X-ray penetration. This was proved by the hump at about 26° which was due to C coming from BP in Figure 4.10a.

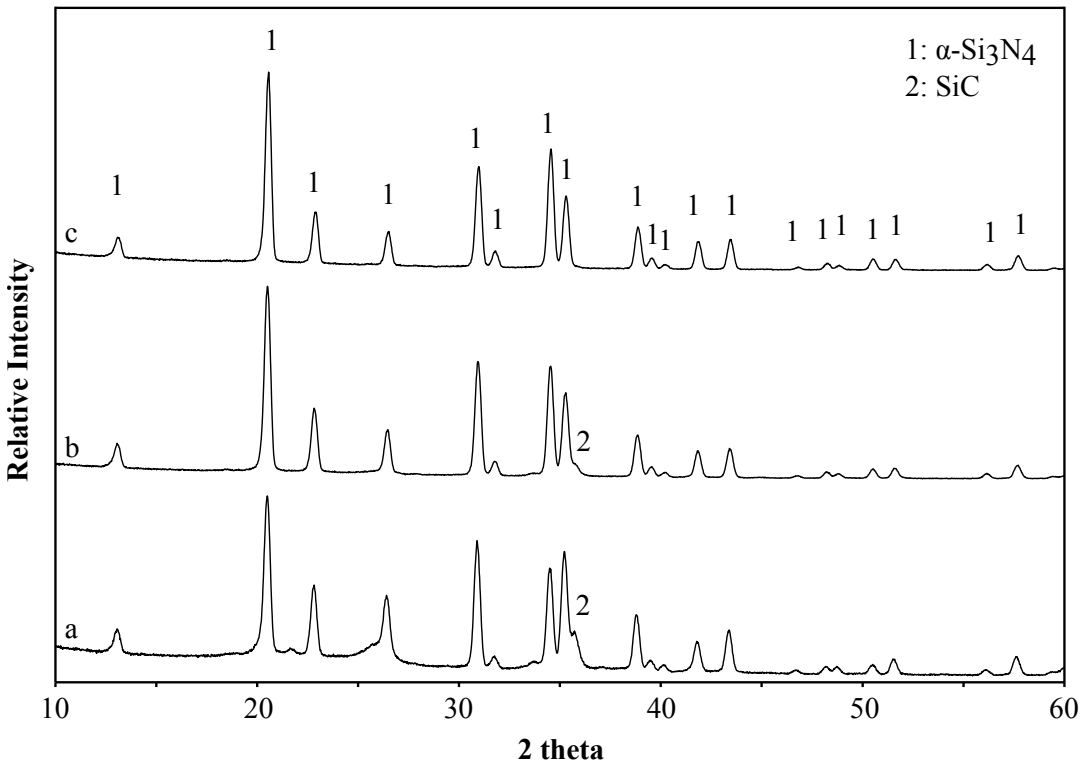

Figure 4.10: XRD patterns of WSL products formed at (a) 1400°C, (b) 1450°C and (c) 1500°C after 1 h at 50 L/h N_2 flow rate on 3 g PRH samples, before the removal of unreacted carbon.

To examine the reaction products as a whole, another set of XRD analyses were conducted on the mixtures which were obtained by the mixing and grinding of the BP and WSL products together. XRD patterns of the mixed products are given in Figure 4.11. Comparing Figures 4.9 and 4.11, it was seen that the mixing of BP and WSL together resulted in a slight increase in the relative intensities of Si_3N_4 peaks. This result was expected since WSLs were mainly identified as Si_3N_4 as shown in Figure 4.10. On the other hand, general view of the XRD patterns remained similar.

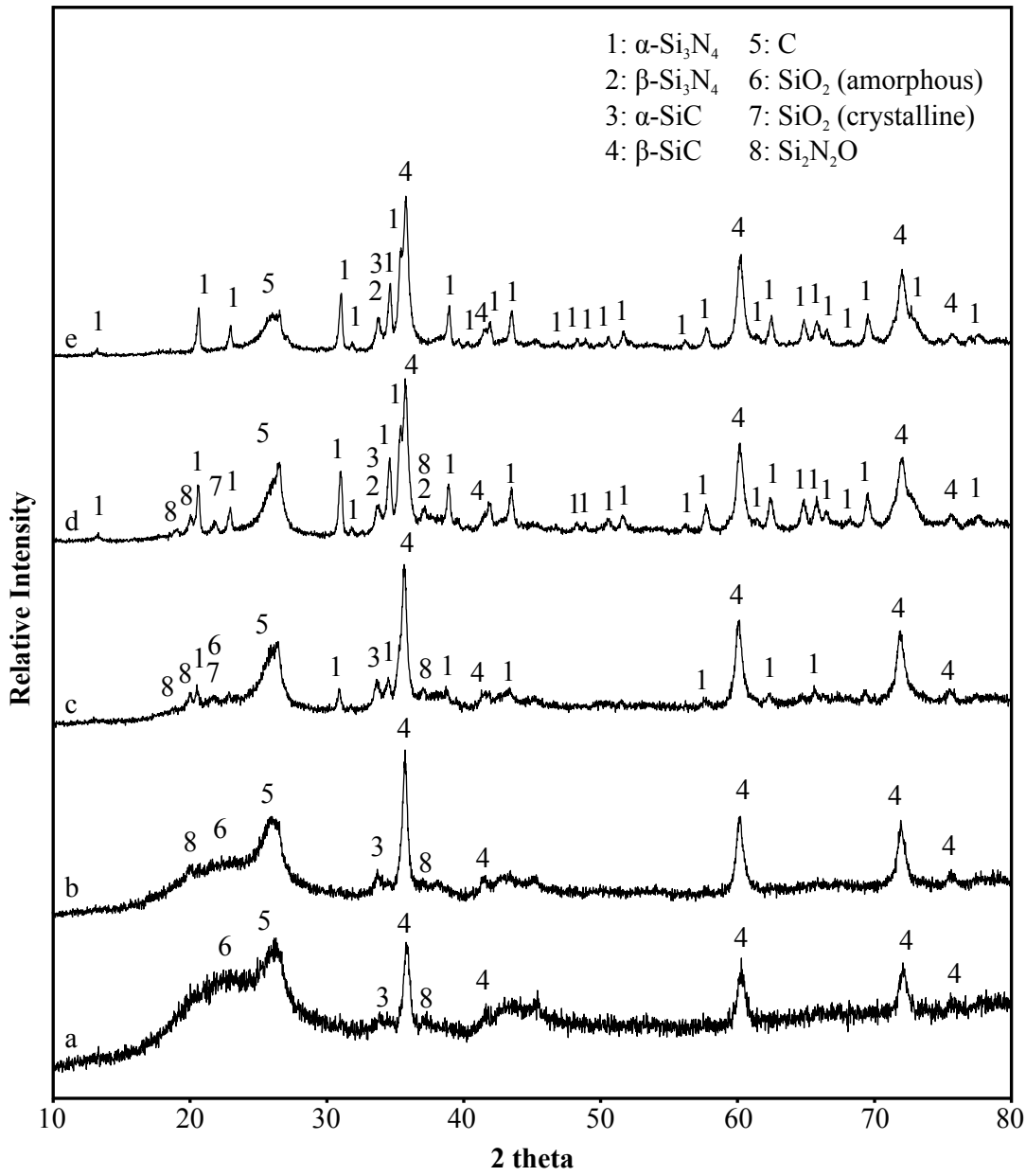

Figure 4.11: XRD patterns of the whole products (mixed and ground BP + WSL) formed at (a) 1300°C, (b) 1350°C, (c) 1400°C, (d) 1450°C and (e) 1500°C after 1 h at 50 L/h N_2 flow rate on 3 g PRH samples, before the removal of unreacted carbon. (no WSL formation was detected at temperatures 1300 and 1350°C, thus their patterns belong to only BP).

Figure 4.12 shows the weight loss and unreacted carbon percentages after the experiments conducted at different temperatures. Weight loss was determined by weighing the sample before and after the experiments. Unreacted carbon was determined by heating the product under air atmosphere at 700°C for 3 h and oxidizing the carbon.

The overall reaction responsible for the carbothermal reduction and nitridation of SiO_2 was previously given as $3SiO_{2(s)} + 6C_{(s)} + 2N_{2(g)} \rightarrow Si_3N_{4(s)} + 6CO_{(g)}$. Theoretical weight loss for this reaction was calculated by $\frac{(3M_{SiO_2}+6M_C)-(M_{Si_3N_4}+M_{unreacted\,C})}{3M_{SiO_2}+6M_C}$ to be 30.62% for C:SiO_2 molar ratio of 5.2 (M represents molecular weight in the formula). It was observed from Figure 4.12 that the weight loss during the experiments increased with the increasing temperature from 25% at 1300°C to 49% at 1500°C. Weight loss was higher than the theoretical value for the experiments conducted above 1350°C. Loss of gaseous species during the experiments may have caused this phenomena. It was also observed from the figure that high amounts of unreacted carbon, around 40-45 wt%, was present in the products, which was found to be located mainly in BP.

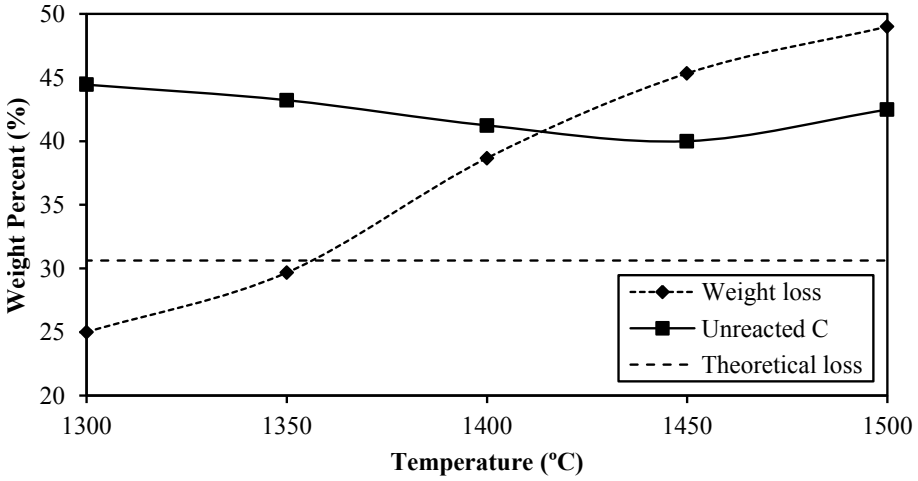

Figure 4.12: Percentages of weight loss and unreacted carbon left in the crucibles at 1300-1500°C for 1 h at 50 L/h N_2 flow rate on 3 g of PRH samples.

Morphological investigation by SEM was carried out on BP and WSL products formed at 1400, 1450 and 1500°C. Figure 4.13 shows the SEM images of the WSL products formed at 1400, 1450 and 1500°C. It was realized from the figure that the WSL products were mainly formed as nano/micro-fibers. Considering the XRD patterns of the WSL products given in Figure 4.10, the fibers shown in the images were identified as Si_3N_4. This was also supported by the detection of Si and N elements on fiber surfaces by EDS analyses. The composition of the fibers were found as around 71 wt% Si, 26 wt% N and 3 wt% O by an EDS analysis, indicating some oxidation of Si_3N_4.

Figure 4.13a showed that a highly contaminated WSL product was formed at 1400°C as compared to the product obtained at 1500°C (Figure 4.13e). This contamination happened probably during separation of BP from WSL. The SiC peak that was detected on the XRD pattern of WSL product formed at 1400°C as given in Figure 4.10a could be also explained by this contamination.

EDS analysis of the particle shown in Figure 4.13f gave C, Ca, O and Si peaks with a composition of 52.8 wt% C, 22.4 wt% Ca, 14.7 wt% O and 10.1 wt% Si. Ca was the second most abundant impurity in the PRH which was used as the starting material for nitridation experiments. Presence of Ca was detected by the ICP analysis which was shown in Table 4.2. Confirming that, Ca was present in most of the particles formed in WSLs.

Silicon and oxygen was found to be present in most of the EDS analyses conducted on the particles at different temperatures. This was explained by the presence of unreacted SiO_2 and crystalline SiO_2.

The diameters of the Si_3N_4 fibers in WSLs were found to be increasing with increasing temperature. This increase was thought to be due to the increasing diffusion rate at higher temperatures. Diameters were measured as between 80-250 nm at 1400°C, 200-500 nm at 1450°C and 0.8-1.85 μm at 1500°C. The lengths of the fibers were not possible to measure or compare, however they were as long as tens of micrometers.

Figure 4.14 shows the SEM images of the BP products formed at 1400, 1450 and 1500°C after the elimination of unreacted carbon by burning the product in air at 700°C for 3 h. The SEM images of BPs were obtained by analyzing the BPs attached to the back side of the WSLs. It was seen that BPs were formed by irregularly shaped and sized flakes and particles.

Upon the EDS analysis of the spherical particles shown in Figure 4.14b, only Si and O were found to be present with the composition of around 59 wt% Si and 41 wt% O. Accordingly they were identified as SiO_2 which was left as unreacted in the BP. Considering that these particles were close to the surface of the PRH in the alumina crucible, probably the rate of nitridation reaction was not high enough to be completed after 1 h.

Figures 4.14c and 4.14d show the interface between WSL and BP of the product obtained at 1450°C. WSL was detected at lower left and BP was detected at upper right corner of the images. High intimate surface contact of WSL and BP shown in the images made the complete separation of WSL from BP impossible. The fibers shown in Figures 4.14e and 4.14f probably originated from WSL attached to BP. Normally, no fibers were thought to be produced in BPs.

There existed wide contradictions on the SiC formation temperature during the carbothermal reduction and nitridation of rice husks reported in the literature. I. A. Rahman et al. stated that the maximum temperature for the formation of Si_3N_4 from rice husks was 1425°C, above which SiC started to form [42]. I. B. Cutler determined this temperature in his study as 1400°C [5]. Kuşkonmaz et al. did not detect the formation of SiC until 1450°C, above which SiC was found to be present in increasing amounts with the increasing temperature [14]. Although there are contradictions on the exact temperature at which SiC starts to form, all of the authors have reported that the SiC formation increased with the increasing temperature. In this thesis study, upon the investigation of the XRD patterns given in Figures 4.9 and 4.11, it was seen that SiC was present at all temperatures. Significant formation of Si_3N_4 was first detected at 1400°C. Considering the reported literature and in the light of the mentioned XRD patterns, to minimize the formation of SiC in the products and to have a high enough reaction rate to produce Si_3N_4 in reasonable durations, the temperature at which the rest of the experiments would be conducted was chosen as 1400°C. The formation of SiC was investigated thermodynamically in detail and explained in a separate section in the final part of the thesis.

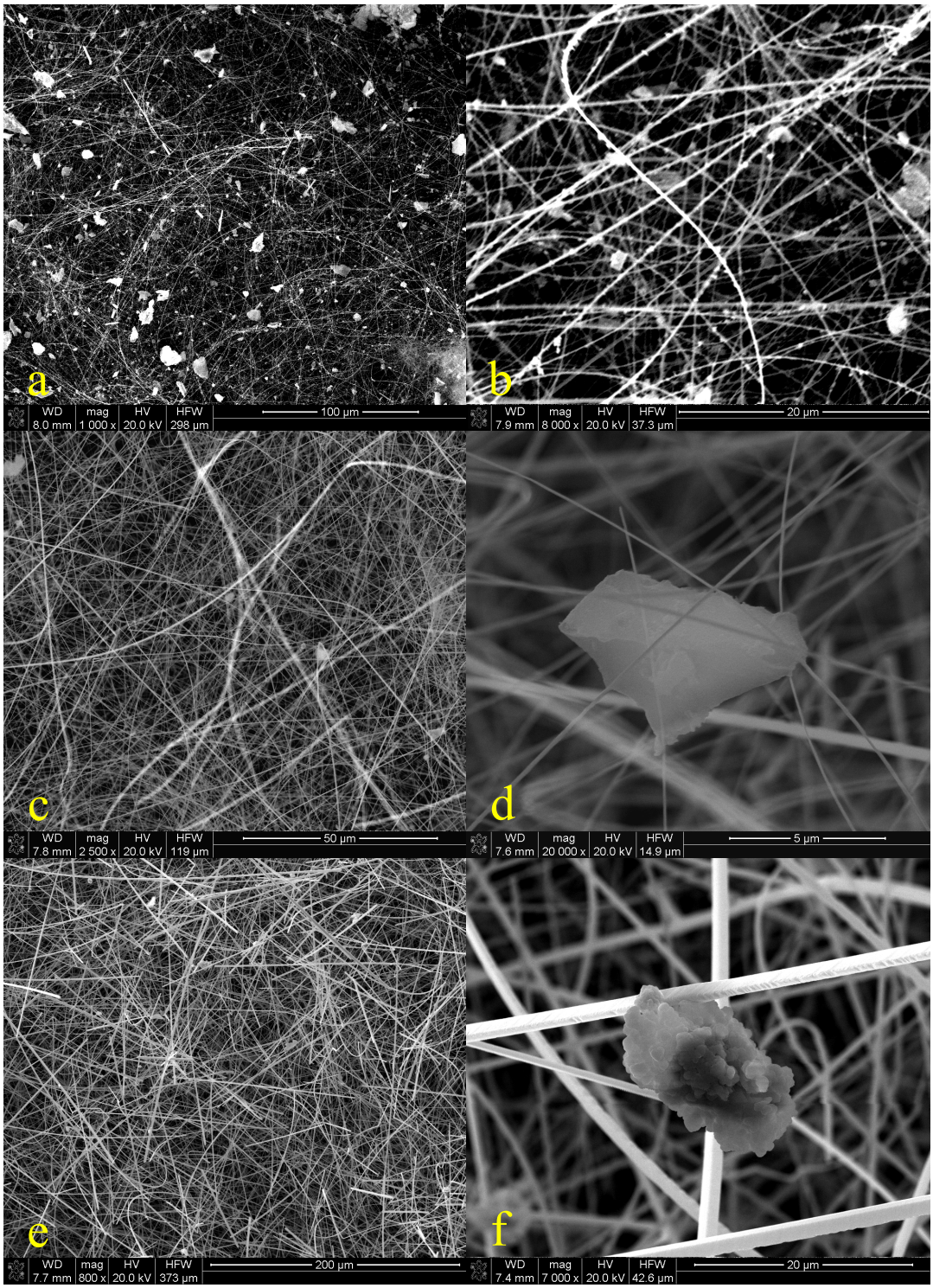

Figure 4.13: SEM images of WSL products obtained at (a, b) 1400°C, (c, d) 1450°C and (e, f) 1500°C after 1 h at 50 L/h N_2 flow rate on 3 g PRH samples, after the removal of unreacted carbon.

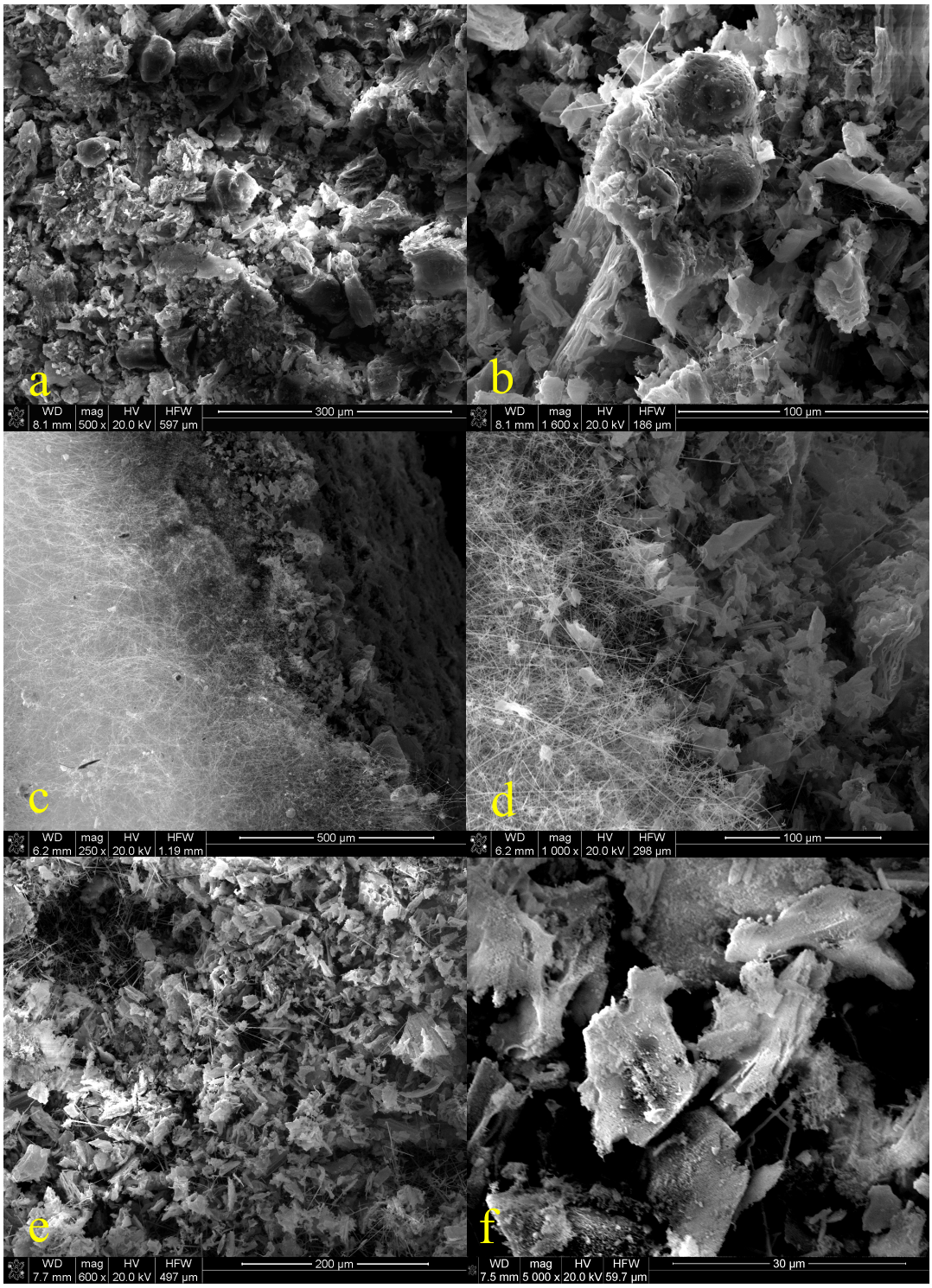

Figure 4.14: SEM images of BP products obtained at (a, b) 1400°C, (c, d) 1450°C and (e, f) 1500°C after 1 h at 50 L/h N_2 flow rate on 3 g PRH samples, after the removal of unreacted carbon.

4.2.3 Effect of Reaction Duration

To examine the effect of reaction duration on the carbothermal reduction and nitridation of acid leached and pyrolyzed rice husks, experiments were conducted for 1, 3, 6, 9 and 24 h at 1400°C at a N_2 flow rate of 50 L/h on 3 g PRH samples.

Upon the visual inspection of the reaction products, WSL formation was detected at all times. BP was formed under the WSL products. WSL products formed after 1 and 3 h looked similar and could not be well separated from the BP. However, experiments conducted for 6, 9 and 24 h produced two thin WSL products on top of each other. The top WSL was very easy to separate from the bottom one without any contamination from BP. The bottom WSL was, however, inseparable from the BP. The XRD patterns of top WSL products for 6 and 24 h are given in Figure 4.15. The top WSL products were not heated to elevated temperatures prior to XRD analysis since they did not contain any unreacted carbon.

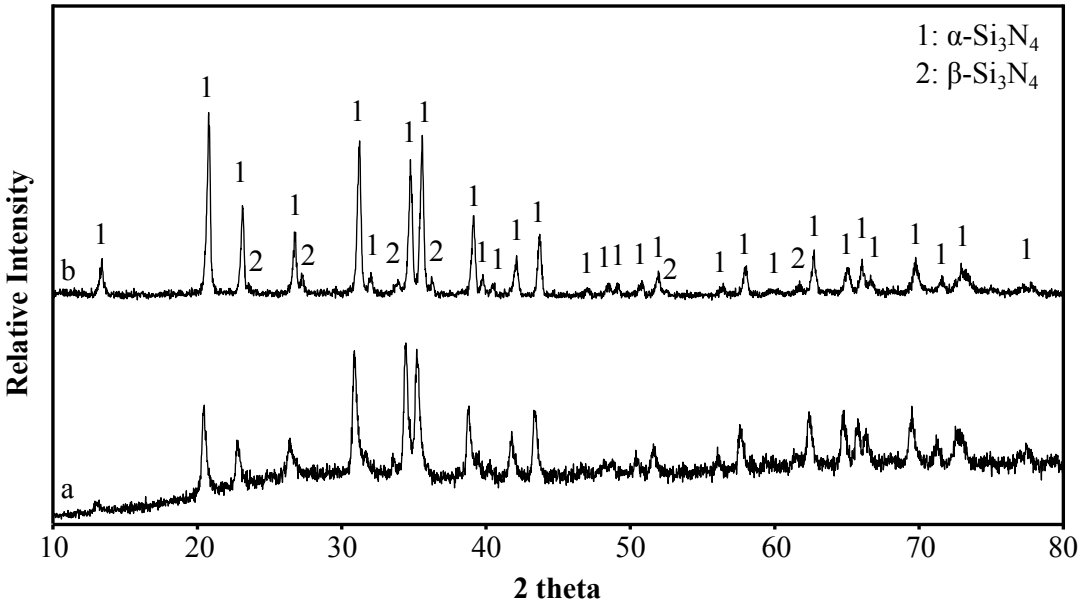

Figure 4.15: XRD patterns of the WSL products formed after (a) 6 h and (b) 24 h reaction durations at 1400°C at a N_2 flow rate of 50 L/h on 3 g PRH samples.

As seen from Figure 4.15, WSL formed after 6 and 24 h experiments were pure Si_3N_4 containing both α and β phases. It was observed from the XRD patterns that the crystallinity of the WSL formed after 24 h was higher than that of WSL formed after 6 h due to a prolonged exposure to high temperature. No SiC peaks were detected in

the XRD patterns since there was no contamination from the BP.

To investigate the reaction products as a whole, BP and WSL formed were ground by hand in a ceramic mortar and mixed thoroughly. The mixtures were then heated to 700°C for 3 h in air atmosphere for the removal of unreacted carbon. XRD analyses were conducted on these carbon-free mixtures and the obtained patterns are given in Figure 4.16.

It was observed from Figure 4.16 that no peaks belonging to SiO_2, Si_2N_2O and α-SiC were detected in the products, at reaction durations longer than 1 h. Thus, these phases were considered to be early intermediate products of the experiments and transformed into other phases at prolonged reaction durations. β-Si_3N_4 was first detected after 3 h and it was found to be present in all of the products formed with a reaction duration greater than 1 h. It was also observed that the fraction of SiC in the products decreased with increasing reaction duration. On the other hand, α-Si_3N_4 fraction in the products was found to be increased with increasing reaction duration, as detected from the XRD pattern. This result was in agreement with the findings of Kuşkonmaz et al. [14]. At reaction durations between 3-24 h, the products were found to be containing the same phases, only differing in their percentages.

Quantitative analyses were conducted on the reaction products obtained after 3-24 h reaction durations based on the XRD patterns given in Figure 4.16, in order to calculate the Si_3N_4 and SiC weight percentages. For these analyses, the method explained by F. H. Chung was used [54]. For the unresolved strongest peak of Si_3N_4 in certain patterns, intensity of the strongest resolved peak was measured and this intensity was converted to the intensity of its strongest line by direct comparison, using the XRD pattern of pure commercial Si_3N_4, which was obtained by the same XRD instrument. Unreacted SiO_2 that may be left in the products was not taken into account in the calculations, since they can be removed by boiling the products in NaOH solution. Figure 4.17 shows the results of the quantitative analyses. It was seen from the figure that the fraction of total Si_3N_4 increased with increasing reaction duration, on the other hand SiC fraction decreased. Si_3N_4 weight percentage was changing approximately between 85 wt% at 3 h to 95 wt% at 24 h.

Figure 4.18 shows the weight loss and unreacted carbon percentages of the products

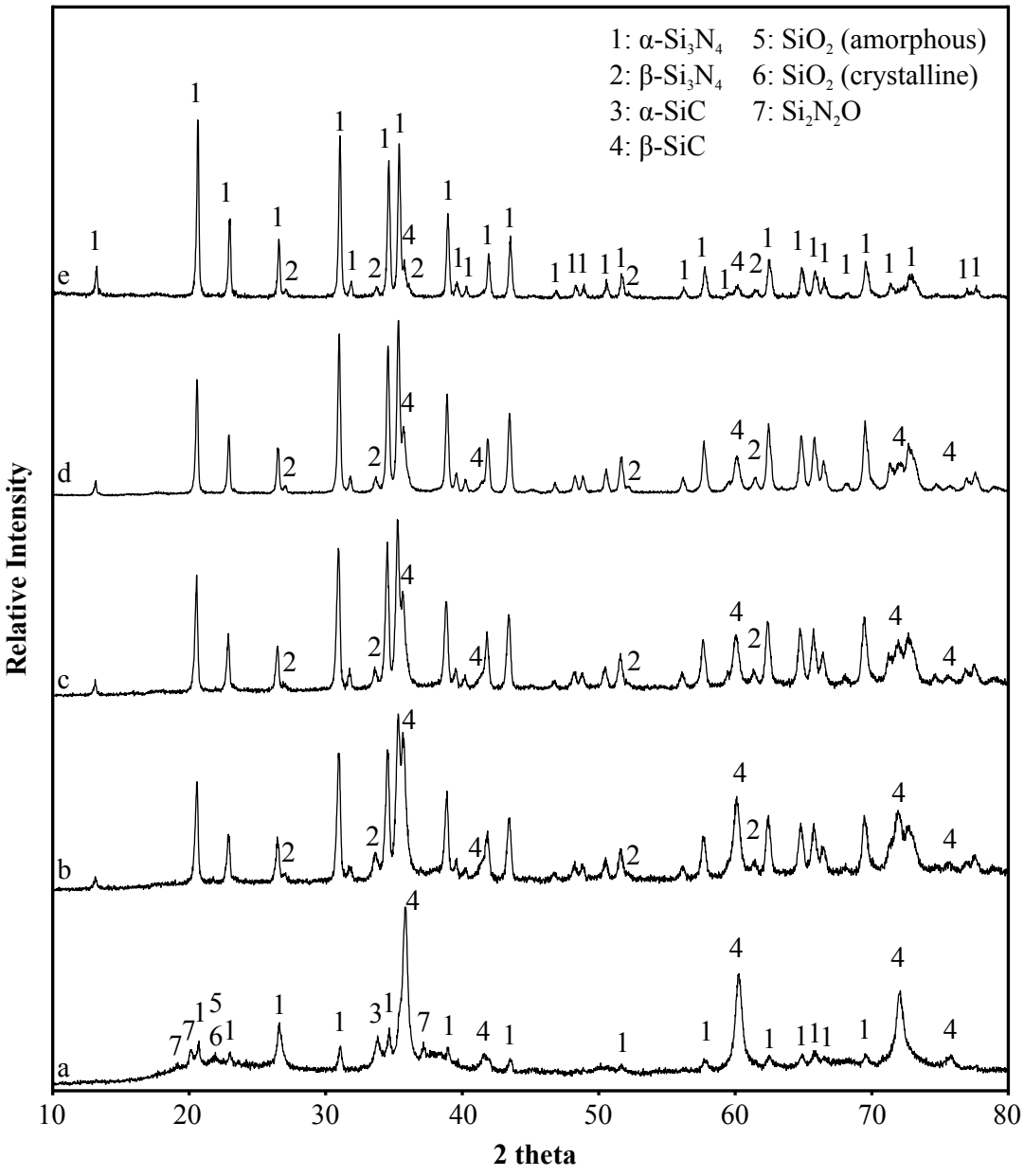

Figure 4.16: XRD patterns of the whole products (mixed and ground BP + WSL) formed after (a) 1 h, (b) 3 h, (c) 6 h, (d) 9 h and (e) 24 h reaction durations at 1400°C at a N_2 flow rate of 50 L/h on 3 g PRH samples, after the removal of unreacted carbon. Unchecked peaks belong to α-Si_3N_4.

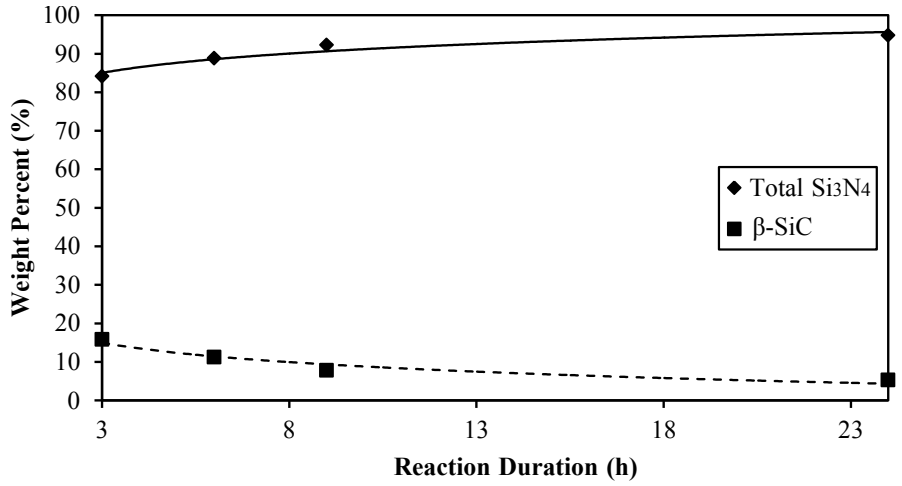

Figure 4.17: Si_3N_4 and SiC weight percentages in the products (mixed and ground WSL + BP) obtained after 3-24 h at 1400°C and 50 L/h N_2 flow rate on 3 g of PRH samples. Si_3N_4 is given as a total of α and β phases.

after the experiments conducted for 1-24 h. It was observed from the figure that the weight loss after the experiments was higher than the theoretical value at all times, which was calculated to be 30.62%. Weight loss percentages of the experiments conducted for 3-24 h were very close to each other and in the close vicinity of 46%. Highest unreacted carbon percentage was observed in 1 h reaction duration. Unreacted carbon percentages of the experiments conducted for 3-24 h were very close to each other and on the close vicinity of 39%.

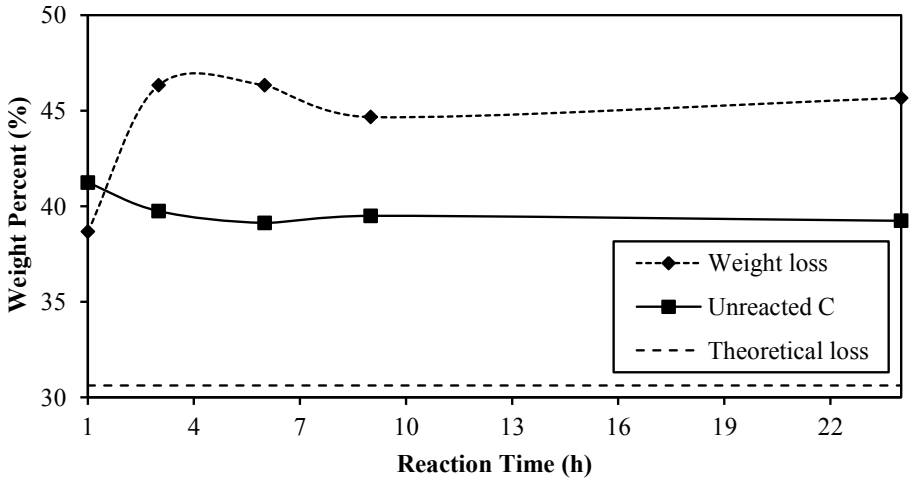

Figure 4.18: Percentages of weight loss and unreacted carbon left in the crucibles after reactions conducted for 1-24 h at 1400°C and 50 L/h N_2 flow rate on 3 g of PRH samples.

Considering both Figures 4.17 and 4.18, it was concluded that the reaction rate was faster at the first hours of the experiments and slowed down after approximately 3 h. Since SiC percentage was decreasing as the Si_3N_4 percentage was increasing without changing the weight loss significantly and no other phases were found to be present in the system, SiC to Si_3N_4 transformation must be considered. These considerations are given in detail in the final part of the thesis.

Figure 4.19 shows the SEM images of WSL products obtained after 1-24 h durations at 1400°C. It was observed from the images that Si_3N_4 fibers were produced at all durations. The diameters of the fibers were observed to be increasing with increasing reaction duration up to 9 h. The diameters of fibers for 24 h reaction duration were smaller than for 9 h reaction duration. The morphology of the fibers produced after 24 h were more like sharp needles rather than fibers and the diameters were more variable than the diameters of WSL products formed at the other reaction durations. Some thick fibers were also detected at the background of the WSL formed after 24 h.

Diameters of the Si_3N_4 fibers were measured as between 80-250 nm after 1 h, 100-340 nm after 3 h, 1-1.82 μm after 6 h, 1.39-2.82 μm after 9 h and 110 nm - 1.49 μm after 24 h reaction durations. The fibers were about tens of micrometers in length.

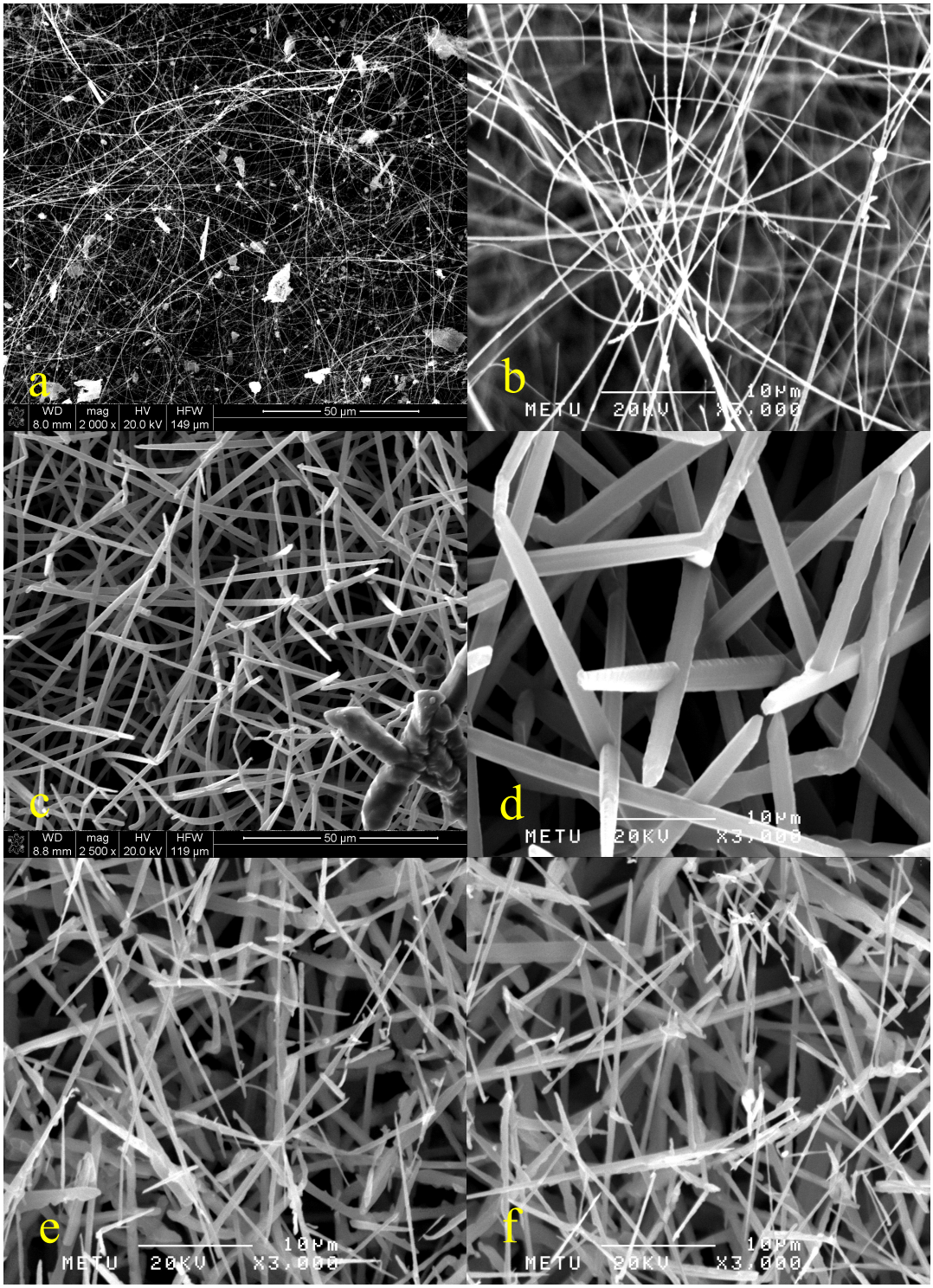

Figure 4.19: SEM images of WSL products obtained after (a) 1 h, (b) 3 h, (c) 6 h, (d) 9 h and (e, f) 24 h at 1400°C and 50 L/h N_2 flow rate on 3 g PRH samples.

4.2.4 Effect of N_2 Flow Rate

To investigate the effect of N_2 flow rate on the carbothermal reduction and nitridation of acid leached and pyrolyzed rice husks, the experiments were conducted at gas flow rates of 10, 20, 30, 40 and 50 L/h at 1400°C on 3 g PRH samples for 6 h.

Upon examining the reaction products with naked eye, WSL formation on top of BP was detected at all gas flow rates. It was observed that two thin WSL were formed on top of each other at gas flow rates of 30, 40 and 50 L/h. Thus, the complete separation of top WSL without any contamination was easily possible. However, only one WSL was formed above the BP at gas flow rates of 10 and 20 L/h. Accordingly, in these cases it was not possible to separate the WSL without the adhering BP on the back side.

Small amounts of White Cotton-like Material (WCM) formation was first detected at 40 L/h N_2 flow rate, on the wall of the alumina crucible which was closer to the gas outlet. Amount of WCM produced was increased with decreasing gas flow rate. At a N_2 flow rate of 10 L/h, most of the crucible walls were covered with WCM. The higher rate of WCM formation at lower gas flow rates were explained by either the carrying of these products or carrying of the reactants which were responsible for the formation of these products, by high N_2 flow rates. Since most of the WCM and/or reactants were swept away from the system at higher gas flow rates, only possible place for the formation of WCM at higher gas flow rates was found to be the bottom of the crucible wall that was closer to the gas outlet, which prevented them from being swept away. WCM and the location where it was formed in the crucible is shown in Figure 4.20.

XRD pattern of the WCM formed at 10 L/h N_2 flow rate is given in Figure 4.21. The produced WCM was not heated to elevated temperatures since it did not contain any unreacted carbon. It was observed from the pattern that WCM was formed as pure Si_3N_4. A rough XRD pattern was obtained, since the WCM collected from the walls of the crucible was soft and had to be pressed down on to the sample holder of the XRD instrument, which formed an irregular and non-continuous surface to be analyzed.

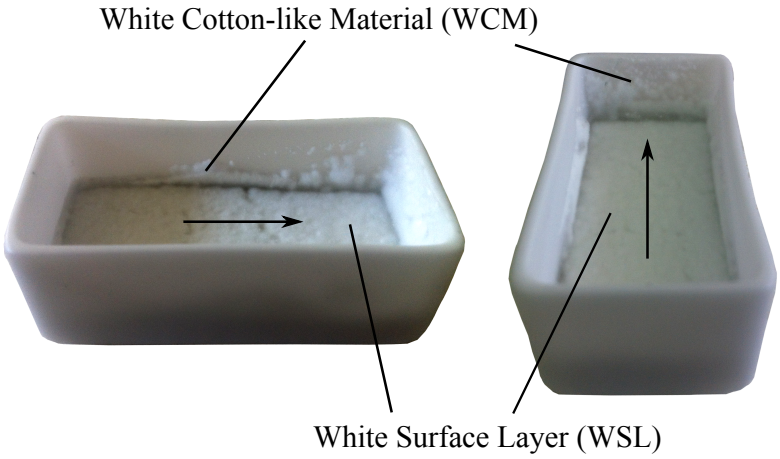

Figure 4.20: Front and side views of the alumina crucibles showing the formation of WCM and WSL. Arrows show the N_2 flow direction.

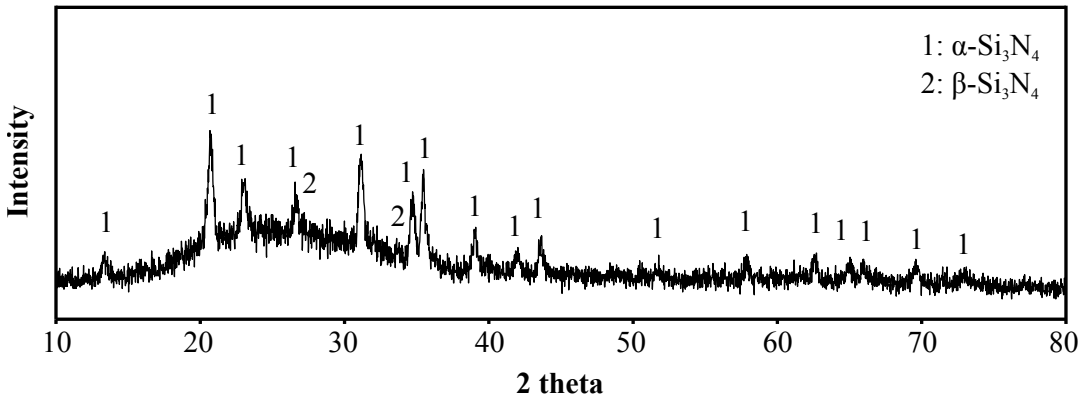

Figure 4.21: XRD pattern of the WCM produced at a N_2 flow rate of 10 L/h at 1400°C for 6 h on 3 g PRH sample.

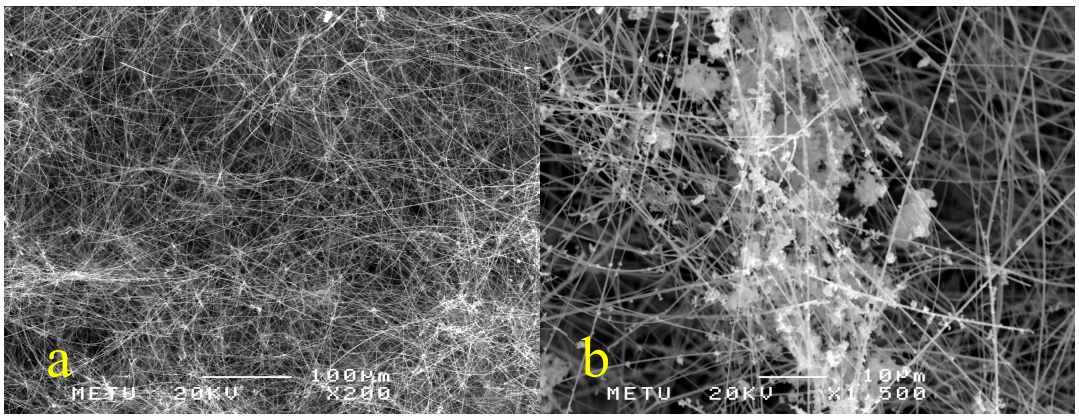

Figure 4.22: SEM images of WCM product obtained at a N_2 flow rate of 10 L/h at 1400°C for 6 h on 3 g PRH sample at a magnification level of (a) x200, (b) x1500.

SEM images of the WCM formed at 10 L/h N_2 flow rate are given in Figure 4.22. It was observed from the figure that Si_3N_4 fibers of hundreds of micrometers length were formed. The diameters of the fibers were measured as between 110-410 nm. Some particles were found to be formed on the fibers at different regions, as shown in Figure 4.22b. Upon EDS analysis of these particles, Si and N elements were detected. Accordingly, the particles were identified as Si_3N_4.

To investigate the reaction products as a whole, BP and WSL formed at various gas flow rates were ground by hand in a ceramic mortar and mixed thoroughly. The mixtures were then heated to 700°C for 3 h in air atmosphere for the removal of unreacted carbon. Figure 4.23 shows the results of the XRD analyses conducted on the carbon-free mixtures.

It was seen from Figure 4.23 that Si_3N_4 and SiC were the only phases detected in the XRD patterns. It was observed from the relative peak intensities that, SiC percentage of the products was increasing with decreasing N_2 flow rate. On the other hand, α-Si_3N_4 fraction of the products was observed to be increasing with increasing gas flow rate. Quantitative analyses were conducted on the XRD patterns in the same fashion explained in the previous section, to investigate the compositional effect of N_2 flow rate on the products. Weight percentages of Si_3N_4 and SiC in the products as a function of N_2 flow rate is given in Figure 4.24.

As seen from Figure 4.24, Si_3N_4 weight fraction in the products was found to be increasing with the increasing N_2 flow rate. Similar results have been reported by T. H Liou et al. and Y. W. Cho et al. in their studies [18,26,28]. Si_3N_4 weight percentage was found to be changing approximately between 78 wt% at 10 L/h to 89 wt% at 40 L/h N_2 flow rate. Weight loss and unreacted carbon percentages after the experiments conducted at 10-50 L/h gas flow rates are given in Figure 4.25.

It was observed in Figure 4.25 that at all gas flow rates, the weight loss percentages were greater than the theoretical weight loss value for the overall reaction responsible for the carbothermal reduction and nitridation of SiO_2 and very close to each other, around 46%. Unreacted carbon percentages were in the close proximity of 39% for all gas flow rates. Comparing Figure 4.25 with the weight loss and unreacted carbon percentages of experiments conducted for 3-24 h as given in Figure 4.18, it was

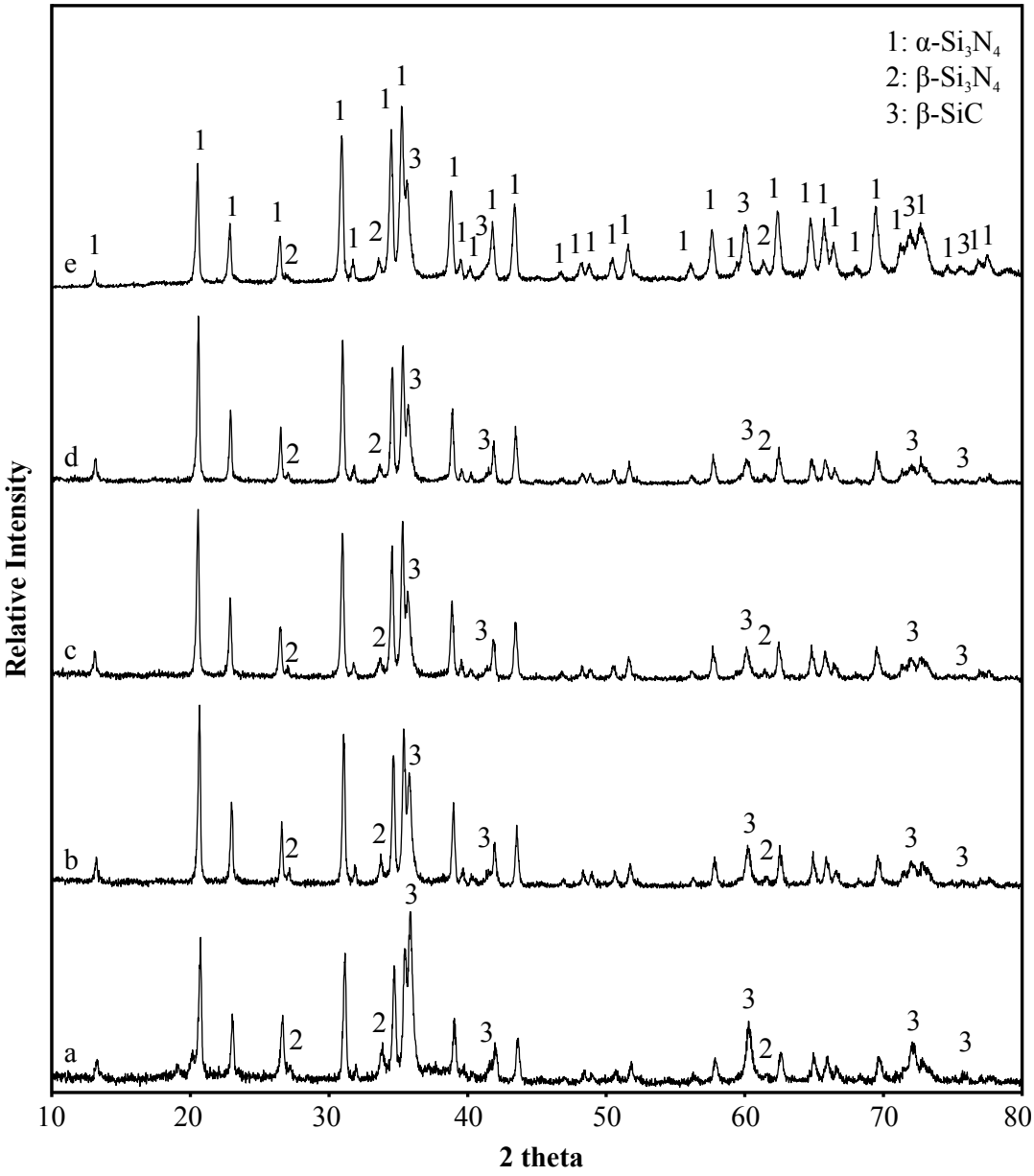

Figure 4.23: XRD patterns of the whole products (mixed and ground BP + WSL) formed at a N_2 flow rate of (a) 10 L/h, (b) 20 L/h, (c) 30 L/h, (d) 40 L/h and (e) 50 L/h at 1400°C for 6 h on 3 g PRH sample, after the removal of carbon. Unchecked peaks belong to α-Si_3N_4.

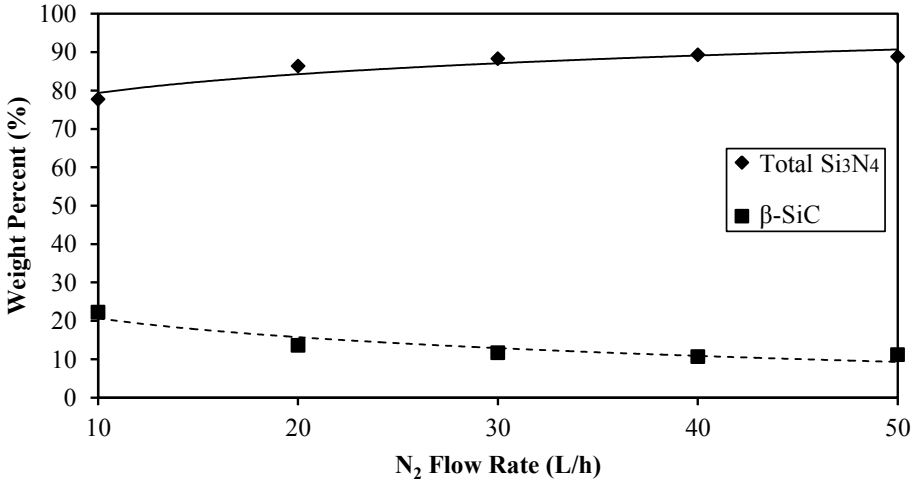

Figure 4.24: Si_3N_4 and SiC weight percentages in the products (mixed and ground WSL + BP) obtained at gas flow rates between 10-50 L/h at 1400°C for 6 h on 3 g of PRH samples. Si_3N_4 is given as a total of α and β phases.

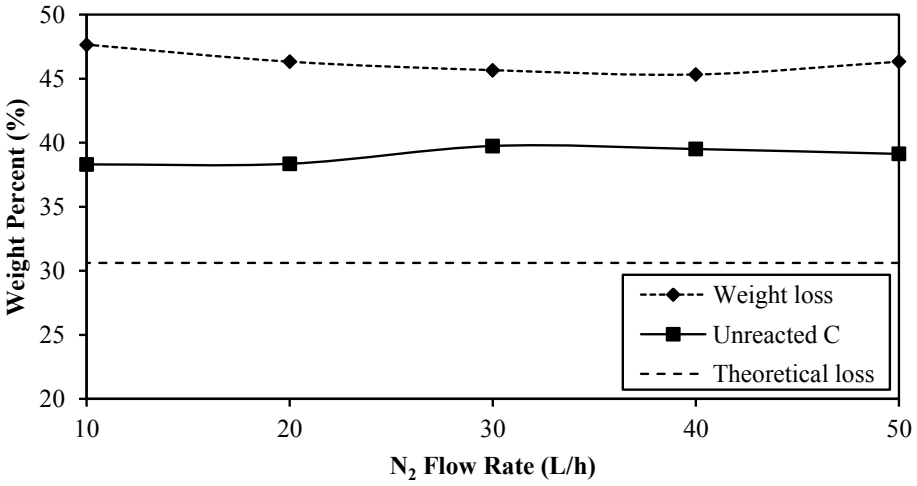

Figure 4.25: Percentages of weight loss and unreacted carbon left in the crucibles after reactions conducted at N_2 flow rates of 10-50 L/h at 1400°C for 6 h on 3 g of PRH samples.

seen that the weight loss and unreacted carbon values obtained at both experiment sets were very similar. This was considered as a proof that the same reactions were responsible for the weight loss during these two experiment sets, provided that the reaction duration was longer than 3 h. Figure 4.26 shows the SEM images of WSLs produced at 10-50 L/h. The produced WSLs were not heated to elevated temperatures prior to SEM analysis since they did not contain any unreacted carbon.

As seen from Figure 4.26, Si_3N_4 fibers were observed to be formed at all N_2 flow rates. The diameters of the fibers were measured as between 275-600 nm at 10 L/h, 880 nm - 1.51 μm at 20 L/h, 170-440 nm at 30 L/h, 122-480 nm at 40 L/h and 1-1.82 μm at 50 L/h. Thus, there were no apparent relationship between the fiber diameters and N_2 flow rates. Fibers were about hundreds of micrometers in length. Formation of a large cluster was detected at 30 L/h gas flow rate as shown in Figure 4.26d. Upon EDS analysis conducted on the particle, Si, Ca, C and O elements were found to be present. Relatively high content of impurity Ca in PRH were thought to be playing an important role in the production of these particles. EDS analysis conducted on the thick fibers forming directly on top of the large cluster shown in Figure 4.26d showed the presence of Si, Ca and C elements. This particle may have acted as a nucleation site for the formation of these non-silicon nitride fibers.

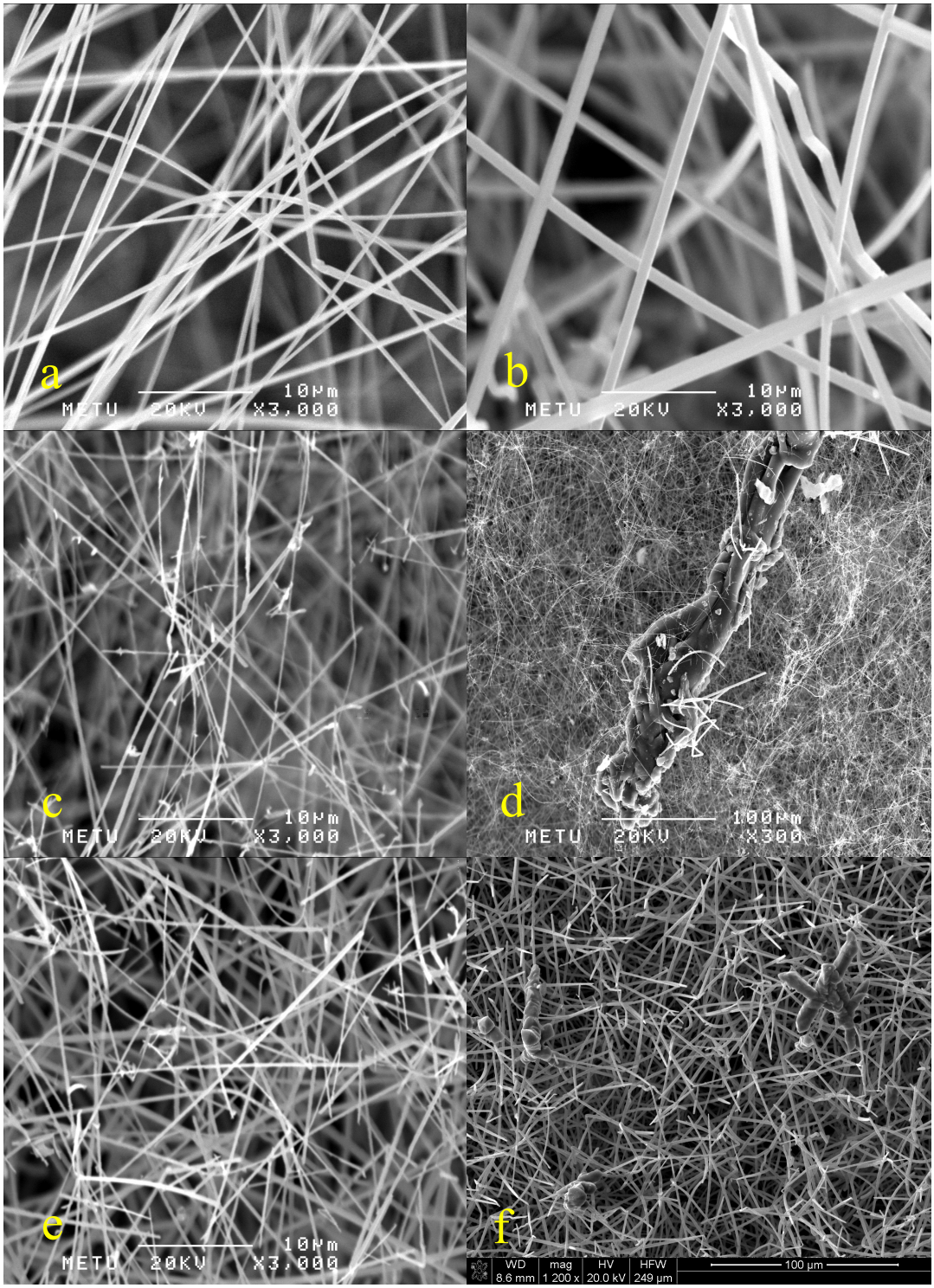

Figure 4.26: SEM images of WSL products obtained at N_2 flow rate of (a) 10 L/h, (b) 20 L/h, (c, d) 30 L/h, (e) 40 L/h and (f) 50 L/h at 1400°C for 6 h on 3 g PRH samples.

4.2.5 Effect of Starting PRH Amount

Since Si_3N_4 was found to be present in the BP and percentage of Si_3N_4 was calculated to be increasing with increasing reaction duration at a slow rate as shown in Figure 4.17, decreasing the starting PRH amount placed in the alumina crucible was thought to be a possible way to increase the Si_3N_4 concentration of the final product (WSL + BP). For this purpose, PRH amount in the crucible was adjusted as 0.25 g, 0,75 g, 1.5 g and 3 g. The corresponding depth of PRH samples in the alumina crucible were measured as 0.3 mm deep for 0.25 g, 1 mm for 0.75 g, 2 mm for 1.5 g and 5 mm for 3 g samples by a vernier caliper. The experiments were conducted at 1400°C for 6 h at a N_2 flow rate of 50 L/h.

Visual inspection of the reaction products revealed that WSL was formed at all PRH amounts. However, when 0.25 g of PRH was used as a starting mixture, the formed WSL was not possible to separate from the BP. Also, the BP formed was more gray than black. Two WSL were formed on top of each other when 0.75 g and more PRH was used, making it easy to separate WSL completely from BP. No significant formation of WCM was detected in this experiment set. To investigate the reaction products as a whole, BP and WSL formed using various amounts of starting PRH mixtures were ground by hand in a ceramic mortar and mixed thoroughly. The mixtures were then heated to 700°C for 3 h in air atmosphere for the removal of unreacted carbon. Figure 4.27 shows the results of the XRD analyses conducted on the carbon-free mixtures.

It was observed from Figure 4.27 that, the percentage of Si_3N_4 was increased with decreasing amounts of PRH introduced to the furnace with the alumina crucible. Also, β-Si_3N_4 percentage of the products were found to be increasing significantly with decreasing PRH amount. Quantitative analyses were conducted on the given XRD patterns as explained in the previous sections to investigate the compositional effect of PRH amount on the products. Si_3N_4 and SiC weight percentages in the products as a function of PRH amount are given in Figure 4.28.

As seen from Figure 4.28, Si_3N_4 fraction of the products were calculated to be increasing with decreasing starting PRH amounts. Accordingly, SiC fraction was found

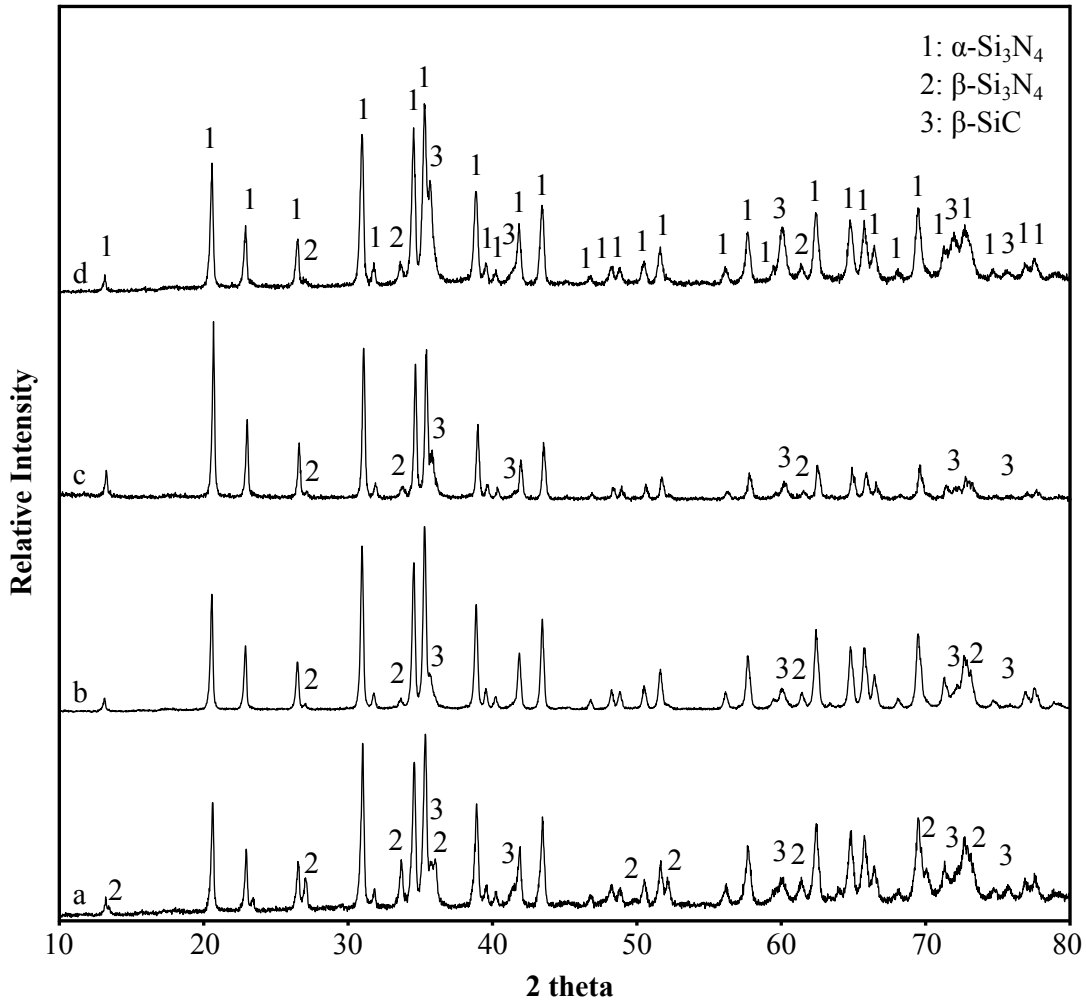

Figure 4.27: XRD patterns of the whole products (mixed and ground BP + WSL) formed on (a) 0.25 g, (b) 0.75 g, (c) 1.5 g and (d) 3 g PRH samples at 1400°C at a N_2 flow rate of 50 L/h for 6 h, after the removal of carbon. Unchecked peaks belong to α-Si_3N_4.

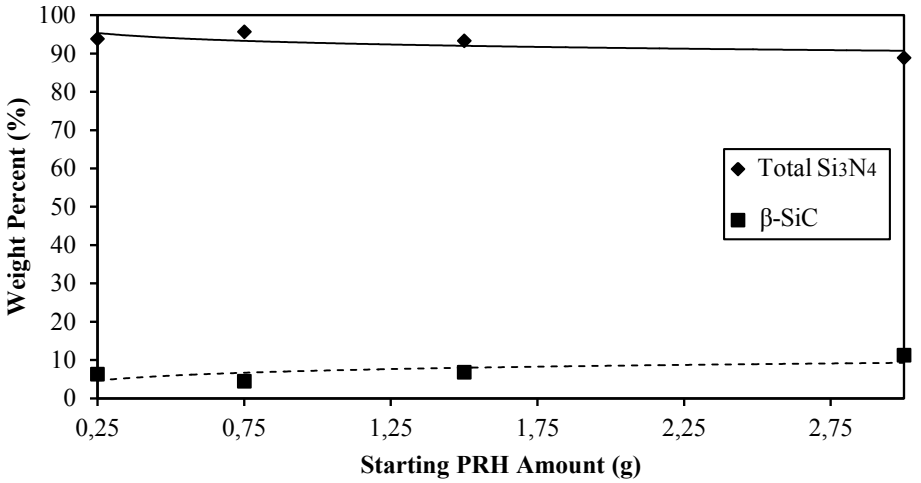

Figure 4.28: Si_3N_4 and SiC weight percentages in the products (mixed and ground WSL + BP) obtained at starting PRH amounts between 0.25-3 g at 1400°C for 6 h at 50 L/h N_2 flow rate. Si_3N_4 is given as a total of α and β phases.

to be decreasing with decreasing PRH amounts. Highest Si_3N_4 weight percentage of the products was achieved as around 96 wt% when 0.75 g of PRH was used as the starting material. Lowest Si_3N_4 weight percentage was obtained as around 89 wt% when 3 g of PRH was used. Weight loss and unreacted carbon percentages after the experiments conducted on 0.25-3 g PRH samples are given in Figure 4.29.

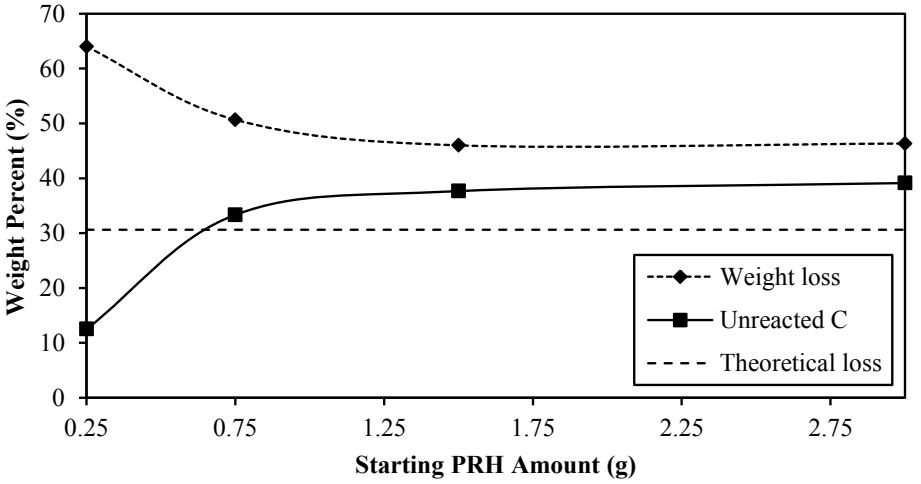

Figure 4.29: Percentages of weight loss and unreacted carbon left in the crucibles after reactions conducted on 0.25-3 g PRH samples at 1400°C for 6 h at a N_2 flow rate of 50 L/h.

Weight loss after the experiments was found to be decreasing with the increasing start-

ing PRH amount as shown in Figure 4.29. At all starting PRH amounts, the weight loss was found to be higher than the theoretical loss. Around 64% and 50% weight losses were detected when 0.25 g and 0.75 g PRH samples were used, respectively. However, the weight loss was decreased to the close vicinity of 46% when 1.5 g or more PRH was used to conduct the experiments. It was observed that the unreacted carbon percentages were increasing with increasing starting PRH amount. Around 39% of unreacted carbon was detected when PRH amounts of 1.5 g or higher was used to conduct the experiments.

SEM images of the WSL products formed when starting amount of PRH was changed between 0.25-3 g are given in Figure 4.30. The produced WSLs were not heated to elevated temperatures since they did not contain any unreacted carbon. It was observed from the images that Si_3N_4 fibers were formed at all conditions. The diameters of the fibers were measured as between 1.75-3.12 μm on 0.25 g, 176-743 nm on 0.75 g, 1.15-1.92 μm and 1-1.82 μm on 3 g PRH samples. Thus, there was no apparent relationship between the fiber diameters and the starting PRH amounts. Large fiber-like particles that were shown in Figure 4.30a were not taken into account when fiber diameters were measured. Upon EDS analyses conducted on those particles, they were found to contain Si, Ca and O, as previously detected many times on the particles formed in WSLs in the other experiment sets.

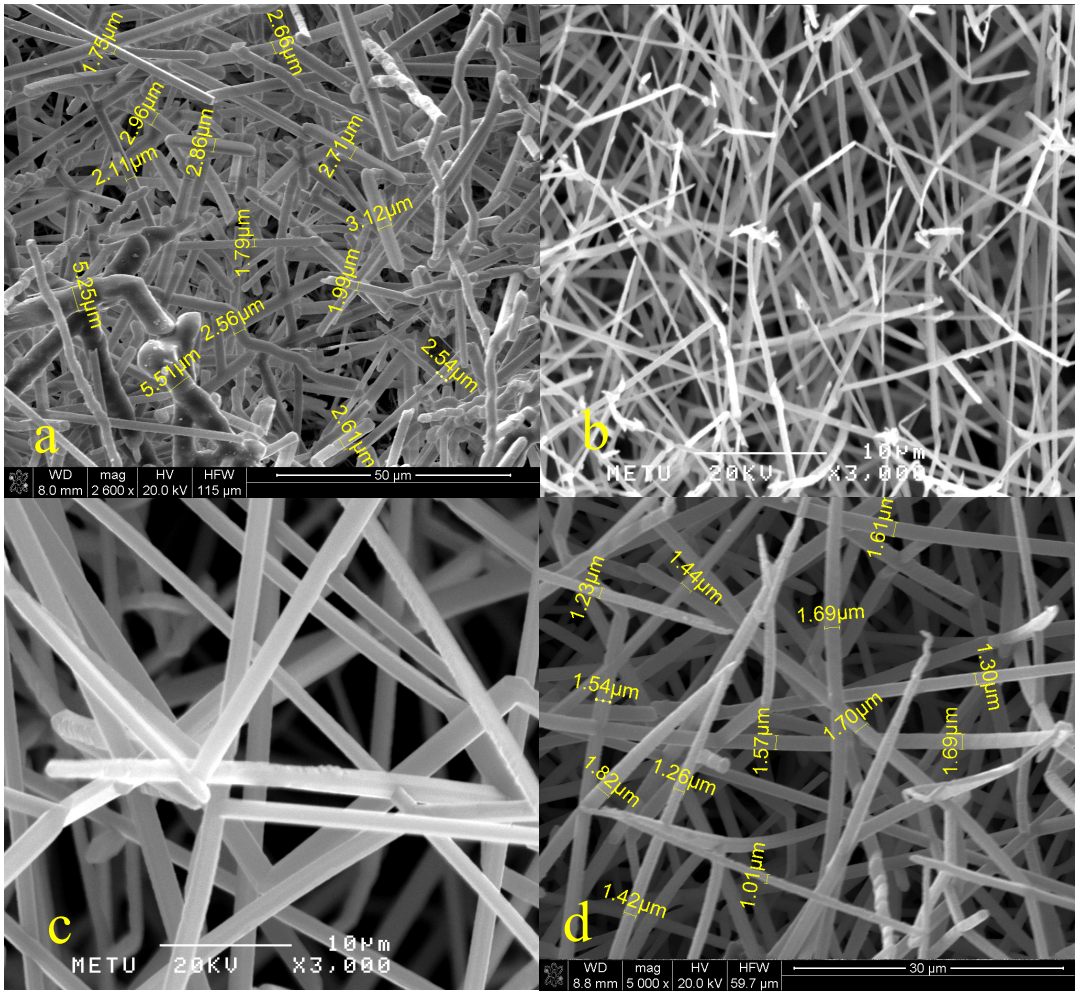

Figure 4.30: SEM images of WSL products obtained on (a) 0.25 g, (b) 0.75 g, (c) 1.5 g and (d) 3 g PRH samples at 1400°C for 6 h at a N_2 flow rate of 50 L/h.

4.2.6 Thermodynamic Considerations and Reaction Mechanism

It is widely accepted that [5, 14, 16, 18, 23, 25–28, 40, 42, 55–59] the overall reaction describing the production of Si_3N_4 by carbothermal reduction and nitridation of SiO_2 can be given by:

$$3SiO_{2(s)} + 6C_{(s)} + 2N_{2(g)} \rightarrow Si_3N_{4(s)} + 6CO_{(g)} \quad (1)$$

However, it is believed that Reaction (1) takes place through two intermediate steps involving $SiO_{(g)}$ vapor. The formation of $SiO_{(g)}$ may occur due to the following reactions:

$$SiO_{2(s)} + C_{(s)} \rightarrow SiO_{(g)} + CO_{(g)} \quad (2)$$

or

$$SiO_{2(s)} + CO_{(g)} \rightarrow SiO_{(g)} + CO_{2(g)} \quad (3)$$

$$CO_{2(g)} + C_{(s)} \rightarrow 2CO_{(g)} \quad (4)$$

and formation of Si_3N_4 can be achieved by a reaction of produced $SiO_{(g)}$ and carbon as follows:

$$3SiO_{(g)} + 3C_{(s)} + 2N_{2(g)} \rightarrow Si_3N_{4(s)} + 3CO_{(g)} \quad (5)$$

or

$$3SiO_{(g)} + 3CO_{(g)} + 2N_{2(g)} \rightarrow Si_3N_{4(s)} + 3CO_{2(g)} \quad (6)$$

$$CO_{2(g)} + C_{(s)} \rightarrow 2CO_{(g)} \quad (4)$$

Reactions (1), (5) and (6) give no information about the structure of produced Si_3N_4. Thus, to investigate whether α or β-Si_3N_4 is favorable by Reaction (1) and its step reactions (5) and (6), simple thermodynamic investigation is necessary. To conduct such an investigation, the standard Gibbs free energy changes of formation of CO, CO_2, SiO and SiO_2 were calculated by using the data tabulated by I. Barin [60]. They were calculated as:

$\Delta G_f^\circ(CO) = -113.94 - 0.0855T(kJ/mol)$
$\Delta G_f^\circ(CO_2) = -395.08 - 0.0004T(kJ/mol)$
$\Delta G_f^\circ(SiO) = -105.63 - 0.0802T(kJ/mol)$ up to 1900 K
$\Delta G_f^\circ(SiO_2) = -812.92 + 0.182T(kJ/mol)$

There is no total agreement on the published standard Gibbs free energies of formation of α and β-Si_3N_4 [61]. Furthermore, there exist no data regarding the β-Si_3N_4 in the thermochemical tables tabulated by I. Barin. Thus, the following data as recommended by A. Hendry [62] was used for the α and β-Si_3N_4:

$\Delta G_f^\circ(\alpha\text{-}Si_3N_4) = -1167.3 + 0.594T\ (kJ/mol)$
$\Delta G_f^\circ(\beta\text{-}Si_3N_4) = -936 + 0.45T$ (kJ/mol)

Change of calculated ΔG_f° values of Si_3N_4 as a function of temperature, according to Reactions (1), (5) and (6) are given in Figure 4.31 depending on whether α or β phase is produced by the mentioned reactions.

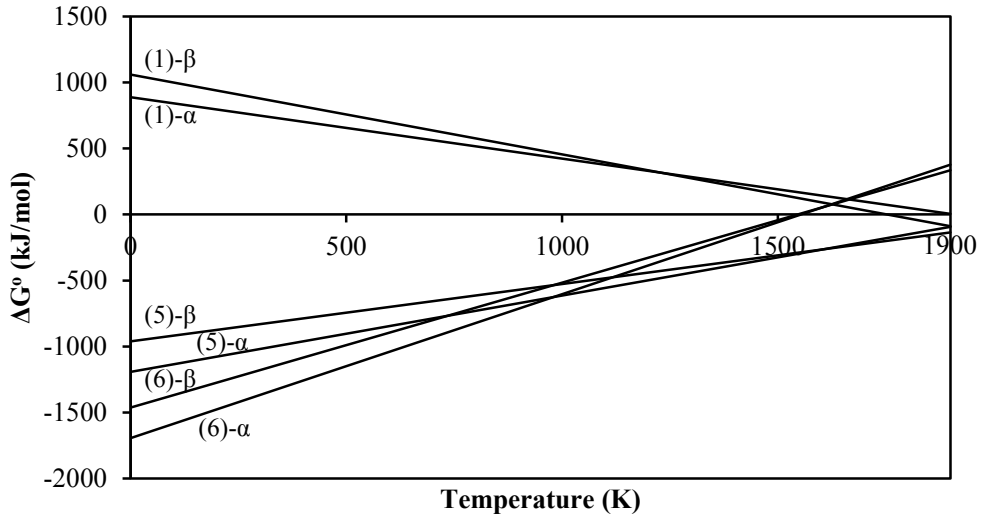

Figure 4.31: Standard free energy changes for Reactions (1), (5) and (6).

In Figure 4.31, (1)-α represents the change of free energy of formation of α-Si_3N_4 according to Reaction (1) and similarly (1)-β represents the change of free energy of formation of β-Si_3N_4 according to Reaction (1). It is seen from the figure that, at lower temperatures α-Si_3N_4 is the favored phase in all reactions. β-Si_3N_4 becomes more favorable with the increasing temperature. Carbothermal reduction and nitridation of SiO_2 was most widely studied between 1200-1500°C in the literature and 1400°C was studied in this work. It is seen from the figure that, at this temperature range β is the more stable phase, independent from the reaction upon which it forms. However, this is not in accordance with the findings of this study and findings of other studies in the literature, since it was previously reported by the XRD patterns that an α-Si_3N_4 rich product was obtained at all conditions. Formation of α-Si_3N_4 instead of thermodynamically favored β-Si_3N_4 was explained by S. A. Siddiqi et al. in their study [59]. They stated that the transformation of low temperature α phase into high temperature β phase was hindered by the higher local P_{SiO} in the reaction bed (alumina crucible). Phase stability can also be affected significantly by the impurities present in the C-SiO_2 source [28].

It is also observed from Figure 4.31 that Reaction (1) is not favorable in the temperature range of carbothermal reduction and nitridation of SiO_2. Although both Reactions (5) and (6) have a negative free energy change up to high temperatures, Reaction (5) is observed to be more favorable at higher temperatures since it has a negative free energy change in the temperature range of interest. Thus, the wide acceptance regarding the production of Si_3N_4 by carbothermal nitridation of SiO_2 taking place in two successive steps instead of directly forming by Reaction (1) was seen to be thermodynamically correct.

The formation of Si_3N_4 by the carbothermal reduction and nitridation of SiO_2 is accompanied by SiO vapor as agreed by many authors [14, 23, 26, 56]. $SiO_{(g)}$ formation may occur due to Reactions (2) and (3). Free energy change of formation of $SiO_{(g)}$ according to these reactions as a function of temperature is given in Figure 4.32.

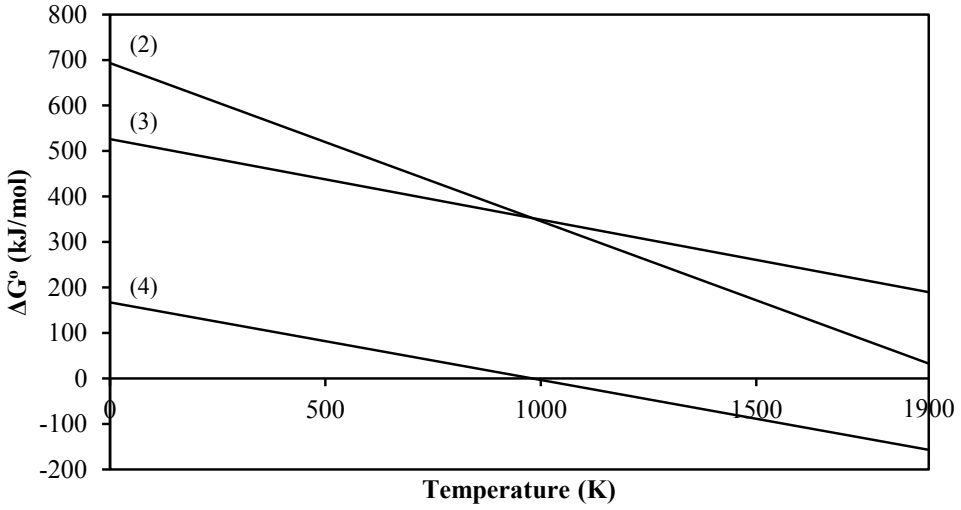

Figure 4.32: Standard free energy changes for Reactions (2), (3) and (4).

As seen from Figure 4.32, Reaction (2) is more favorable than Reaction (3) in the production of SiO vapor. However, both reactions have positive free energy change over the temperature range of interest. Therefore, the produced $CO_{(g)}$ through Reaction (2) or $CO_{2(g)}$ through Reaction (3) must be swept away from the system effectively, in order to prevent them from hindering the reactions [26]. Reaction (4) is favored especially at higher temperatures as observed from the figure.

Significant amounts of β-SiC was detected in the final products obtained at various conditions in the present study. Many authors have also reported the formation of

β-SiC in their studies [5, 14, 42]; however some reported production of pure Si_3N_4 without any SiC present [16,39]. SiC formation may be due to the following reactions [23, 55, 58, 63]:

$$SiO_{(g)} + 2C_{(s)} \rightarrow SiC(s) + CO_{(g)} \quad (7)$$

$$SiO_{2(s)} + 2C_{(s)} \rightarrow SiC(s) + CO_{2(g)} \quad (8)$$

$$SiO_{2(s)} + 3C_{(s)} \rightarrow SiC(s) + 2CO_{(g)} \quad (9)$$

$$SiO_{2(s)} + 4CO_{(g)} \rightarrow SiC(s) + 3CO_{2(g)} \quad (10)$$

Standard Gibbs free energy change of formation of SiC was calculated using the data given by I. Barin [60] as follows:

$\Delta G_f^\circ(SiC) = -73.123 + 0.0078T\ (kJ/mol)$ up to 1700 K
$\Delta G_f^\circ(SiC) = -121.55 + 0.0366T\ (kJ/mol)$ above 1700 K

Accordingly, Figure 4.33 was drawn to investigate the formation of SiC thermodynamically. As observed from the figure, Reactions (8) and (10) have positive free energy changes over the temperature range. Reaction (9) only becomes favorable at very high temperatures. On the other hand, Reaction (7) has a negative free energy change at all temperatures and therefore it is the most favorable reaction for the formation of SiC in the considered temperature range. Reaction (7) is thought to be the reaction responsible for the formation of significant amount of SiC in the final products at temperatures as low as 1300°C, in this study.

As seen by the XRD patterns given in Figure 4.16, most of the SiC was formed after 1 h reaction duration. As also represented in Figure 4.17, SiC percentage was at the minimum when the reaction duration was set to maximum (24 h). The reason for the high formation rate of SiC in the early stage of the experiment is thought to be an indication of high SiO vapor formation rate early in the experiment. Formed SiO vapor then reacts with already present C in PRH according to Reaction (7) and forms SiC.

The reason for the high rate of formation of SiO vapor in the early stages is considered to be related to Reaction (2). Reaction (2) was previously shown to be the more favorable reaction for the production of SiO vapor. Considering the reactants

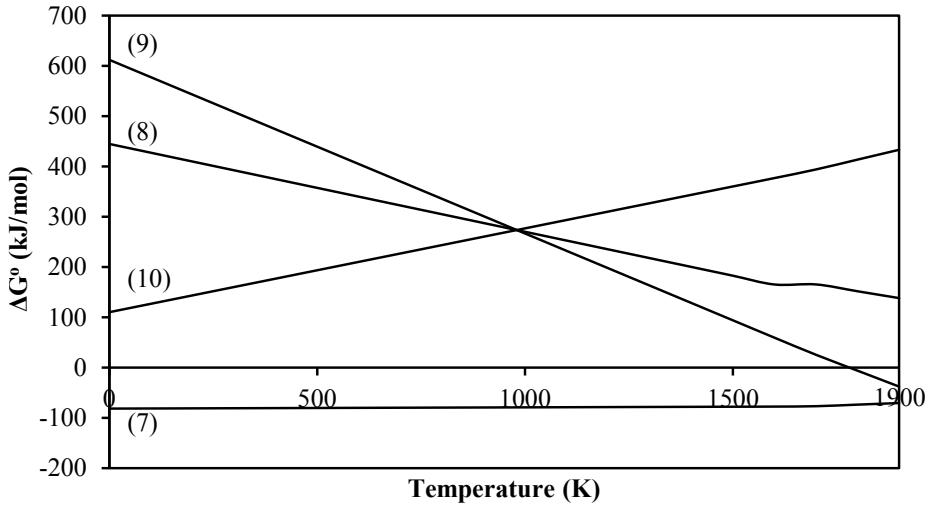

Figure 4.33: Standard free energy changes for Reactions (7), (8), (9) and (10).

of Reaction (2), it is seen that $C_{(s)}$ is reacting with $SiO_{2(s)}$ to form $SiO_{(g)}$. Both $C_{(s)}$ and $SiO_{2(s)}$ is present in PRH in intimate contact. Therefore, due to high amount of contact points between $C_{(s)}$ and $SiO_{2(s)}$, the reaction rate is considered to be high at early stages. However, as the contact points between $C_{(s)}$ and $SiO_{2(s)}$ diminish due to the formation of SiO vapor, Reaction (2) slows down and stops when there are no contact points left. After this point, SiO is thought to be produced only by Reaction (3) at a slower rate.

Considering the XRD patterns given in Figures 4.16, 4.23 and 4.27 and the quantitative analyses based on them, it was determined that only phases present in the system at all times longer than 1 h reaction duration were Si_3N_4 and SiC. SiC percentage in the final products was decreasing with the increasing reaction duration, increasing N_2 flow rate and decreasing starting PRH amount. On the other hand, the percentage of Si_3N_4 was found to be increasing with decreasing SiC percentage. Therefore, either SiC present in the final products was decomposing into gaseous species under these conditions and leaving the system or transforming into Si_3N_4, because there were no other phases detected in the given XRD patterns. Since the decomposition temperature of SiC is around 3100 K, only plausible explanation of the decrease in SiC percentage and increase in Si_3N_4 lies in the transformation of SiC into Si_3N_4. Following reactions may be written for the transformation of SiC into Si_3N_4 [28, 55, 59]:

$$3SiC_{(s)} + 2N_{2(g)} \rightarrow Si_3N_{4(s)} + 3C_{(s)} \quad (11)$$

$$2SiC_{(s)} + SiO_{2(s)} + 2N_{2(g)} \rightarrow Si_3N_{4(s)} + 2CO_{(g)} \quad (12)$$

Weight loss percentages during the course of the various experiment sets are tabulated in Table 4.6.

Table 4.6: Weight Loss Percentages After Various Experiments

Experiment Set 2*		**Experiment Set 3****		**Experiment Set 4*****	
Reaction duration (h)	**Weight loss (%)**	**N_2 flow rate (L/h)**	**Weight loss (%)**	**Starting PRH (g)**	**Weight loss (%)**
1	38.7	10	47.7	0.25	64.0
3	46.3	20	46.3	0.75	50.7
6	46.3	30	45.7	1.50	46.0
9	44.7	40	45.3	3.00	46.3
24	45.7	50	46.3		

*Conducted at 1400°C on 3 g PRH at a N_2 flow rate of 50 L/h .
**Conducted at 1400°C on 3 g PRH for 6 h.
***Conducted at 1400°C at a N_2 flow rate of 50 L/h for 6 h.

Considering the weight loss data given in Table 4.6 for various reaction durations, it was observed that at reaction durations longer than 1 h, the weight loss percentages were almost the same, around 46%. This meant that approximately after 3 h of a reaction duration, the weight of material in the alumina crucible did not change significantly. It was previously shown that SiC percentage was decreasing and Si_3N_4 percentage was increasing with increasing experiment duration. Thus, it is concluded that the reaction responsible for the transformation of SiC to Si_3N_4 should not change the weight of the product, i.e. $M_{\text{solid reactants}}=M_{\text{solid products}}$, so that the weight of material in the alumina crucible remained constant. Reaction (12) is such a reaction, however Reaction (11) is not. Thus, this provides a strong evidence of the SiC to Si_3N_4 transformation through Reaction (12). Furthermore, the same effect is observed for all N_2 flow rate experiments and starting PRH experiments with PRH more than 1.5 g.

Considering Reaction (12), following considerations can be made:

$\Delta G_{(12)} = \Delta G^{\circ}_{(12)} + RTlnQ$
$\Delta G^{\circ}_{(12)}$ was calcuated by using the data tabulated by I. Barin [60], thus:
$\Delta G^{\circ}_{(12)} = -336.014 + 0.2254T + RTln(P^2_{CO})$

solving this equation for T=1400°C (1673 K) and R=0.008314 kJ gives;

$$\Delta G_{(12)} = 41.0802 + 13.909 \ln(P_{CO}^2)$$

the equilibrium partial pressure of CO is found as $P_{CO} = 0.228$ atm. P_{CO} must be kept below this value for Reaction (12) to occur. Assuming $P_{N_2} + P_{CO} = 1$ atm in the system, the equilibrium nitrogen partial pressure is found as $P_{N_2} = 0.772$ atm. Thus, low CO partial pressures can be achieved by maintaining a high nitrogen partial pressure, which can be done by increasing the N_2 flow rate. This can be supported by the findings of N_2 flow rate experiments as given in Figures 4.23 and 4.24. As it was observed from these figures, SiC percentage in the products was decreasing with increasing N_2 flow rate. Furthermore, the highest SiC percentage was achieved at the lowest N_2 flow rate (10 L/h), since SiC to Si_3N_4 transformation was hindered by CO gas.

Similar reasoning can be conducted on Reaction (1), the overall reaction for the carbothermal production of Si_3N_4. Calculations are as follows:

$$\Delta G_{(1)} = \Delta G^{\circ}_{(1)} + RT\ln Q$$
$$\Delta G_{(1)} = 887.82 - 0.465T + RT\ln\frac{P_{CO}^6}{P_{N_2}^2}$$

at equilibrium,

$$\ln\frac{P_{CO}^6}{P_{N_2}^2} = \frac{-887.82 + 0.465T}{RT}$$
$$\frac{P_{CO}^3}{P_{N_2}} = \exp\left(\frac{-887.82 + 0.465T}{2RT}\right)$$

$\frac{P_{CO}^3}{P_{N_2}}$=0.01926 is obtained when $T = 1400°C\ (1673 K)$ and $R = 0.008314$ kJ. Assuming $P_{N_2} + P_{CO} = 1$ atm in the system, it can be written that $P_{N_2} = 1 - P_{CO}$. By solving $\frac{P_{CO}^3}{1 - P_{CO}} = 0.01926$, the equilibrium partial pressure of CO and N_2 are found as $P_{CO} = 0.244$ atm and $P_{N_2} = 0.756$ atm. Thus, it is observed from the calculations that maintaining the $P_{CO} < 0.244$ atm plays an important role on the reaction. Since CO gas forms due to Reaction (1), it must be removed from the system efficiently to decrease its partial pressure. This can be done by sweeping the formed CO gas by a flow of N_2. The higher the flow rate of N_2 the lower the P_{CO} will be kept, thus the

reaction will commence. It was observed that almost the same N_2 flow rate conditions that favor the transformation of SiC to Si_3N_4 also favors the formation of Si_3N_4 by the overall Reaction (1).

Using Reactions (1), (9) and (12) and their calculated free energy changes of formation, a predominance diagram was constructed based on the partial pressures of N_2 and CO for 1400°C. Diagram is given in Figure 4.34.

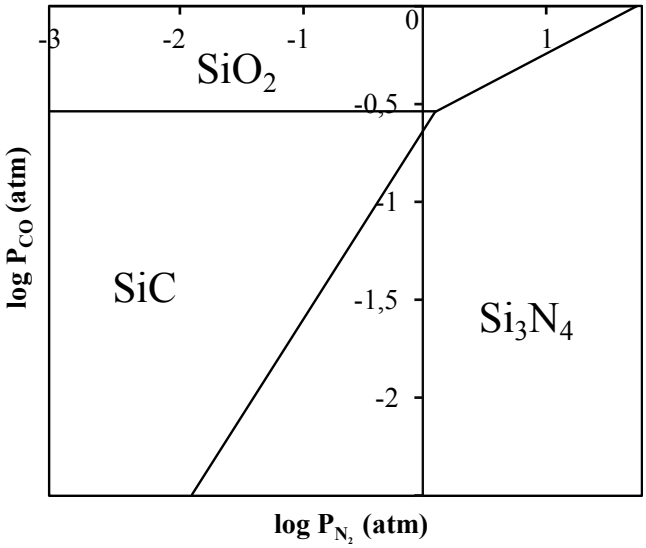

Figure 4.34: Predominance diagram showing stability regions of SiO_2, Si_3N_4 and SiC at 1400°C.

As observed from Figure 4.34, lower partial pressures of CO favors both the formation of SiC and Si_3N_4. However, SiC is seen to be more stable at lower N_2 pressures, on the other hand, Si_3N_4 becomes stable at higher N_2 pressures. Therefore, the SiC formed at the early stages of the experiments transforms to Si_3N_4 at high N_2 flow rates.

When the formation of WCM, as shown in Figure 4.20, was considered, it was observed that it was formed on the crucible walls. SEM investigation (Figure 4.22) showed that it was formed as Si_3N_4 fibers. Since the formation of WCM took place outside of the PRH powder bed, it was considered that it must be formed by a gas phase reaction [16]. Thus, the formation of WCM was thought to be due to Reaction (6). Siddiqi et al. stated that Reaction (6) was not a likely reaction to occur, since it involved a reaction between three gas phases in an extremely complex stoichiometry

(they have considered α-Si_3N_4 as $Si_{76}N_{100}O_2$) [59]. However, some authors have disagreed with Siddiqi et al. and stated that the reaction may be considered as a possible formation and growth reaction of Si_3N_4 [16, 28, 56].

WSL was observed to be formed on top of the PRH powders as a continuous white layer as shown in Figure 4.8. WSL was shown to be made of Si_3N_4 fibers with a similar morphology to that of WCM by various SEM images. Formation of Si_3N_4 fibers was considered to be due to a vapor-solid mechanism [16]. Thus, Reaction (5) was thought to be the reaction responsible for the formation of WSL. It was detected from the reaction duration experiments that after 1 and 3 h long experiments, a single layer of WSL was formed on top of the PRH powder. However, when the experiment duration was increased to 6 h and beyond, two separate WSLs were observed to be formed on top of each other. The top WSL had no connection with the PRH powder and could be completely separated from the bottom WSL. Thus, the formation of top WSL was thought to be due to a gas phase reaction like the formation of WCM. Accordingly, Reaction (6) was thought to be responsible for the formation of second layer of WSL.

It was observed from Figure 4.9 that significant amounts of Si_3N_4 were produced in BPs at 1400 and 1450°C even after only 1 h. V. Pavarajarn et al. reported the formation of amorphous silicon oxycarbide species in BPs [16]. It was stated that this oxycarbide was formed by a solid-state reaction between C and SiO_2 and then reacted with N_2 to produce Si_3N_4. They concluded that the contact points between C and SiO_2 would diminish after some time and the formation of silicon oxycarbide species would be stopped. Therefore, they observed a high rate of formation of Si_3N_4 in the early stage of the reaction and no further formation of Si_3N_4 after the early stages.

SiC formation in BP was reported in all of the experiments conducted. It was previously proposed that SiC was formed by Reaction (7) and then transformed into Si_3N_4 at a slow rate by Reaction (12). In order to explain the similar weight loss data given in Table 4.6, no reactions other than Reaction (12) should occur in BP after experiment durations longer than 3 h. However, the formation of SiC and formation of Si_3N_4 in BP must also be considered as possible reactions to occur. Considering the

mechanism proposed by V. Pavarajarn et al. above, Si_3N_4 would only be formed at early reaction durations in BP and the formed Si_3N_4 would remain in the BP at all reaction durations unchanged. It was also previously explained that SiC formation was thermodynamically favored by Reaction (7). For this reaction to take place, SiO vapor supply was necessary. As mentioned earlier SiO vapor formation in the reaction bed is mainly due to Reaction (2) which involves C and SiO_2. Similarly, the rate for this reaction is expected to be high at early stages of the reaction since there exists an intimate contact between C and SiO_2. However, this reaction would not occur after the early stages due to the destroyed contact points. Accordingly, the SiO vapor supply for Reaction (7) would be decreased significantly and the reaction rate would be slowed down greatly. On the other hand, CO is observed to be a product of many reactions considered. High rate of formation of CO is thought to be increasing the local partial pressure of CO in the reaction bed and preventing the Reaction (7) to take place, especially when SiO vapor formation rate is slowed down. Although N_2 gas is supplied into the reaction tube at a high rate, the produced CO may not be swept away from the system completely since the WSL formed on top of the alumina crucible could be hindering the diffusion of N_2 coming in and CO going out. Therefore, it was concluded that after about 3 h and longer reaction durations, only reaction occurring in BP was Reaction (12). Thus, the weight of the BP would remain at a constant level from 3 h to the end of the reaction.

It was observed from Figure 4.9 that Si_2N_2O was detected in BPs produced at 1300-1450°C after 1 h reaction duration. The formation of Si_2N_2O may be explained by the following reaction as given by F. L. Silva et al. [55]:

$$SiO_{(g)} + C_{(s)} + N_{2(g)} \rightarrow Si_2N_2O_{(s)} + CO_{(g)} \quad (13)$$

Si_2N_2O is considered to be a product of early treatment times and then converted into Si_3N_4 by following reactions [55]:

$$Si_2N_2O_{(s)} + SiO_{2(s)} + 3C_{(s)} + N_{2(g)} \rightarrow Si_3N_{4(s)} + 3CO_{(g)} \quad (14)$$

$$Si_2N_2O_{(s)} + SiC_{(s)} + N_{2(g)} \rightarrow Si_3N_{4(s)} + CO_{(g)} \quad (15)$$

The conversion of Si_2N_2O to Si_3N_4 may be confirmed by the removal of the peaks belonging to Si_2N_2O at higher reaction durations as given by XRD patterns in Figure 4.16.

CHAPTER 5

CONCLUSION

Synthesis of Si_3N_4 through the carbothermal reduction and nitridation of SiO_2 present in the acid leached and pyrolyzed rice husks was investigated. Rice husks obtained from Black Sea region (Bafra) of Turkey were subjected to a pretreatment process including purification, pyrolysis and grinding. Pretreated powder was used as the starting material for the carbothermal reduction and nitridation experiments. Effects of reaction parameters such as temperature, duration, N_2 flow rate and starting PRH amount were examined. The products were analyzed by X-ray diffraction and scanning electron microscopy. Following results were obtained after the study:

1. Purification of as-received rice husks by successive sieving, water washing and acid leaching steps was proved to be a valid method for obtaining high purity rice husks containing almost only C and SiO_2.

2. Acid leaching of RHs was found to be increasing the crystallinity of the phases present in RHs.

3. Pyrolysis of RHs was found to be taking place in three stages.

4. XRD and elemental analyses results of the PRH samples indicated that it was possible to produce a mixture of C and amorphous SiO_2 by the pyrolysis of RHs at 600°C under argon atmosphere.

5. XRD analysis result of RHA showed that the amorphous SiO_2 in RHs partially transformed into crystalline SiO_2 at 900°C.

6. Three different Si_3N_4 containing products were observed to form after carboth-

ermal nitridation experiments, namely, White Surface Layer (WSL), Black Powder (BP) and White Cotton-like Material (WCM). No WSL formation was observed in the products obtained after the experiments conducted at 1300 and 1350°C. WSL formation was observed at 1400, 1450 and 1500°C, even after only 1 h reaction duration. Formed WSLs were detected as Si_3N_4, rich in α phase, independent of their formation conditions, by XRD analyses. WSLs were detected to have a fibrous morphology containing Si_3N_4 fibers by SEM analyses.

7. WCM was observed to be formed on crucible walls. It was analyzed as Si_3N_4, rich in α phase, by XRD analysis. WCM was found to have a fibrous morphology by SEM analysis. The formation of WCM became significant only at N_2 flow rates lower than 30 L/h.

8. BPs were found to contain both Si_3N_4 and SiC. The weight fraction of Si_3N_4 in BP was found to be increasing with increasing temperature.

9. The diameters of the Si_3N_4 fibers in WSLs were found to be increasing with increasing temperature.

10. Weight percentage of Si_3N_4 in the products was found to be increasing with increasing reaction duration. After 3 h reaction duration the Si_3N_4 weight percentage was calculated as approximately 85 wt% and it was increased to around 95 wt% after 24 h.

11. Weight percentage of Si_3N_4 in the products was found to be increasing with increasing N_2 flow rate. Si_3N_4 weight percentage in the product obtained at a N_2 flow rate of 10L/h was calculated to be around 78 wt%. This was increased to its maximum of approximately 89 wt% when the gas flow rate was increased to 40 L/h.

12. Weight percentage of Si_3N_4 in the products was found to be increasing with decreasing starting PRH amounts. The highest percentage was obtained as around 96 wt% when 0.75 g of PRH was used as the starting material, the lowest percentage was obtained as 89 wt% when 3 g of PRH was used.

13. The highest formation of β-Si_3N_4 was detected when 0.25 g of PRH was used as the starting material for the experiment as detected by the XRD analysis.

In conclusion, it was seen from the experimental results that it was possible to obtain both pure Si_3N_4 and Si_3N_4/SiC composite powder by the carbothermal reduction and nitridation of Turkish rice husks. For the production of pure Si_3N_4, the optimum conditions were given at 1400°C on 3 g PRH at a N_2 flow rate of 50 L/h as 6 h and longer durations, so that the top WSL formation occurs. For the production of Si_3N_4/SiC composite powder having less than 80 wt% Si_3N_4, the optimum conditions were found as 6 h at 1400°C on 3 g PRH at a N_2 flow rate of 10 L/h. For the production of Si_3N_4/SiC composite powder having a composition between 80-90 wt% Si_3N_4, the optimum conditions were found as 6 h at 1400°C on 3 g PRH at a N_2 flow rate between 20-50 L/h. For the production of Si_3N_4/SiC composite powder having more than 90 wt% Si_3N_4, the optimum conditions were found as 6 h at 1400°C at a N_2 flow rate of 50 L/h on 0.25-1.5 g PRH or 9 h or longer durations at 1400°C on 3 g PRH at a N_2 flow rate of 50 L/h.

As possible future studies, to increase the Si_3N_4 formation, following methods are suggested. The formed WSL should be disturbed at certain time intervals by mixing it together with BP using a thin alumina rod or such, inside the tubular furnace at the reaction temperature. This way, the BP would be exposed to the N_2 flow again and more WSL formation would take place. Also, the effect of Si_3N_4 addition into the PRH could be investigated to see whether or not it would increase the Si_3N_4 formation by acting as nucleation sites. Effect of addition of other oxides into the PRH powder like Al_2O_3, Y_2O_3, ZrO_2, TiO_2, CeO_2, Fe_2O_3, NiO and V_2O_5 could also be investigated in future studies.

REFERENCES

[1] D.A. Taylor, *Advanced Ceramics – The Evolution, Classification, Properties, Production, Firing, Finishing and Design of Advanced Ceramics*. Materials Australia, 2001. **33** (1), p. 20-22.

[2] Hagen Klemm, *Silicon Nitride for High-Temperature Applications*. Journal of the American Ceramic Society, 2010. **93** (6), p. 1501-1522.

[3] L. Sun, K. Gong, *Silicon-Based Materials from Rice Husks and Their Applications*. Industrial & Engineering Chemistry Research, 2001. **40**, p. 5861-5877.

[4] P. Koohafkan, B. A. Stewart, *Water and Cereals in Drylands*. The Food and Agriculture Organization of the United Nations and Earthscan, 2008.

[5] Ivan B. Cutler, *Production of silicon nitride from rice hulls*. U.S. Patent 3,855,395, 1974.

[6] Frank L. Riley, *Silicon Nitride and Related Materials*. Journal of the American Ceramic Society, 2000. **83** (2), p. 245–265.

[7] H. Sainte-Claire Deville, F. Wöhler, *On the Direct Compound Silicon Nitride*. Liebigs Ann. Chem. Pharm., 1859. **110**, p. 248–250.

[8] H. Melner, *Verfahren zür darstellung von Nitriden*. Ger. Pat. No. 88 999, 1896.

[9] S. Somiya et al. (Eds.), *Handbook of Advanced Ceramics - Chapters 9.1, 11.1, 11.2 and 15.1*. Elsevier Ltd., 2003.

[10] K. L. Roberts, L. Covington Jr., *Nitrides*. Kirk-Othmer Encyclopedia of Chemical Technology, John Wiley & Sons, Inc., 2005. **16**, p. 1-36.

[11] H. Lange, G. Wotting, G. Winter, *Silicon Nitride-From Powder Synthesis to Ceramic Materials*. Angewandte Chemie International Edition, 1991. **30**, p. 1579-1597.

[12] Michael J. Hoffmann, *Si_3N_4-Ceramics: Processing, Microstructure and Mechanical Properties*. IV. Ceramic Congress, Eskişehir, Türkiye, 1998.

[13] D. R. Askeland, P. P. Fulay, D. K. Bhattacharya, *Essentials of Materials Science and Engineering*. Second Edition, SI, Cengage Learning, 2010.

[14] N. Kuskonmaz, A. Sayginer, C. Toy, E. Acma, O. Addemir, A. Tekin, *Studies on the Formation of Silicon Nitride and Silicon Carbide from Rice Husk*. High Temperature Materials and Processes, 1996. **15** (1-2), p. 123-127.

[15] O. Addemir, A. Tekin, C.K. Gupta, *Nitridation in the Processing and Preparation of Metals and Ceramics*. High Temperature Materials and Processes, 1996. **15** (4), p. 273-280.

[16] V. Pavarajarn, R. Precharyutasin, P. Praserthdam, *Synthesis of Silicon Nitride Fibers by the Carbothermal Reduction and Nitridation of Rice Husk Ash*. Journal of the American Ceramic Society, 2010. **93** (4), p. 973–979.

[17] C. Real, M. D. Alcala, J. M. Criado, *Synthesis of Silicon Nitride from Carbothermal Reduction of Rice Husks by the Constant-Rate-Thermal-Analysis (CRTA) Method*. Journal of the American Ceramic Society, 2004. **87** (1), p. 75-78.

[18] T. H. Liou, F. W. Chang, *The Nitridation Kinetics of Pyrolyzed Rice Husk*. Industrial & Engineering Chemistry Research, 1996. **35**, p. 3375-3383.

[19] M. N. Rahaman, *Ceramic Processing*. CRC Press, 2006.

[20] I. J. McColm, N. J. Clark, *Forming, Shaping and Working of High-Performance Ceramics*. Blackie and Son Ltd, 1988.

[21] D. Mallette, C. A. Pickles, C. Simpson, *Carbothermal Production of Silicon Nitride*.

[22] A. O. Kurt, Y. Güzelvardar, *Dinamik Karbotermal Yöntem ile* α-Si_3N_4 *Seramik Tozu Üretimi*. Afyon Kocatepe Üniversitesi Fen Bilimleri Dergisi. **Özel Sayı**, p. 125-140.

[23] M. Ekelund, B. Forslund, *Carbothermal Preparation of Silicon Nitride: Influence of Starting Material and Synthesis Parameters*. Journal of the American Ceramic Society, 1992. **75** (3), p. 532-539.

[24] A. Ortega, M. D. Alcala, C. Real, *Carbothermal synthesis of silicon nitride* (Si_3N_4)*: Kinetics and diffusion mechanism*. Journal of Materials Processing Technology, 2008. **195**, p. 224-231.

[25] S. J. P. Durham, K. Shanker, R. A. L. Drew, *Carbothermal Synthesis of Silicon Nitride: Effect of Reaction Conditions*. Journal of the American Ceramic Society, 1991. **74** (1), p. 31-37.

[26] T. H. Liou, F. W. Chang, *Kinetics of Carbothermal Reduction and Nitridation of Silicon Dioxide/Carbon Mixture*. Industrial & Engineering Chemistry Research, 1995. **34**, p. 118-127.

[27] Shi-Chang Zhang, W. R. Cannon, *Preparation of Silicon Nitride from Silica*. Journal of the American Ceramic Society, 1984. **67** (10), p. 691-695.

[28] Y. W. Cho, J. A. Charles, *Synthesis of nitrogen ceramic powders by carbothermal reduction and nitridation Part 1 Silicon nitride*. Materials Science and Technology, 1991. **7**, p. 289-298.

[29] International Rice Research Institute. *World Rice Statistics Online Query Facility*. Available: http://ricestat.irri.org:8080/wrs2/entrypoint.htm. Last accessed on 10th of January 2014.

[30] M.R. Giddel, A.P. Jivani, *Waste to Wealth - Potential of Rice Husk in India a Literature Review*. Proceedings of the International Conference on Cleaner Technologies and Environmental Management PEC, Pondicherry, India. January 4-6, 2007. p. 586-590.

[31] Rice Millers Association, http://www.pdd.org.tr/sector-report. Last accessed on 6th of June 2013.

[32] N. K. Sharma, W. S . Williams, A. Zangvil, *Formation and Structure of Silicon Carbide Whiskers from Rice Hulls*. Journal of the American Ceramic Society, 1984. **67**, p. 715-720.

[33] S. Chandrasekhar, K. G. Satyanarayana, P. N. Pramada, P. Raghavan, T. N. Gupta, *Review Processing, properties and applications of reactive silica from rice husk—an overview*. Journal of Materials Science, 2003. **38**, p. 3159 – 3168.

[34] H. Kurama, S.K. Kurama, *The Effect of Chemical Treatment on the Production of Active Silica from Rice Husk*. 18th International Mining Congress and Exhibition of Turkey-IMCET, 2003.

[35] V. M. H. Govindarao, *Utilization of rice husk - A preliminary analysis*. Journal of Science & Industrial Research, 1980. **39**, p. 495-515.

[36] M. G. A. Vieira, A. F. de Almeida Neto, M. G. C. da Silva, C. C. Nobrega, A. A. M. Filho, *Characterization and Use of In Natura and Calcined Rice Husks for Biosorption of Heavy Metals Ions from Aqueous Effluents*. Brazilian Journal of Chemical Engineering, 2012. **29** (03), p. 619-633.

[37] S. D. Genieva, S. Ch. Turmanova, A. S. Dimitrova, L. T. Vlaev, *Characterization of Rice Husks and the Products of its Thermal Degradation in Air or Nitrogen Atmosphere*. Journal of Thermal Analysis and Calorimetry, 2008. **93** (2), p. 387–396.

[38] Y. A. R. Yücel, *Silicon Carbide Whisker Production from Rice Husks of Black Sea and Thrace Regions of Turkey*. M.Sc. Thesis in Metallurgical and Materials Engineering, 1997. Middle East Technical University: Ankara.

[39] T. H. Liou, F. W. Chang, J. J. Lo, *Pyrolysis Kinetics of Acid-Leached Rice Husk*. Industrial & Engineering Chemistry Research, 1997. **36**, p. 568-573.

[40] I. A. Rahman, *The Formation of Different Si_3N_4 Phases in the Presence of V_2O_5 During Carbothermal Reduction of Untreated and Acid Treated Rice Husk*. Ceramics International, 1998. **24**, p. 293-297.

[41] I. A. Rahman, *Preparation of Si_3N_4 by Carbothermnal Reduction of Digested Rice Husk*. Ceramics International, 1994. **20**, p. 195-199.

[42] I. A. Rahman, F. L. Riley, *The Control of Morphology in Silicon Nitride Powder Prepared from Rice Husk*. Journal of the European Ceramic Society, 1989. **5**, p. 11-22.

[43] Piotr Klimczyk, *Mechanical properties of Si_3N_4-SiC composites sintered by HPHT method*. Advances in Science and Technology, 2010. **63**, p. 396-401.

[44] L. Hegedusova, M. Kasiarova, J. Dusza, M. Hnatko, P. Sajgalik, *Mechanical properties of carbon-derived Si_3N_4+SiC micro/nano-composite*. International Journal of Refractory Metals & Hard Materials, 2009. **27**, p. 438-442.

[45] P. Sajgalik, M. Hnatko, F. Lofaj, P. Hvizdos, J. Dusza, P. Warbichler, F. Hofer, R. Riedel, E. Lecomte, M. J. Hoffmann, *SiC/Si_3N_4 nano/micro-composite – processing, RT and HT mechanical properties*. Journal of the European Ceramic Society, 2000. **20**, p. 453-462.

[46] X. Bao, M. J. Edirisinghe, *Different strategies for the synthesis of silicon carbide–silicon nitride composites from preceramic polymers*. Composites, 1999. Part A **30**, p. 601-610.

[47] M. Balog, J. Keckes, T. Schöberl, D. Galusek, F. Hofer, J. Krestan, Z. Lences, J. L. Huang, P. Sajgalik, *Nano/macro-hardness and fracture resistance of Si_3N_4/SiC composites with up to 13 wt.% of SiC nano-particles*. Journal of the European Ceramic Society, 2007. **27**, p. 2145-2152.

[48] M. Herrmann, H. Klemm, B. Göbel, Chr. Schubert and W. Hermel, *SiC/Si_3N_4 Nanocomposites with Excellent High-Temperature Long-Term Behaviour*. Key Engineering Materials, 1999. **161-163**, p. 377-380.

[49] J. F. Yang, T. Ohji, T. Sekino, C. L. Li, K. Niihara, *Phase transformation, microstructure and mechanical properties of Si_3N_4/SiC composite*. Journal of the European Ceramic Society, 2001. **21**, p. 2179-2183.

[50] Koichi Niihara, *New Design Concept of Structural Ceramics – Ceramic Nanocomposites*. The Centennial Memorial Issue of The Ceramic Society of Japan, 1991. **99** (10), p. 974-982.

[51] A. S. Saygıner, *Pirinç Kabuklarından Karbotermik Redüksiyon ve Nitrürleme Yöntemiyle SiC-Si_3N_4 Seramik Kompozit Tozu Üretimi*. Yüksek Lisans Tezi, 1995. İstanbul Teknik Üniversitesi: Fen Bilimleri Enstitüsü.

[52] N. Johar, I. Ahmad, A. Dufrense, *Extraction, preparation and characterization of cellulose fibres and nanocrystals from rice husk*. Industrial Crops and Products, 2012. **37**, p. 93-99.

[53] M. Sarangi, P. Nayak, T. N. Tiwari, *Effect of temperature on nano-crystalline silica and carbon composites obtained from rice-husk ash*. Composites: Part B, 2011. **42**, p. 1994-1998.

[54] Frank H. Chung, *Quantitative Interpretation of X-ray Diffraction Patterns of Mixtures. II. Adiabatic Principle of X-ray Diffraction Analysis of Mixtures*. Journal of Applied Crystallography, 1974. **7**, p. 526-531.

[55] F. L. Silva, J.M. Vieira, *Carbothermal reduction and nitridation of silica: nuclei planar growth controlled by silicon monoxide diffusion on the reducer surface*. Journal of Materials Processing Technology, 1999. **92-93**, p. 112-117.

[56] S. L. Chung, C. W. Chang, *Carbothermal reduction and nitridation synthesis of silicon nitride by using solution combustion synthesized precursors*. Journal of Materials Science, 2009. **44**, p. 3784-3792.

[57] R. Koc, S. Kaza, *Synthesis of α-Si_3N_4 from Carbon Coated Silica by Carbothermal Reduction and Nitridation*. Journal of the European Ceramic Society, 1998. **18**, p. 1471-1477.

[58] M. V. Vlasova, T. S. Bartnitskaya, L. L. Sukhikh, L. A. Krushinskaya, T. V. Tomila, S. Yu. Artyuch, *Mechanism of Si_3N_4 nucleation during carbothermal reduction of silica*. Journal of Materials Science, 1995. **30**, p. 5263-5271.

[59] S. A. Siddiqi, A. Hendry, *The influence of iron on the preparation of silicon nitride from silica*. Journal of Materials Science, 1985. **20**, p. 3230-3238.

[60] Ihsan Barin, *Thermochemical Data of Pure Substances*. Weinheim; New York; Basel; Cambridge; Tokyo: VCH, 1995. Third edition.

[61] Zdenek Panek, *Standard Gibbs Energy of Formation of β-Silicon Nitride*. Journal of the American Ceramic Society, 1995. **78** (4), p. 1087-1088.

[62] A. Hendry, *Proceedings of the 11th RISOE International Symposium on Metallurgy and Materials Science*. RISO National Laboratory, Roskilde, Denmark, 1990, p. 27-38.

[63] B. K. Padhi and C. Patnaik, *Development of Si_2N_2O, Si_3N_4, and SiC Ceramic Materials Using Rice Husk*. Ceramics International, 1995. **21**, p. 213-220.